Sunlight to Signals: Solar Panel as an Optical Wireless Communication Receiver for Sustainable Communication Systems

Submitted By

Rahul

under the supervision of

Prof. Vivek Ashok Bohara
Professor, IIIT-Delhi
&
Prof. Anand Srivastava
Professor, IIIT-Delhi

INDRAPRASTHA INSTITUTE *of* INFORMATION TECHNOLOGY **DELHI**

Department of Electronics and Communication Engineering
Indraprastha Institute of Information Technology - Delhi
New Delhi-110020 (India)

September 2026

Sunlight to Signals: Solar Panel as an Optical Wireless Communication Receiver for Sustainable Communication Systems

Dissertation submitted to

Indraprastha Insititute of Information Technology-Delhi

in partial fulfillment of the requirements for the award of the degree of

Doctor of Philosophy

Submitted By

Rahul

Roll No: PhD19111

under the supervision of

Prof. Vivek Ashok Bohara

Professor, IIIT-Delhi

Prof. Anand Srivastava

Professor, IIIT-Delhi

Department of Electronics and Communication Engineering

Indraprastha Institute of Information Technology - Delhi

New Delhi-110020 (India)

September 2026

मातृ देवो भव ।
पितृ देवो भव ।
आचार्य देवो भव ।

With profound reverence and gratitude,
I dedicate this thesis to my beloved parent's and my respected teachers.
Their faith has been my foundation,
their values my compass,
and their affection my strength.

I also dedicate this work, with love and affection,
to my sister and my wife,
whose unwavering support, understanding, and patience
have illuminated my path through every challenge.

Indraprastha Institute of Information Technology-Delhi
Okhla Industrial Estate, Phase III
New Delhi-110020, India
September 2026

Certificate

This is to certify that the thesis titled **Sunlight to Signals: Solar Panel as an Optical Wireless Communication Receiver for Sustainable Communication Systems** being submitted by **Rahul** to the Indraprastha Institute of Informattion Technology-Delhi, for the award of the degree **Doctor of Philosophy**, is an original research work carried out by her under our supervision. In our opinion, the thesis has reached the standards fulfilling the requirements of the regulations relating to the degree. The results contained in this thesis have not been submitted in part or in full to any other university or institute for the award of any degree/diploma.

Prof. Vivek Ashok Bohara
Professor
Dept. of Electronics & Communication Eng.
IIIT Delhi, 110020

Prof. Anand Srivastava
Professor
Dept. of Electronics & Communication Eng.
IIIT Delhi, 110020

Place: New Delhi
Date: September 2026

Indraprastha Institute of Information Technology-Delhi
Okhla Industrial Estate, Phase III
New Delhi-110020, India
September 2026

Declaration

This is to certify that the dissertation entitled **Sunlight to Signals: Solar Panel as an Optical Wireless Communication Receiver for Sustainable Communication Systems** being submitted by **Rahul** to the **Indraprastha Institute of Information Technology-Delhi**, for the award of the degree of **Doctor of Philosophy**, is a bonafide work carried out by me. This research work has been carried out under the supervision of **Prof. Vivek Ashok Bohara and Prof. Anand Srivastava.**

The study pertains to this dissertation has not been submitted in part or in full, to any other University or Institution for the award of any other degree.

Rahul
PhD19111
ECE Department
IIIT-Delhi, India

Indraprastha Institute of Information Technology-Delhi
Okhla Industrial Estate, Phase III
New Delhi-110020, India
September 2026

Declaration Regarding Use of AI in Thesis

I acknowledge that I am fully responsible for the entire content of my thesis, including any sections assisted by online tools, including Artificial Intelligence-based tools. I accept full accountability for any violations of ethical standards in publications arising from the use of such tools.

Rahul
PhD19111
ECE Department
IIIT-Delhi, India

Acknowledgements

"Curiosity sets the journey in motion; perseverance shapes it into something significant."

— Author's reflection

This thesis reflects not only the outcome of my research efforts but also the collective guidance, encouragement, and support I received throughout my doctoral journey. What began as curiosity gradually transformed into learning, growth, and perseverance, made possible by the many individuals and institutions who believed in me, challenged my thinking, and stood by me at every stage.

I sincerely express my deepest gratitude to my supervisors, **Prof. Vivek Ashok Bohara** and **Prof. Anand Srivastava**, for their constant guidance, motivation, and unwavering belief in me throughout this journey. Their thoughtful feedback, patience, and high standards shaped not only this research but also my approach to problem-solving and independent thinking. They have been true role models, and it has been both a privilege and a dream come true to work under their mentorship.

I am deeply grateful to **Dr. Abhijit Mitra** for his constant presence, encouragement, and invaluable support. His ability to simplify complex problems into clear, structured steps helped me better understand challenges and approach them with confidence. His critical insights and broad perspective consistently encouraged me to look beyond technical details and appreciate the practical and market relevance of my work. I also thank **Mr. Deepak Solanki**, CEO of Velmenni R&D Pvt. Ltd., for his valuable guidance and industry-oriented insights, which helped bridge the gap between academic research and real-world product development.

I owe my deepest gratitude to my research colleague, my most honest critic, and my wife, Mrs. Akanksha Sneh, whose quiet strength and unwavering support sustained me throughout this journey. She helped me see what I could not recognize on my own, stood beside me during the most challenging moments, and supported me through long and demanding hours of coding.

Her presence brought calm during uncertainty, and this work reflects her patience and belief as much as my own efforts.

I would also like to thank my colleagues from the **Wirocomm Research Group** and the **CoE Li-Fi Lab** at IIIT-Delhi for their collaboration and encouragement. I sincerely acknowledge my seniors Dr. Anand Singh for teaching me the value of calmness, Dr. Rana Kumar Jana for instilling the importance of constructive critique, Dr. Akshita Gupta for her constant willingness to help, and Dr. Saumya Chaturvedi for her encouragement to keep moving forward. I also thank my colleagues Dr. Priyanka Singh, Dr. Neetu R. R., and Kainat Yasmeen for valuable discussions and continued motivation. I am grateful to my fellow researchers Saswati Paramita, Rehana Salam, Hanshita Prabhakar, Suhail Khan, Anant Agarwal, Gaurav Gupta, Anshu Kumar, Ebha Dipti Singh, Misbha Fatima, Sumit Kumar, and Ankit Kumar Pal for their enriching ideas, collaboration, and the positive research environment they fostered.

A special thanks to my thesis examination committee **Prof. Eiji Oki**, Kyoto University, **Prof. Moussa Ayyash**, Chicago State University, and **Prof. Swades De**, IIT-Delhi, for their thoughtful questions, constructive feedback, and insightful discussions during the defense.

I am deeply grateful to IIIT-Delhi for its excellent research environment, world-class infrastructure, and continuous support throughout my PhD journey. My sincere thanks to the Ph.D. and IRD administration, academic, IT, library, examination, administrative, facilities, housekeeping, and security teams for their invaluable support in making this journey comfortable and enriching.

Finally, this journey, shaped by the joy of learning, personal growth, and the courage to pursue meaningful aspirations, would not have been possible without the unconditional love, patience, and sacrifices of my parents, Mr. Dharampal and Mrs. Kusuma Devi, and my sister, Mrs. Malti Aggarwal.

ABSTRACT

The increasing adoption of intelligent transportation systems, smart cities, and energy-efficient wireless networks has further fueled the need for communication technologies that are not only high-speed and reliable but also sustainable and economical. Optical wireless communication (OWC) has been identified as a promising addition to existing radio frequency technologies because of its vast unregulated bandwidth, security features, and resistance to electromagnetic interference. However, the use of traditional optical receivers like photodiodes and avalanche photodiodes is accompanied by the need for separate power sources and is also prone to performance degradation due to high ambient light intensities, smaller receiver area, and the need for a complex optical design at the receiver to collect more energy, therefore increasing the system cost.

In recent years, solar panels have gained attention as promising alternatives to conventional optical receivers because they can harvest energy and receive data at the same time. Although photovoltaic devices are primarily designed for power generation, their large sensing area, tolerance to strong ambient light, and widespread availability make them appealing for use in sustainable optical wireless communication systems. However, the inherent electrical properties of commercial silicon solar panels—such as high junction capacitance, which results in limited bandwidth—create major obstacles for achieving high data rates. In addition, much of the existing research has been limited to custom-built photovoltaic devices, controlled laboratory

environments, or short-range indoor setups. As a result, the potential of commercially available solar panels for practical, real-world communication applications remains an unexplored research area.

This thesis explores the feasibility, design, and optimization of solar panels as optical receivers, with a main emphasis on the use of commercial silicon solar panels and light-emitting diode (LED) transmitters for reliable communication. This thesis systematically examines the communication performance of solar panel receivers, derives the bandwidth and sensitivity limits, and introduces new analog front-end designs to improve optical receiver communication performance.

The first part of this thesis presents an in-depth experimental study of silicon solar panels used as communication receivers under various optical and electrical conditions. The performance of solar panel receivers in terms of frequency response, time-domain response, received optical power sensitivity, and communication distance is examined. The effects of transmission distance, optical irradiance, modulation frequency, and ambient light on system performance are comprehensively explored. These experiments show that, although solar panels have very limited bandwidth, their performance can be greatly improved by proper analog signal processing.

To overcome these challenges, this thesis develops and experimentally validates new analog front-end receiver designs specifically optimized for commercial solar panels. The proposed architectures employ carefully engineered impedance matching, filtering, and amplification techniques to extend the usable communication bandwidth beyond the photovoltaic device's inherent electrical limitations. In contrast to earlier approaches based on reverse-biased operation or custom-fabricated receivers, the proposed solutions remain fully compatible with energy harvesting and are built entirely from off-the-shelf components, making them more practical for real-world deployment. Experimental evaluations show significant gains in both bandwidth and achievable data rates, enabling dependable optical communication with standard indoor LED sources under realistic operating conditions.

The thesis also investigates simultaneous light information and power transfer (SLIPT) using solar panel–based receivers, with particular attention to the trade-off between harvested energy and communication quality. By examining multiple operating points and receiver configurations, this work offers valuable insight into joint optimization strategies that balance power collection with data throughput. These findings support the development of self-powered or energy-assisted optical wireless systems aimed at low-power and sustainable communication applications.

In addition to the indoor environment, this thesis also encompasses the uncharted area of optical wireless communication in vehicular systems with solar-panel receivers. The vehicular system poses distinct challenges, including mobility issues, misalignment, limited orientation, and dead zones. The experimental work of this thesis explores these challenges and validates the use of solar panel receivers in vehicular communication systems, including vehicle-to-vehicle and vehicle-to-infrastructure communication. The discussion emphasizes the significant shortcomings of current receiver designs and the need for orientation-resilient, robust receivers in dynamic environments.

Overall, this thesis makes the following key contributions: (i) a comprehensive experimental characterization of commercial silicon solar panels as optical communication receivers, (ii) the design and validation of novel analog front-end circuits that significantly enhance communication bandwidth using off-the-shelf components, (iii) an in-depth investigation of SLIPT trade-offs in solar panel–based receivers, and (iv) an early exploration of vehicular optical wireless communication using solar panels, identifying open challenges and future research directions.

By bridging the gap between laboratory demonstrations and real-world deployment, this work establishes solar panels as viable, sustainable, and low-cost optical receivers, paving the way for their integration into future intelligent transportation systems and energy-efficient wireless networks.

Table of contents

List of figures

List of tables

Nomenclature

Abbreviations

6G	Sixth generation
AC	Alternating Current
ADC	Analog to Digital Converter
APD	Avalanche Photodiode
AWG	Arbitrary Waveform Generator
BEC	Bandwidth Enhancement Circuit
DAC	Digital-to-Analog Converter
DC	Direct Current
DSP	Digital Signal Processing
FOV	Field-of-View
FSO	Free-Space Optical
FV	Following Vehicle
IoT	Internet-of-Things

LC	Light Communication
LD	LASER Diode
LED	Light-Emitting Diodes
Li-Fi	Light Fidelity
LV	Leading Vehicle
OFDM	Orthogonal Frequency Division Multiplexing
OOK	On–Off Keying
OPV	Organic Photovoltaic
OWC	Optical Wireless Communication
PAM	Pulse-Amplitude Modulation
PHY	Physical Layer
PV	Photo-voltaic
QoS	Quality of Service
RF	Radio frequency
RTT	Round-Trip Time
Tx-AFE	Receiver Analog Front End
Si	Silicon
SLIPT	Simultaneous Light Information and Power Transfer
SNR	Signal-to-Noise Ratio
TIA	Trans-Impedance Amplifier

TIR	Total Internal Reflection
Tx-AFE	Transmitter Analog Front End
V2I	Vehicle-to-Infrastructure
V2V	Vehicle-to-Vehicle
VLC	Visible Light Communication

Chapter 1

Introduction

This chapter introduces the motivation and background of the research presented in this thesis. It provides an overview of optical wireless communication and highlights the limitations of conventional receiver technologies in energy-constrained and outdoor environments. The potential of solar panels as sustainable optical receivers capable of simultaneous energy harvesting and data reception is briefly discussed. Key challenges related to bandwidth, receiver design, and practical deployment are outlined. The chapter further motivates the need for improved analog front-end architectures using commercially available components. Finally, it presents the problem statement, summarizes the thesis's main contributions, and describes the dissertation's overall organization.

1.1 Motivation

The unprecedented growth in data traffic driven by bandwidth-hungry applications such as high-definition video streaming, extended and virtual reality, autonomous systems, and massive Internet-of-Things (IoT) deployments has exposed fundamental limitations of conventional radio frequency (RF) communication systems. Spectrum scarcity, escalating licensing costs, and increasing energy consumption have made it increasingly challenging to meet the performance and sustainability requirements of next-generation wireless networks. These challenges are further intensified by the emerging vision of 6G communication systems, which emphasizes ubiquitous connectivity, ultra-high data rates, low latency, and environmentally sustainable operation.

In response to these challenges, optical wireless communication (OWC) , and in particular visible light communication (VLC) , has gained significant attention as a complementary technology to RF communication systems. Operating in the unlicensed visible spectrum spanning 400–800 THz [1–3], VLC offers orders-of-magnitude higher available bandwidth compared to RF [3, 4], enabling multi-gigabit data rates without contributing to RF spectrum congestion. The highly directional nature of optical links results in low co-channel interference and enhanced spatial reuse, making VLC especially suitable for dense indoor environments and last-mile access scenarios. These advantages have led to strong academic and industrial interest, culminating in the standardization of light communication technologies under IEEE 802.15.7 [5] and IEEE 802.11bb [6], thereby reinforcing light communication's (LC) potential as a mainstream wireless access technology.
A key enabler of LC is the widespread deployment of light-emitting diodes (LEDs) for illumination. Modern white LEDs, realized through phosphor-coated blue chips or Red-Green-Blue combinations, offer high energy efficiency, long operational lifetimes, and the ability to support data rates approaching 1 Gbps under controlled conditions [7–10]. The dual use of LEDs for both lighting and communication [11–13] significantly reduces infrastructure costs and enhances energy efficiency, aligning VLC with sustainable networking goals [14–18]. However, while transmitter technologies have matured rapidly, the receiver side of LC systems remains a critical bottleneck.

Conventional LC receivers predominantly employ PIN photodiodes or avalanche photodiodes (APDs) owing to their high-speed response and linear detection characteristics [19–23]. Although their practical deployment is constrained by several inherent limitations. The need for an external electrical bias increases power consumption and system complexity, particularly in energy-constrained or remote scenarios. In addition, the small active area of photodiodes renders LC links highly sensitive to alignment and orientation errors, where even slight misalignment between the transmitter and receiver can lead to significant signal degradation, reduced signal-to-noise ratio, and compromised quality of service (QoS). Addressing these challenges often requires optical concentrators and precise alignment mechanisms, which further increase system cost and hinder scalability.

These limitations motivate the exploration of alternative optical receivers that can enhance link robustness while reducing energy consumption and system complexity. In this regard, solar panels have emerged as a compelling candidate for light communication. Owing to their large photosensitive area, solar panels significantly relax alignment constraints and improve tolerance to receiver orientation and mobility. More importantly, solar panels inherently enable simultaneous optical communication and energy harvesting, allowing the received optical power to be partially converted into electrical energy that can power the receiver circuitry itself. This dual functionality offers a pathway toward energy self-sufficient and green communication systems, which are key requirements for future wireless networks.

The primary objective of this work is to demonstrate that a commercially available solar panel can serve as a practical and reliable optical wireless communication receiver. This approach reduces system cost and power consumption while enabling scalable LC deployment across diverse applications, including rural connectivity, smart cities, and intelligent transportation systems, thereby supporting the development of sustainable and resilient 6G communication networks.

1.2 Light Communication Background

The origins of optical communication can be traced back to early visual signaling methods such as beacon fires, semaphore systems, and mirror-based heliographs. A major scientific milestone was achieved in 1880 when Alexander Graham Bell demonstrated the photophone, enabling wireless voice transmission using modulated sunlight, as shown in Fig. 1.1 [24]. This invention

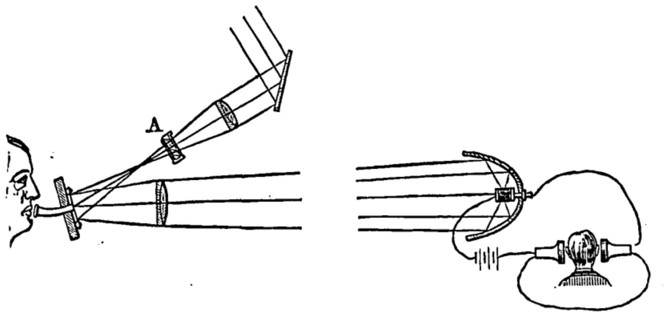

Figure 1.1: Sound by light

is widely regarded as the conceptual foundation of modern optical wireless communication [25]. The field progressed significantly following the invention of the laser in the 1960s, which enabled stable, coherent, and high-intensity optical beams. This advancement led to the development of Free-Space Optical (FSO) communication systems for terrestrial, airborne, and deep-space links [26–31]. Further progress in semiconductor optoelectronics during the 1990s facilitated the deployment of infrared optical links, while the early 2000s marked a major breakthrough with the emergence of VLC. In VLC, solid-state light sources such as LEDs enable simultaneous illumination and data transmission [32–35]. This evolution culminated in the introduction of Li-Fi (Light Fidelity) as a high-speed light-based networking paradigm, followed by international standardization efforts such as IEEE 802.15.7 and ITU-T initiatives, establishing OWC as a practical component of next-generation wireless systems [5, 6, 36].

Figure 1.2 illustrates the electromagnetic spectrum, highlighting the position of OWC within the infrared, visible, and ultraviolet bands [25]. Unlike conventional RF systems operating in the congested and tightly regulated kHz-GHz spectrum, OWC exploits optical frequencies spanning hundreds of terahertz, offering orders-of-magnitude larger bandwidth. This vast spectral availability enables ultra-high data rates, increased user capacity, and low-latency communication, as predicted by Shannon's capacity limits. Moreover, the optical spectrum is globally unlicensed, eliminating spectrum licensing costs and regulatory constraints associated with RF systems. The visible light band uniquely supports dual functionality by enabling

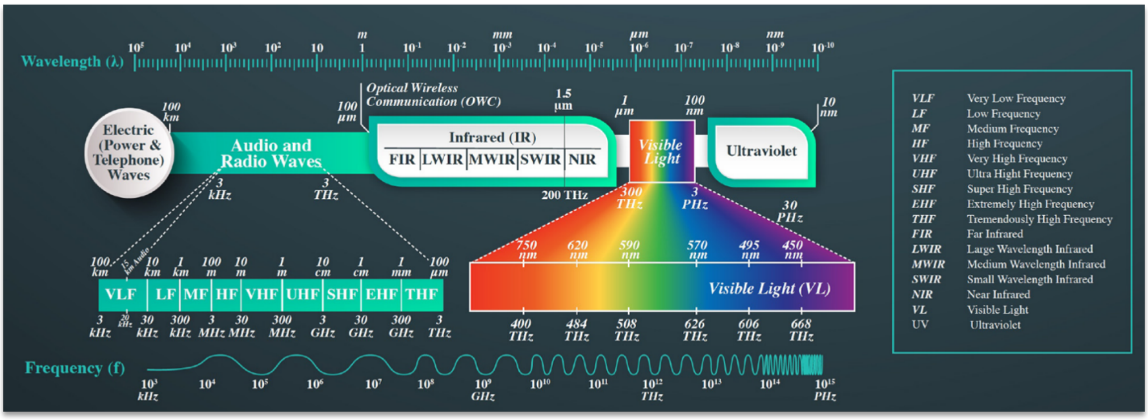

Figure 1.2: Electromagnetic spectrum highlighting the optical bands

both illumination and communication via existing LED infrastructure, while the infrared and ultraviolet bands facilitate highly directional, interference-free links.

1.3 Light Communication Architecture

An end-to-end OWC system that transmits Ethernet data from a server to a remote client using an optical link is shown in Fig. 1.3. The system consists of digital baseband processing, transmitter analog front end (Tx-AFE), optical wireless channel, receiver analog front end (Rx-AFE), and digital signal processing at the receiver.

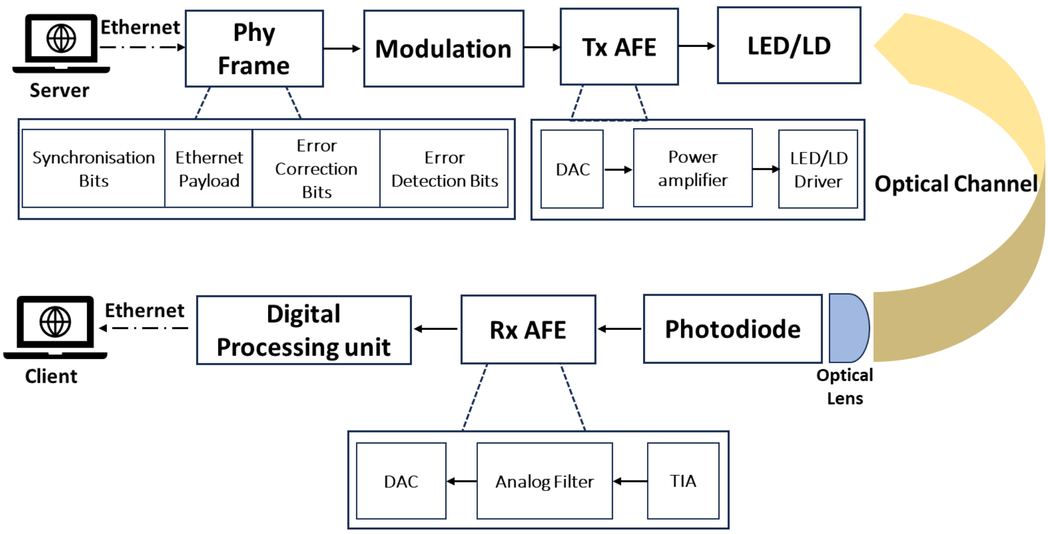

Figure 1.3: Block diagram of optical wireless communication system

1.3.1 Digital Baseband and PHY Frame

An Ethernet-connected server generates a binary data stream that is encapsulated into physical layer (PHY) frames comprising synchronization, payload, and error-correction/detection fields, where the synchronization enables reliable frame detection and timing recovery, the payload conveys user information, and the redundancy enhances robustness to channel impairments. The resulting framed bitstream is then mapped onto a non-negative baseband waveform using intensity-modulation–compatible schemes such as on–off keying (OOK), pulse-amplitude modulation (PAM), or orthogonal frequency division multiplexing (OFDM), ensuring suitability for optical intensity transmission.

1.3.2 Transmitter Analog Front End

The digitally modulated samples are converted into an analog waveform by a digital-to-analog converter (DAC) and then amplified before being applied to an LED or laser diode (LD) driver. The optical source is biased to operate within its linear region, i.e., between the turn-on threshold and saturation, ensuring a linear relationship between the emitted optical power and the injected current while avoiding nonlinear distortion, and clipping at higher modulation schemes [37, 38]. Under proper biasing, the transmitted optical power can be expressed as

$$P_t(t) = P_{\mathrm{DC}} + \eta\, i(t), \tag{1.1}$$

where P_{DC} denotes the optical power due to the DC bias, η is the electro–optical conversion efficiency, and $i(t)$ represents the modulating electrical current. Accordingly, the Tx-AFE is designed to provide stable biasing and linear current control, enabling faithful conversion of the digitally modulated waveform into a high-quality optical signal for reliable, high-data-rate optical wireless communication.

1.3.3 Optical Wireless Channel

The modulated optical signal propagates through a free-space optical channel between the transmitter and the receiver. The channel introduces impairments such as path loss, ambient light interference, shot noise, shadowing, and misalignment. The received optical power can be expressed as

$$P_r = H(0)P_t, \tag{1.2}$$

where P_t is the transmitted optical power and $H(0)$ denotes the channel DC gain, which depends on the transmitter radiation pattern, propagation distance, and receiver aperture. The channel DC gain is given by [39]:

$$H(0) = \begin{cases} (m+1)\frac{A_r}{2\pi D_d^2}\cos^m(\phi)T_s(\psi)g(\psi)\tau(D_d)\cos(\psi), & 0 \leq \psi \leq \psi_c \\ \\ 0, & \psi \geq \psi_c \end{cases} \tag{1.3}$$

where the absorption and scattering of light through the atmosphere are figured by $\tau(D_d)$, the transmittance at the distance D_d from the transmitter. ϕ is the irradiance angle, ψ is the incidence angle, ψ_c is the critical incident angle, m is the lambertian order. A_r is the detector's physical area of the photodiode, $T_s(\psi)$ is the filter transmission in the receiver.

An idealized non-imaging concentrator having an internal refractive index of n achieves a gain

$$g(\psi) = \begin{cases} \frac{n^2}{\sin^2\psi_c}, & 0 \leq \psi \leq \psi_c \\ \\ 0, & \psi > \psi_c \end{cases} \tag{1.4}$$

The order m is related to $\phi_{1/2}$ by

$$m = -\frac{\ln 2}{\ln \cos \phi_{1/2}}. \tag{1.5}$$

1.3.4 Receiver Analog Front End

At the receiver, the incident optical signal is collected by an optical lens that enlarges the effective aperture and focuses the light onto the photodiode's active area, thereby improving optical gain and enhancing the received signal-to-noise ratio (SNR). The photodiode converts the received optical power into an electrical current via the photoelectric effect, with the generated photocurrent proportional to the incident light intensity. Since the photodiode output current is typically weak, it is amplified and converted into a voltage by a trans-impedance amplifier (TIA). The TIA plays a pivotal role in the receiver front end, as its gain, bandwidth, and noise performance directly impact receiver sensitivity and dynamic range, particularly in high-speed optical wireless systems that demand wide bandwidth and low input-referred noise. The amplified signal is subsequently passed through an analog filter to suppress out-of-band components, including high-frequency thermal noise and low-frequency ambient-light variations, and to mitigate aliasing prior to digitization. The conditioned signal is then sampled and quantized by an analog-to-digital converter (ADC), whose sampling rate and resolution are chosen to capture the signal bandwidth and dynamic range accurately. The resulting digital samples are finally processed by the digital signal processing (DSP) unit for synchronization, demodulation, channel equalization, and decoding.

1.3.5 Digital Signal Processing and Data Recovery

The digitized signal is processed to perform synchronization, channel equalization, demodulation, and error-correction decoding. The synchronization bits are used to align the receiver clock and identify frame boundaries. After decoding, the recovered payload data is delivered to the client device through an Ethernet interface.

1.4 Research Contribution

To overcome the limitations of conventional optical wireless communication (OWC) systems and enable practical real-world deployment, it is necessary to address the fundamental challenges faced by optical receivers. First and foremost, optical receivers operating in ambient light face the challenge of strong ambient light, resulting in high shot noise. Second, the smaller size of photodetectors often leads to receiver misalignment or signal power loss. The PD also requires external power to operate, thereby increasing the receiver's power consumption. The above-mentioned challenges often require specialized optical arrangements, multiple receiver units, complex front-end circuitry, and high power consumption, which significantly increase system cost and complexity. These requirements severely limit the scalability and large-scale deployment of conventional OWC systems, particularly in remote areas, mobile environments, vehicular scenarios, and outdoor applications.

To address these limitations, this thesis proposes using a *solar panel as an optical wireless communication receiver*. A solar panel inherently converts incident optical intensity into an electrical signal, utilizing ambient light to harvest energy, thereby enabling a unified platform for both communication and power delivery. Unlike conventional photodiode-based receivers, solar panels possess a large photosensitive area, high optical power handling capability, and inherent tolerance to strong ambient illumination. These properties enable solar-panel-based receivers to naturally overcome several critical OWC challenges, including saturation in bright light, limited field of view, shadowing, and high receiver cost, making them particularly attractive for outdoor, vehicular, and large-scale deployments. However, solar panels are not originally designed for high-speed communication and pose their own challenges, including limited electrical bandwidth due to large junction capacitance, weak signal conversion in the presence of strong DC photocurrent, low frequency response, and a trade-off between energy harvesting and information decoding. Overcoming these limitations requires specialized circuit design, signal extraction techniques, and system-level optimization.

The major research contributions of this work include the design, modeling, and experimental validation of solar panel-based optical receivers for robust OWC systems. This thesis systematically addresses the fundamental limitations of conventional optical wireless receivers through the following major contributions:

- An experimental framework is developed to validate the feasibility of solar panels as optical wireless communication receivers. A dedicated bandwidth enhancement circuit (BEC) (Design 1) is proposed to overcome the intrinsic low-pass response of solar panels caused by their large junction capacitance. Using a white LED transmitter in an indoor testbed, this study demonstrates that solar panels can reliably detect intensity-modulated optical signals, thereby establishing their viability as practical communication receivers.

  – ***Rahul****, A. Mitra, A. Srivastava, V. A. Bohara, and D. Solanki, "Experimental Validation of Optical Wireless Receiver using Solar Panel with Bandwidth Enhancement Circuit," 2022 IEEE 95th Vehicular Technology Conference (VTC2022-Spring), Helsinki, Finland, 2022, pp. 1–6, doi:10.1109/VTC2022-Spring54318.2022.9860765.*

- An enhanced receiver architecture bandwidth enhancement circuit (Design 2) is introduced to significantly improve both bandwidth and sensitivity, enabling extended-range in indoor visible light communication using solar panels. In addition, the optical transmitter is optimized by incorporating a total internal reflection (TIR) lens on the LED to improve beam collimation and increase the achievable communication distance.

  – ***Rahul****, A. Srivastava, V. A. Bohara, D. Solanki, and A. Mitra, "Demonstration of Broad-band Data Link over off-the-shelf Solar Module with White LED,"* Journal of Lightwave Technology*, 2025, doi:10.1109/JLT.2025.3541831.*

  –***Rahul****, V. A. Bohara, A. Mitra, D. Solanki, and A. Srivastava, "Sunlight to Signals:*

Solar Panel as Active Data Receiver," 17th International Conference on COMmunication Systems and NETworks (COMSNETS), Bengaluru, India, 2025, pp. 1359–1361, doi:10.1109/COMSNETS63942.2025.10885740.

- A simultaneous light information and power transfer (SLIPT) framework is developed in which the solar panel and BEC (Design 3) simultaneously harvest optical energy and decode communication signals. This contribution jointly optimizes energy harvesting and data reception, demonstrating the potential of solar-panel-based receivers for energy-autonomous optical wireless systems.

  – ***Rahul**, V. A. Bohara, A. Mitra, D. Solanki and A. Srivastava, "Experimental Validation of Simultaneous Power and Data Transfer over Solar Panels for 5G and Future Network," 2024 IEEE Future Networks World Forum (FNWF), Dubai, United Arab Emirates, 2024, pp. 867-872, doi: 10.1109/FNWF63303. 2024. 11028868.*

- A comprehensive comparative evaluation of multiple solar panel configurations is conducted to reflect practical, real-world deployment scenarios. The impact of different panel arrangements on bandwidth, sensitivity, signal characteristics, and communication reliability is quantified, providing important design guidelines for scalable solar-panel-based optical wireless systems.

  – ***Rahul**, A. Mitra, V. A. Bohara, A. Srivastava and D. Solanki, "Leveraging Solar Panels for Light Communication: Analyzing the Role of Configuration in Signal Reception," 2025 IEEE 26th International Conference on High Performance Switching and Routing (HPSR), Suita, Osaka, Japan, 2025, pp. 1-3, doi: 10.1109/ HPSR64165. 2025. 11038895.*

  – ***Rahul**, A. K. Pal, P. Aggarwal, V. A. Bohara, and A. Mitra, "Modeling and Measurement of Communication Characteristics in Parallel-Configured Solar Panel Optical Receivers,"* IEEE Transactions on Circuits and Systems*, 2026.(Under Review)*

- The proposed receiver architecture is further adapted for outdoor operation by incorporating ambient-light suppression techniques that ensure reliable performance under intense sunlight conditions. Infrared LEDs are used as optical transmitters to improve energy efficiency, and experimental validation demonstrates that the solar-panel-based receiver successfully alleviates dead-zone issues as well as sensitivity to orientation, misalignment, and partial shading.

  *– **Rahul**, A. Mitra, A. Srivastava, V. A. Bohara, and D. Solanki, "Solar Module as a High-Speed Data Receiver with Ambient Light Suppression in an Outdoor Scenario,"* Optics Letters*, 2025, doi:10.1364/OL.545006.*

  *– **Rahul**, V. A. Bohara, A. Srivastava, D. Solanki, and A. Mitra, "Dead Zone Mitigation in Vehicular Platoon via Solar Panel as a Communication Receiver,"* IEEE Transactions on Intelligent Transportation Systems*, 2025, doi:10.1109/TITS.2025.3627293.*

1.5 Other Contributions

Apart from the main contribution mentioned above, the author of this thesis has also contributed to the following publications.

1. **Rahul**, S. Chaturvedi, A. Srivastava, V. A. Bohara and A. Mitra, "Energy Management Strategy for Drone-Based Optical Wireless Communication Network," in *Physical Communication*, vol. 76, p. 103075, 2026, doi: 10.1016/j.phycom.2026.103075.

2. D. Solanki, **Rahul**, A. Mitra, A. Srivastava and V. A. Bohara, " Long Range High Speed Optical Wireless Communication Link", submitted to *Optics Letters*, 2026.

3. A. K. Pal, **Rahul**, V. A. Bohara, and A. Mitra, "Toward Low-Power Free-Space Optical Communication over Solar Panel," *Proc. of 19th IEEE ANTS*, Delhi, India, 2025.

4. A. K. Pal, **Rahul**, A. Mitra, and V. A. Bohara, "Mirror-Assisted Non-Line-of-Sight Voice Communication Over Solar Panels as Receivers for Long-Range Low-Power Links," *18th*

International Conference on COMmunication Systems and NETworks (COMSNETS), Bengaluru, India, 2026.

5. Naman Singhal, A. K. Pal, **Rahul**, V. A. Bohara, and A. Mitra, "A Graphical User Interface Driven Method for Static and Dynamic Parameter Extraction of Solar Panels for Optical Communication," *18th International Conference on COMmunication Systems and NETworks (COMSNETS)*, Bengaluru, India, 2026.

1.6 Thesis Organization

The primary objective of this dissertation is to establish commercially available solar panels as practical optical wireless communication receivers. The research progresses systematically from establishing the fundamental feasibility of solar-panel-based communication, followed by bandwidth enhancement, simultaneous information and power transfer, comparative analysis of different photovoltaic configurations, and finally outdoor and vehicular communication scenarios. Accordingly, Fig. 1.4 illustrates the complete research roadmap. The figure summarizes

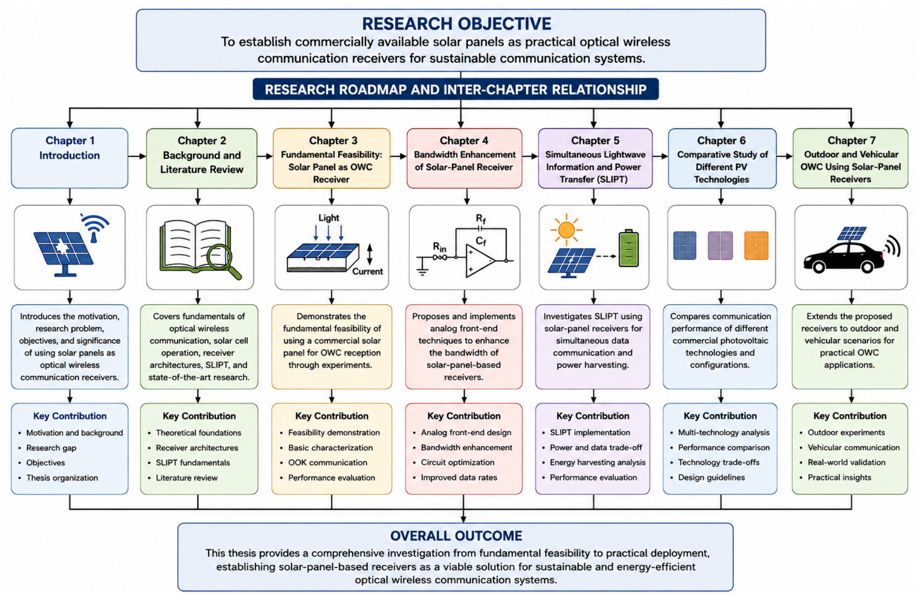

Figure 1.4: Research roadmap illustrating the technical flow and inter-chapter relationships of the dissertation.

how each chapter contributes to the overall research objective and demonstrates the logical evolution of the work from fundamental receiver characterization to practical deployment scenarios. Chapter 2 reviews the existing literature on optical wireless communication systems, with emphasis on receiver technologies and their limitations. Chapter 3 presents the experimental validation of solar panels as optical wireless receivers using a bandwidth-enhanced indoor VLC testbed. Chapter 4 introduces an enhanced receiver and transmitter architecture to extend indoor communication range and performance. Chapter 5 develops an SLIPT framework using solar panels. Chapter 6 provides a comparative evaluation of different solar panel configurations and their impact on communication performance. Chapter 7 extends the proposed system to outdoor environments with ambient-light suppression and infrared-based transmission. Finally, Chapter 8 concludes the thesis and outlines future research directions.

- Appendix **A** lists the publications resulting from this dissertation.
- **References** provides the complete list of cited works.

Chapter 2

Background and Related Work

This chapter provides the essential theoretical foundations and technical background necessary to contextualize the research contributions of this thesis. It reviews the core principles of optical wireless communication, with particular emphasis on optical receiver architectures and the emerging paradigm of employing solar panels as optical receivers. Furthermore, the chapter discusses key aspects of analog front-end design, simultaneous light information and power transfer, and vehicular optical wireless communication, collectively establishing the groundwork for the proposed research.

2.1 Rationale and Necessity of Solar Panel–Based Optical Receivers

OWC consists of multiple building blocks as illustrated in Fig. 2.1. At higher layers, including medium access control, interference mitigation, mobility support, and networking protocols, many concepts are analogous to those in RF systems. However, the unique propagation characteristics of optical channels, such as strong directionality, susceptibility to blockage, and sensitivity to ambient light, necessitate fundamentally different design approaches.

Importantly, the effectiveness of higher-layer solutions is intrinsically dependent on the

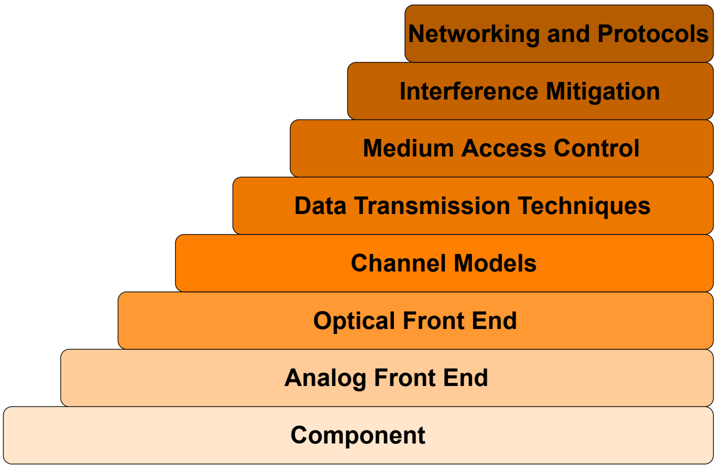

Figure 2.1: Building blocks of OWC network

lower-layer foundations, namely accurate channel models, efficient optical front-end systems, analog front-end, and the underlying optical devices and components. Among these, optical devices and components are particularly critical, as they directly determine key system-level parameters such as peak data rates, achievable link distance, and energy efficiency.
In this context, the receiver plays a pivotal role in enabling reliable and high-performance OWC systems across diverse application domains. While advances in optical transmitters and modulation techniques continue to enhance system capabilities, the ultimate performance is often limited by the receiver's ability to efficiently convert optical signals into electrical signals in the presence of ambient light interference, mobility, and hardware constraints. Consequently, the system-level design and optimization of optical receivers, optical front-end circuits, analog front-end, and signal processing techniques form the cornerstone of scalable and robust OWC systems, directly aligning with the layered architecture and domain diversity.

Optical receivers are a fundamental building block of OWC systems, converting the received optical signal into a usable electrical representation for subsequent processing and decoding. Unlike RF receivers, optical receivers must operate under stringent constraints imposed by the physical properties of light, such as unidirectional propagation, susceptibility to blockage, and strong dependence on environmental illumination. The comparison of conventional optical

Table 2.1: Comparison of conventional optical receivers based on PIN photodiodes and avalanche photodiodes (APDs).

Parameter	PIN Photodiode	Avalanche Photodiode (APD)	Refs.
Operating principle	Incident photons absorbed in the intrinsic region generate electron–hole pairs, which drift under a small reverse bias. No internal gain ($M = 1$).	Operates near reverse breakdown where photogenerated carriers undergo impact ionization, providing avalanche gain ($M \approx$ 10–100).	[40–42]
Receiver sensitivity	Lower sensitivity; thermal noise dominates at low received optical power.	Typically, 5–10 dB better sensitivity due to internal gain, although avalanche excess noise limits performance.	[40, 42]
Bandwidth	Very high; limited by carrier transit time and junction capacitance.	High but limited by the gain–bandwidth product.	[40, 42]
Active area	Typically below 1 mm^2; increasing the area increases capacitance and reduces bandwidth.	Generally smaller than PIN photodiodes to preserve gain uniformity and speed.	[43, 44]
Alignment/FOV	Requires accurate alignment or optical concentrators because of the small active area.	Requires similar or stricter alignment owing to the smaller active area.	[43, 44]
Ambient-light tolerance	Ambient light introduces shot noise and may saturate the receiver.	Lower tolerance because background-induced shot noise is also multiplied.	[43]
Power consumption	Low reverse bias (typically ≤ 5 V).	Requires high reverse bias (tens to hundreds of volts) with temperature compensation.	[41, 42]
Receiver complexity	Simple receiver consisting mainly of a photodiode and TIA.	Requires high-voltage bias, gain control, and temperature-compensation circuitry.	[41, 42]
Cost	Low.	Higher owing to the device and associated circuitry.	[40, 41]
Dominant noise	Thermal noise.	Avalanche excess noise and thermal noise.	[40, 42]

receivers based on PIN photodiodes and avalanche photodiodes (APDs) is presented in the Table 2.1.

Despite significant progress, the design of optical receivers faces several critical challenges. Solar panels, as optical receivers, can mitigate most challenges and contribute to sustainable, eco-friendly, and ubiquitous communication design. The comparison of conventional optical receivers based on PIN photodiodes and avalanche photodiodes (APDs) with a solar panel as an optical receiver are presented in the Table 2.2.

Table 2.2: Comparison of conventional photodiode (PIN/APD) receivers and solar-panel-based receivers.

Criterion	**Conventional PIN/APD Receivers**	**Solar-Panel-Based Receivers**	**Refs.**
Primary function	Detection only; requires external electrical power.	Simultaneous light detection and energy harvesting (SLIPT); self-powered operation is possible.	[45, 46]
Sensitivity/data rate	High sensitivity and capable of multi-Gb/s communication.	Limited bandwidth (typically kHz to tens of MHz) due to large junction capacitance. Demonstrated data rates include 11.84 Mb/s using OFDM with a Si solar panel, 17.05 Mb/s using DMT with self-reverse biasing, and up to 0.5 Gb/s using a GaAs photovoltaic cell.	[46–48]
Active area / FOV	Small active area with a relatively narrow field of view (FOV); often requires concentrating optics.	Large active area (cm^2 to m^2) providing a wide FOV; lens-free reception is feasible.	[44, 49]
Alignment requirement	Requires accurate pointing, acquisition, and tracking.	Relaxed alignment due to the large aperture; more tolerant to mobility, misalignment, and atmospheric/oceanic turbulence.	[44, 49]
Ambient light	Acts as an interference source, increasing shot noise; optical filtering is generally required.	Ambient and solar illumination can be harvested as useful energy while simultaneously supporting optical communication.	[44, 45]
Power consumption	Requires reverse-bias circuitry and receiver electronics; APD receivers additionally require high-voltage bias.	Can operate in photovoltaic mode without external bias, enabling energy-neutral or energy-positive operation.	[45, 47, 50]
Receiver complexity	Requires photodiode, TIA, bias circuitry, and optical components; APD receivers additionally require gain control and temperature compensation.	Relatively simple architecture using passive separation of DC (energy harvesting) and AC (communication) components, without high-voltage circuitry.	[47, 48]
Cost	Moderate for PIN receivers and relatively high for APD receivers.	Low cost because commercially available solar panels can be directly employed as optical receivers.	[44, 47]
Best-fit applications	High-speed indoor VLC/LiFi, optical fiber communication, and long-range free-space optical (FSO) links.	Energy-autonomous IoT devices, remote and rural optical backhaul, underwater optical wireless communication (UOWC), satellite–air–ground–ocean integrated networks, and vehicular VLC.	[44, 46, 47, 49]

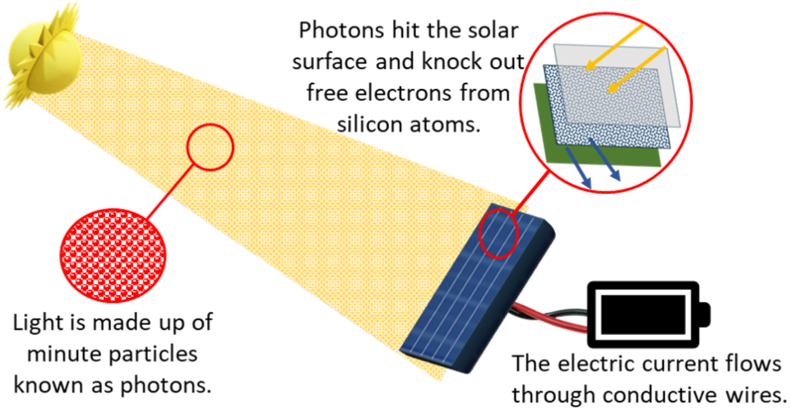

Figure 2.2: Illustration of the photovoltaic effect and operating principle of a solar panel.

2.2 Solar Panels as Optical Receivers

Solar panels are a cornerstone of renewable energy technologies, enabling the conversion of optical radiation into electrical energy through the photovoltaic (PV) effect, as shown in Fig.2.2. Continuous advancements in PV technology have led to significant improvements in efficiency, durability, and cost-effectiveness, resulting in widespread deployment of solar panels across diverse applications. Various solar panel technologies exist, including monocrystalline, polycrystalline, thin-film, perovskite, organic, and bifacial structures, each offering distinct performance characteristics. Fundamentally, solar panels operate by absorbing incident light within semiconductor materials—typically silicon—where photon absorption generates electron–hole pairs and produces an electrical current. Importantly, solar panels respond not only to natural sunlight but also to artificial light sources. This inherent photo-responsivity allows solar panels to detect variations in incident optical intensity, thereby extending their functionality beyond energy harvesting. As a result, solar panels can be repurposed as optical receivers capable of supporting optical wireless communication, enabling a unified platform for simultaneous energy harvesting and information reception.

2.2.1 Communication Receivers Using Silicon Solar Panels

Early studies established the feasibility of employing commercial silicon (Si) solar cells as optical receivers for OWC systems. These works demonstrated that PV panels can detect modulated optical signals.

Kim and Won [51] first introduced the concept of using a Si solar cell as a VLC receiver in 2013. Using a white LED transmitter and a commercial Si solar panel, they demonstrated a data rate of 3 kb/s over a distance of 40 cm. The achievable data rate was primarily limited by the solar cell's low intrinsic electrical bandwidth (approximately 10 kHz), yet this work laid the foundation for solar panel-based optical receivers. The feasibility of Si solar panels for VLC was further demonstrated in application-oriented scenarios. In [52], a solar panel-based VLC receiver was employed in a pipe inspection system to extend the lifetime of sensing nodes. Experimental results showed reliable communication in both air and water, with bit error rates of 0.27% and 0.34%, respectively, over a 1-m link. In [53], an indoor positioning system using a solar panel receiver was experimentally validated. At a transmission distance of 2 m and an illumination level of approximately 300 lux, a data rate of 2 kb/s was achieved using OOK. Noise resilience using solar panels was investigated in [54], where a VLC receiver architecture exploited the inherent properties of solar panels to suppress ambient light noise caused by indirect sunlight and artificial lighting. The system operated at a modulation frequency of 5.78 kHz over a 40 cm link. Bandwidth enhancement techniques for Si solar panel receivers have also been explored. In [55], a parallel resistance loading approach increased the bandwidth from 70 kHz to 130 kHz, albeit at the cost of a significant magnitude response degradation of approximately 18.37 dB. Comparative studies in [56] evaluated photovoltaic modules and APDs under high ambient light conditions. The results showed that solar panels maintained reliable communication under sunlight intensities up to 800 W/m^2, whereas APDs saturated beyond 200 W/m^2. The impact of detector type on transmission distance and angular coverage was studied in [57], where PIN photodiodes, 1 V solar panels, and 5.5 V solar panels were compared for OWC performance.

2.2.2 Simultaneous Communication and Energy Harvesting with Silicon Solar Panels

SLIPT enables concurrent data reception and energy harvesting from the same optical signal. In solar panel-based SLIPT systems, receiver design must balance harvested power and achievable communication bandwidth.

In [50], a polycrystalline Si solar panel combined with an external low-pass filter and amplifier was used to demonstrate OFDM-based optical communication in an indoor environment. A data rate of 7.01 Mb/s was achieved over a short distance of 39 cm and 2.1 mW of power harvested. Das *et al.* [58] demonstrated bidirectional OWC using off-the-shelf lasers and Si solar panels, achieving data rates up to 8 Mb/s over a 30-m free-space link while harvesting up to 5 W of optical power. Subsequent studies focused on bandwidth enhancement. Passive equalization techniques in [47] extended the -3 dB bandwidth to approximately 300–500 kHz, but significantly reduced the receiver magnitude response. In [48], reverse-biasing the solar panel improved the bandwidth from 90 kHz to 120 kHz, although the communication distance was limited to 10 cm. A practical SLIPT implementation was demonstrated in [59], where a 940-nm laser transmitter enabled simultaneous communication and energy harvesting. The system achieved a peak throughput of 28.3 Mb/s while harvesting up to 4.5 W using maximum power point tracking (MPPT), with the harvested energy stored in a 38 Wh lithium-ion battery.

2.2.3 Material-Dependent Solar Panel Optical Receivers

Beyond silicon-based devices, alternative photovoltaic materials have been explored to overcome bandwidth and efficiency limitations. Monocrystalline silicon, thin-film (CdTe, CIGS, a-Si), III–V (GaAs), perovskite, and organic PV (OPV), framed around the four physical parameters that couple PV material choice to communication capability:

1. **Junction capacitance / RC bandwidth** — sets the 3-dB electrical bandwidth of the cell acting as a receiver or as a power source feeding a switching regulator.

2. **Spectral responsivity/bandgap** — determines quantum efficiency at the transmitter's wavelength and hence achievable SNR.

3. **Series/shunt resistance and dark current** — governs noise floor, fill-factor degradation, and nonlinear distortion at high modulation frequencies.

4. **Temperature coefficient of power (γ, %/°C)** — governs long-term link-budget stability under thermal drift, relevant to duty-cycled or continuously transmitting nodes.

Monocrystalline Silicon (mono-Si) Mono-Si has a single continuous lattice with far fewer grain-boundary recombination centers than polycrystalline material, giving lower series resistance and higher shunt resistance. This translates into a cleaner *I–V* knee and a lower thermal-noise contribution. Commercial mono-Si efficiencies sit around 22–24%, versus lower figures for multicrystalline material, and mono-Si is the substrate used in most high-speed solar-cell-as-receiver demonstrations, including an OFDM-based visible-light communication (VLC) link achieving 11.84 Mbps at a bit error rate (BER) of 1.6×10^{-3} using a standard solar panel as the receiver [60]. The larger single-crystal grains reduce trap-state density that would otherwise slow carrier extraction, so mono-Si generally supports a wider communication bandwidth than poly-Si at comparable cell area and thickness.

Thin-Film: CdTe and CIGS CdTe and CIGS are direct-bandgap compound semiconductors that are strong absorbers, allowing very thin active layers — a CdTe layer is roughly 8 μm thick and a CIGS layer roughly 2 μm, both deposited on glass via co-evaporation or MOCVD with monolithic module integration [61]. The thinner intrinsic region reduces junction capacitance per unit area relative to bulk silicon, favorable for bandwidth, but this is offset by higher series resistance from the polycrystalline compound structure and back-contact interfaces, which raises the RC time constant and can dominate over the capacitance benefit. Thin-film modules use roughly 1% of the semiconductor material required for crystalline silicon and exhibit lower temperature coefficients, meaning they lose less output in hot climates — beneficial for link power stability in thermally variable outdoor deployments [62]. CIGS additionally offers mechanical flexibility for building-integrated applications, though it has struggled to reach manufacturing scale [62]. Because CdTe/CIGS efficiency (approximately 22.1% and 23.4%, respectively) trails mono-Si [63], the effective received SNR for a given illuminance is correspondingly lower unless compensated by a larger active area.

Amorphous Silicon (a-Si) a-Si has a wider, tunable optical bandgap and a much higher defect-state density (dangling bonds) than crystalline silicon, giving it comparatively poor carrier mobility and pronounced Staebler–Wronski light-induced degradation. Its efficiency is markedly lower, around 14.0% [63], and the higher trap density increases carrier transit time, lowering usable modulation bandwidth relative to both mono-Si and CdTe/CIGS. a-Si remains relevant mainly for low-rate, low-power indoor or building-integrated PV (BIPV) nodes rather than for high-throughput links. Amorphous silicon thin-film solar cells were explored in [64] for ultra-low-power wake-up receivers. The system achieved wake-up distances of up to 14 m without interference and supported a maximum data rate of 1.12 kb/s.

III–V (GaAs and Multijunction) GaAs and related III–V cells have the highest carrier mobility and radiative recombination efficiency of any PV material system, and correspondingly the best-documented high-speed performance as simultaneous power/data receivers. This material system underlies the highest-bandwidth solar-cell communication links reported to date, including a 0.5 Gb/s OFDM-based laser data-and-power transfer link [46] and a subsequent 1 Gb/s GaAs VCSEL/photovoltaic link [65]. GaAs also has the best thermal stability of the group, with a temperature coefficient of approximately 0.09%/°C, surpassing every thin-film and perovskite alternative [63], making it the material of choice where both bandwidth and thermal robustness matter — at the cost of very high fabrication cost, which is why GaAs is generally reserved for space and concentrator-PV applications rather than terrestrial IoT deployment. In 2018, Fakidis *et al.* demonstrated a high-speed optical wireless link using a single-junction GaAs solar cell [66]. A data rate of 0.5 Gb/s was achieved over a 2-m OFDM-based laser link, with a -3 dB bandwidth of 24.5 MHz and a power conversion efficiency of approximately 42%.

Perovskite Perovskite solar cells (typically ABX_3 halide structures) combine a tunable, high-absorption-coefficient bandgap with solution-processable thin films, giving efficiencies now competitive with mono-Si — laboratory-scale perovskite-silicon tandems have surpassed 33.9% efficiency, exceeding silicon's theoretical single-junction limit of 29.4% [67] — and a sharp spectral response favorable for VLC-type links where the emitter (typically a blue/white LED) spectrum can be matched to the absorber. Perovskite has already been demonstrated specifically for VLC using triple-cation perovskite solar cells [68]. However, perovskite's ionic migration and hysteresis under bias introduce nonlinearity and settling-time effects at the device level not present in crystalline Si or GaAs, and long-term encapsulation/stability issues (moisture, thermal cycling) can degrade communication-link consistency over the node's operational lifetime, even though instantaneous bandwidth can be high. More recently, triple-cation perovskite solar cells were optimized for VLC in [69]. By adjusting the active layer thickness, the -3 dB bandwidth increased from 114 kHz to 400 kHz, enabling data rates up to 56 Mb/s over a 40 cm free-space link.

Organic Photovoltaics (OPV) OPV cells use conjugated polymer or small-molecule absorbers with much lower carrier mobility than any inorganic material discussed above, fundamentally limiting electrical bandwidth. Despite this, organic photovoltaics have been demonstrated for simultaneous energy harvesting and high-speed MIMO optical wireless communication [70], showing that careful device and circuit design (e.g., reducing active-layer thickness to shorten carrier transit time) can partially offset the intrinsic mobility disadvantage. OPV's principal advantages for communication nodes are mechanical flexibility and low-cost roll-to-roll fabrication, rather than raw bandwidth. Organic photovoltaic receivers were investigated in [71], where PTB7:PC71BM-based solar cells enabled simultaneous communication and energy harvesting. Despite a modest PCE of 7%, a -3 dB bandwidth of 1.3 MHz supported a data rate of 34.2 Mb/s over a 1-m link using OFDM. Further investigations in [72] demonstrated that the bandwidth of organic photovoltaic (OPV) receivers strongly depends on shading conditions and operating modes.

Table 2.3: Comparison of PV material families for optical communication.

Technology	PCE	Temp. Coeff.	Comm. BW	Limiting Factor
Mono-Si	22–24%	-0.35 to -0.45	Medium–High	Junction capacitance
Poly-Si (baseline)	18–20%	-0.40 to -0.50	Medium	Grain-boundary recombination
CdTe	$\sim$22.1%	Lower than c-Si	Medium	Series resistance, back contact
CIGS	$\sim$23.4%	Lower than c-Si	Medium	Series resistance, scale-up variability
a-Si	$\sim$14.0%	Low	Low	Defect-state trapping, low mobility
GaAs (III–V)	Up to $\sim$29%	~ -0.09	Very High	High fabrication cost
Perovskite	Up to $\sim$29%	Moderate	High	Ionic migration, hysteresis
OPV	Lower	Moderate	Low	Low carrier mobility

2.2.4 Vehicular Applications of Solar Panel Optical Receivers

Vehicular OWC is a promising technology for vehicle-to-vehicle (V2V) and vehicle-to-infrastructure (V2I) connectivity, leveraging headlights, taillights, and traffic signals as transmitters. However, vehicular environments introduce challenges such as dynamic misalignment, mobility-induced blockages, ambient light interference, and orientation constraints.

Despite extensive research on solar panel-based VLC systems, vehicular applications remain largely underexplored. In [73], a vehicular VLC system employing a solar panel receiver achieved a data rate of 24.4 kb/s over a distance of 70 cm, demonstrating initial feasibility.

Nevertheless, existing studies do not adequately address critical vehicular challenges such as limited receiver orientation, dead-zone conditions, and rapidly varying channel geometry, highlighting the need for further investigation into solar panel-based receivers for vehicular optical wireless communication.

2.3 Comparison with the State-of-the-Art

Table 2.4 presents a consolidated comparison between the proposed research contributions and the closest state-of-the-art in solar panel-based optical wireless communication. The table provides a unified overview of the research area's evolution by eliminating redundant references and comparing all relevant works using common performance metrics, including receiver architecture, communication bandwidth, achievable data rate, communication distance, energy-harvesting capability, and the primary technical contribution. This consolidated comparison clearly positions the research presented in this thesis within the existing literature. The earliest

Table 2.4: Comparison of the proposed works with the existing state-of-the-art in solar panel-based optical communication.

Reference	Year	Receiver Architecture	PV Receiver	Data Rate	Distance	3-dB BW	Energy Harvested	Major Contribution
[50]	2014	Analog	Poly-Si	7.01 Mbps	39 cm	350 kHz	2.1 mW	First OFDM solar communication
[47]	2015	Passive Equalization	Poly-Si	11.84 Mbps	95 cm	300–500 kHz	30 mW	Passive bandwidth enhancement
[51]	2013	Direct Load	Mono-Si	3 kbps	40 cm	10 kHz	1.02 mW	Initial solar communication
[66]	2021	MIMO OFDM	Organic PV	363 Mbps	40 cm	2.8 MHz	10.9 mW	Organic photovoltaic receiver
[48]	2016	Reverse Bias	Mono-Si	17.05 Mbps	10 cm	120 kHz	–	Bandwidth enhancement using reverse bias
[55]	2018	Parallel Resistance	Amorphous	1.25 Mbps	15 cm	130 kHz	–	Bandwidth enhancement
[56]	2020	Analog	CIGS	5 Mbps	23 cm	40 kHz	–	Outdoor solar communication
[73]	2023	OOK	GaAs/Mono	24.4 kbps	110 cm	53 kHz	–	OOK solar communication
IEEE JLT (Chapter 4)	2024	BEC	Poly-Si	**18.85 Mbps**	**330 cm**	**3.27 MHz**	–	Bandwidth enhancement circuit
IEEE FNWF (Chapter 5)	2024	RC–RL SLIPT	Poly-Si	12.4 Mbps	200 cm	2.77 MHz	**38.4 mW**	Simultaneous communication and energy harvesting
IEEE T-ITS (Chapter 7)	2025	BEC	Poly-Si	17.9 Mbps	200 cm	**3.57 MHz**	–	Vehicular communication with blockage and orientation robustness

reported studies primarily established the feasibility of using photovoltaic cells as optical receivers for visible light communication. Initial demonstrations, such as [51] and [50], verified that commercially available solar panels could receive optical signals while simultaneously harvesting energy. However, the large junction capacitance of photovoltaic cells restricted the communication bandwidth to only a few tens or hundreds of kilohertz, thereby limiting the achievable data rate and communication distance. Subsequent works attempted to alleviate this limitation using passive equalization, reverse-biased operation, or resistive loading techniques [47, 48, 55]. Although these approaches improved the communication bandwidth to some extent, they often suffered from reduced signal magnitude, additional biasing requirements, or increased receiver complexity. Furthermore, most existing studies focused primarily on improving communication performance without considering simultaneous energy harvesting or practical deployment challenges.

The first contribution of this thesis (Chapter 4) directly addresses the fundamental bandwidth limitation of photovoltaic receivers through the development of a Bandwidth Enhancement Circuit (BEC). Compared with previously reported analog receiver architectures, the proposed receiver increases the effective communication bandwidth to 3.27 MHz while achieving a communication distance of 330 cm and a data rate of 18.85 Mbps using a commercially available white LED transmitter. This represents a substantial improvement over earlier solar panel-based receivers that employed passive equalization or reverse-biased techniques, and demonstrates that high-speed optical communication can be achieved without sacrificing the simplicity of the receiver architecture.

Building upon this communication-oriented receiver, the second contribution (Chapter 5) extends the receiver functionality to Simultaneous Lightwave Information and Power Transfer (SLIPT). Existing literature has largely investigated communication enhancement and energy harvesting independently, with limited emphasis on their interaction. The proposed RC–RL frequency-selective receiver introduces a passive architecture that simultaneously recovers the communication signal and harvests optical energy. Experimental investigations further demonstrate that appropriate selection of the communication and harvesting filters effectively isolates the two branches, enabling independent tuning of the communication bandwidth while maintaining nearly constant harvested power. This constitutes one of the principal contributions of this thesis, as it experimentally validates the coexistence of high-speed communication and efficient energy harvesting using a single photovoltaic receiver.

The third contribution (Chapter 7) further extends the proposed receiver architecture towards practical intelligent transportation system (ITS) applications. While previous studies were primarily conducted in controlled indoor laboratory environments, the proposed infrared LED-based communication system addresses several practical challenges associated with vehicular optical communication, including receiver misalignment, limited orientation, and partial blockage. Experimental results demonstrate reliable communication for receiver orientations up to $\pm 50^\circ$ and under blockage conditions covering up to 90% of the receiver surface, while maintaining communication over a 2 m vehicular link. These investigations considerably broaden the practical applicability of photovoltaic communication receivers beyond conventional point-to-point indoor demonstrations.

Overall, the comparison presented in Table 2.4 demonstrates the systematic progression of the research carried out in this thesis. Rather than addressing a single performance metric, each contribution builds upon the previous one to overcome a different limitation identified in the literature. The research evolves from bandwidth enhancement of photovoltaic receivers (Chapter 4), to simultaneous communication and energy harvesting through passive frequency-selective receiver design (Chapter 5), and finally to robust deployment in realistic vehicular environments using infrared optical communication (Chapter 7). Collectively, these contributions significantly advance the state-of-the-art by demonstrating that commercially available solar panels can serve as practical self-powered optical receivers capable of supporting high-speed communication, efficient energy harvesting, and reliable operation under realistic deployment conditions.

2.4 Comparison with Dedicated SLIPT Receiver Designs

The literature on simultaneous lightwave information and power transfer (SLIPT) encompasses a wide range of receiver architectures with substantially different design objectives. While several studies focus on maximizing communication throughput using custom-designed photovoltaic devices or dedicated optical receivers, the primary objective of this dissertation is fundamentally different. Specifically, this work investigates the communication capability of commercially available silicon solar panels without requiring any modification to the photovoltaic device itself. Therefore, direct performance comparisons should be interpreted carefully because the receiver technologies, optimization objectives, implementation complexity, and intended application scenarios differ significantly.

To provide a comprehensive perspective, Table 2.5 compares representative SLIPT and optical wireless communication receivers reported in the literature. The compared works are grouped into three categories: (i) commercially available off-the-shelf solar panel receivers, (ii) dedicated or custom-fabricated photovoltaic receivers, and (iii) non-photovoltaic dedicated SLIPT architectures. This comparison highlights the trade-offs among achievable communication performance, hardware complexity, manufacturability, and practical deployment.

Table 2.5 demonstrates that the proposed receiver achieves one of the highest communication data rates reported for commercially available off-the-shelf solar-panel-based optical receivers. Within the *off-the-shelf* category, the proposed bandwidth-enhancement circuit (BEC) enables an unmodified polycrystalline silicon solar panel to achieve communication data rates of 17.9 Mbps using an infrared LED transmitter and 18.85 Mbps using a broadband white LED transmitter. To the best of the author's knowledge, these represent the highest reported communication rates achieved using an unmodified commercial silicon solar panel operating simultaneously as an optical receiver and an energy-harvesting device. Earlier off-the-shelf implementations reported communication rates ranging from only 24.4 kbps to 17.05 Mbps, with performance primarily limited by the inherently low bandwidth of photovoltaic devices. Existing approaches generally rely on passive equalization, reverse-bias operation, or low-order modulation schemes. While reverse bias improves communication bandwidth, it requires an external power supply, thereby partially compromising the self-powered operation, one of the key advantages of SLIPT receivers.

In contrast, *dedicated or custom-fabricated photovoltaic receivers* are specifically designed to maximize communication bandwidth rather than preserving compatibility with commercially available photovoltaic modules. For example, GaAs photovoltaic receivers combined with GaAs VCSEL transmitters have demonstrated communication data rates approaching 1 Gb/s, whereas laboratory-fabricated organic photovoltaic (OPV) receivers have reported communication rates exceeding 300 Mbps. These impressive results are achieved through research-grade semiconductor epitaxy, optimized device geometries, millimeter-scale active

Table 2.5: Comparison of Off-the-Shelf Solar Panel Receivers with Dedicated/Custom SLIPT Receiver Designs

Reference	**Receiver Type**	**Optical Source**	**Data Rate**	**Distance**	**Off-the-shelf?**	**Key Limitation**
Off-the-shelf solar panel receivers						
Chapter 7	Polycrystalline Si + BEC	IR LED (850 nm)	**17.9 Mbps**	2 m	Yes	–
Chapter 4	Polycrystalline Si + TIR lens + BEC	White LED	**18.85 Mbps**	330 cm	Yes	–
Chapter 5	Polycrystalline Si (2 cell sizes)	White LED	12.4 / 2.5 Mbps	2 m	Yes	Rate-vs-harvested-power trade-off
[47]	Polycrystalline Si	White LED	11.84 Mbps	95 cm	Yes	Passive equalization only
[48]	Monocrystalline Si, reverse-biased	White LED	17.05 Mbps	10 cm	Yes*	Needs external reverse bias; very short range
[51]	Monocrystalline Si	White LED	3 kbps	40 cm	Yes	Early proof-of-concept; no BW enhancement
[55]	Amorphous crystalline	White LED	1.25 Mbps	15 cm	Yes	Very short range
[73]	GaAs + Monocrystalline	White LED	24.4 kbps	50–110 cm	Yes	No BW enhancement; low rate
[58]	Polycrystalline Si	White LED	7.01 Mbps	39 cm	Yes	No dedicated BW-enhancement circuit
[74]	CIGS thin film	White LED	5 Mbps	23 cm	No	Custom-grown thin-film stack
Dedicated / Custom-Fabricated Photovoltaic Receivers						
[46]	GaAs PV cell	Laser (VCSEL precursor)	0.5 Gb/s	Short bench	No	Same fabrication constraints as above
[65]	GaAs PV cell	GaAs VCSEL (laser)	**1 Gb/s**	∼2 m	No	Research-grade PV epitaxy with specialized VCSEL; mm-scale active area
[70]	Organic PV (OPV)	White LED	363 Mbps	40 cm	No	Lab-fabricated organic photovoltaic cell
[71]	Organic solar cell	Laser diode	34.2 Mbps	1 m	No	Custom high-speed organic photovoltaic fabrication
Non-Photovoltaic / Dedicated SLIPT Architectures						
[75]	Photodiode-based analytical model	VLC/IR (simulated)	Simulation only	N/A	N/A	Purely analytical; no hardware validation
[76]	$Nd:YVO_4$ gain medium + retro-reflector	808 nm pump laser	Up to 3 Gb/s (sim.)	3 m (20° FOV)	No	Requires custom laser-cavity resonator hardware
[77]	Coupled spatially distributed resonator	Laser (SHG-based)	Simulation-based	Variable	No	Complex bulk optics; laboratory-only demonstration
[78]	$Nd:YVO_4$ crystal + telescope optics	808 nm fiber-coupled pump	Power focused	Lab bench	No	Precision optical bench; not a compact receiver
[79]	Multicrystalline Si + avalanche photodiode	Laser/LED (underwater)	Reported via EH/ID metrics	Short-range UW	Partial	APD front-end increases cost and complexity
[80]	3×3 custom photodetector array	Multiple LED beams	High-throughput	Indoor bench	No	Custom photodetector array with optical multiplexing hardware

*Off-the-shelf solar cell requiring an external reverse-bias supply, partially compromising self-powered SLIPT operation.

areas, specialized laser transmitters, and custom fabrication processes not available in commercially manufactured solar panels. Consequently, although these systems demonstrate the upper performance limits of photovoltaic communication receivers, they cannot be directly compared with low-cost commercial silicon solar panels in terms of manufacturing cost, scalability, ease of deployment, or compatibility with practical energy-harvesting applications.

Similarly, *non-photovoltaic dedicated SLIPT architectures*, including resonant-beam systems, coupled optical cavities, avalanche-photodiode-assisted receivers, and custom multi-photodetector arrays, pursue fundamentally different design objectives. These systems typically aim to maximize wireless power-transfer efficiency, achieve long-range energy delivery, enable self-alignment, or support high-capacity, multiplexed optical communication through sophisticated optical components. Such architectures generally require precision optical alignment, laser resonators, telescope optics, avalanche photodiodes, or custom photodetector arrays, resulting in significantly greater hardware complexity than commercially available solar-panel receivers. While these approaches provide excellent communication performance for their intended applications, they are not directly comparable to the simple single-panel receiver architecture investigated in this dissertation, particularly with respect to deployment cost, implementation complexity, misalignment tolerance, and large-area optical energy harvesting.

Overall, the comparison presented in Table 2.5 illustrates that communication performance should not be evaluated solely on the basis of the maximum achievable data rate. Dedicated receiver architectures achieve substantially higher throughput by employing specialized photovoltaic devices and sophisticated optical hardware, whereas the proposed receiver retains the practical advantages of commercially available silicon solar panels, including low cost, self-powered operation, large optical collection area, mechanical robustness, and tolerance to optical misalignment and partial shading. Consequently, although the proposed receiver does not match the gigabit-per-second performance of dedicated laboratory prototypes, it significantly narrows the performance gap while preserving the characteristics that make commercial solar panels attractive for practical SLIPT applications, including vehicular visible-light communication, intelligent transportation systems, and energy-constrained Internet of Things deployments.

Summary

This chapter reviewed the state of the art in solar panel-based optical receivers for VLC and OWC systems. Early studies demonstrated the feasibility of using silicon solar cells as low-cost communication receivers, highlighting their robustness to strong ambient light at the expense of limited electrical bandwidth. Subsequent works investigated simultaneous communication and energy harvesting through SLIPT frameworks, revealing inherent trade-offs between harvested power, receiver sensitivity, and achievable data rate. To overcome the intrinsic limitations of silicon devices, several studies explored alternative photovoltaic materials such as GaAs, organic, amorphous silicon, and perovskite solar cells, achieving higher bandwidths and data rates under controlled laboratory conditions.

However, most existing solutions rely on specialized photovoltaic materials, short-range indoor testbeds, or reverse-biased, custom-fabricated devices, thereby limiting their practical deployability. In particular, the design of efficient analog front-end architectures tailored to *commercially available and widely deployed silicon solar panels*, in conjunction with *off-the-shelf LED transmitters*, remains largely underexplored. Furthermore, prior works predominantly focus on static scenarios and do not adequately address challenges arising in dynamic environments.

These limitations are especially pronounced in vehicular optical wireless communication, where receiver orientation, mobility-induced misalignment, and dead-zone effects critically impact link reliability. Addressing these gaps motivates the development of novel analog receiver designs that enhance the communication bandwidth of commercial silicon solar panels while preserving energy harvesting capability, thereby enabling practical, low-cost, and scalable optical wireless systems for real-world vehicular applications.

Chapter 3

Experimental Validation of Optical Wireless Receiver over Solar Panel

Motivated by the limited bandwidth and poor practical deployability of existing solar panel-based receivers, this chapter presents a novel analog front-end design for commercially available silicon solar panels using off-the-shelf LEDs, and investigates bandwidth enhancement under varying distance, received optical power, and frequency- and time-domain operating conditions.

3.1 Motivation

Solar cells may use electromagnetic radiation from lasers, LEDs, and sunlight to create electrical energy. To enable communication over a solar panel, it should respond to high-frequency signals that switch between high and low (peak-to-peak) values. Also, optical communication is affected by ambient light, resulting in increased shot noise and clipping of the retrieved analog signal. As the solar panels are not designed to respond to such a high-frequency signal, there is a need for external circuitry to enhance this response.

3.2 Chapter Contributions

The main contributions of this chapter are summarized as follows:

- A robust analog front-end architecture is proposed to suppress the adverse impact of ambient light originating from surrounding natural and artificial illumination sources. The design effectively mitigates the dominant direct current (DC) and low-frequency components induced by ambient light, thereby preventing receiver saturation and improving the signal-to-noise ratio of the information-bearing optical signal under varying illumination conditions.
- An active filter–based bandwidth enhancement technique is developed to overcome the intrinsic low-pass characteristics of solar panels. By proper selection of load resistance and filter components, the effective 3-dB bandwidth of the solar panel receiver is significantly extended, enabling higher data rates and improved modulation support in solar panel–based optical communication systems.

3.3 Fundamentals of Solar Panel as a Communication Receiver

Solar panels convert every incoming optical signal to its electrical equivalent, irrespective of signal behavior (DC or AC). The response to a time-varying signal depends on the receiver bandwidth. In this section, we will discuss the fundamental principles of solar as a receiver and the challenges.

3.3.1 Principle of Operation for a Solar Panel

Traditionally, solar modules are primarily used for optical energy harvesting. Their electrical behavior under steady illumination is well described using a well-established DC equivalent circuit model [81, 82], as illustrated in Fig. 3.1. When incident optical radiation impinges on the solar module, it generates a photocurrent (I_{PH}) proportional to the received optical intensity. One of the key parameters governing the magnitude of the generated photocurrent is the responsivity (ρ) of the solar module, which relates the incident optical power to the output electrical current.

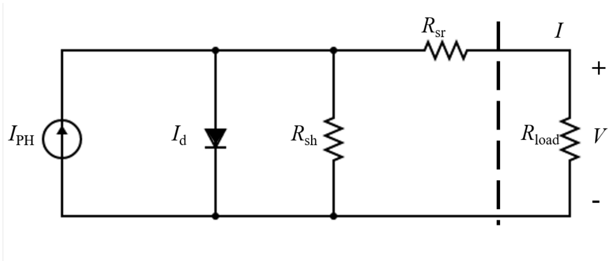

Figure 3.1: DC model of solar module.

The generated photocurrent flows through the internal elements of the solar module, including the diode and parasitic resistances, while the remaining current is delivered to the external load. Based on the single-diode equivalent circuit, the current–voltage (I–V) relationship of the solar module can be expressed as

$$I = I_{PH} - I_d - \frac{V + IR_{sr}}{R_{sh}}, \tag{3.1}$$

where the diode current I_d is given by

$$I_d = I_0 \left(\exp\left[\frac{V + IR_{sr}}{nV_T} \right] - 1 \right). \tag{3.2}$$

From (3.1), it is evident that the relationship between the output current (I) and voltage (V) is nonlinear. In this model, the photocurrent source I_{PH} is connected in parallel with the diode, whose forward conduction current is denoted by I_d. In practical solar modules, non-idealities arise due to parasitic resistive elements. The series resistance (R_{sr}) accounts for losses associated with metallic contacts, interconnections, and solder bonds, whereas the shunt resistance (R_{sh}) represents leakage paths across the p–n junction [83]. The parameter

I_0 denotes the diode reverse saturation current, n represents the number of series-connected cells within the module, V_T is the thermal voltage of the diode, and R_{load} is the external load resistance.

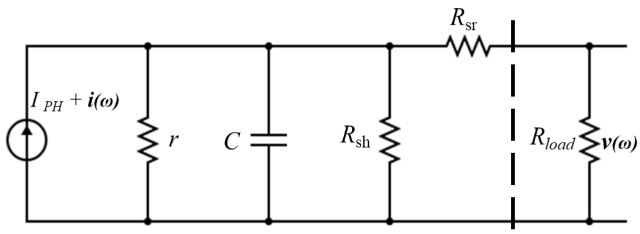

Figure 3.2: AC model of solar module.

While the DC model accurately captures the energy-harvesting behavior, it is insufficient to characterize the solar module's dynamic response to rapidly varying optical signals. Therefore, to analyze the alternating current (AC) behavior relevant to optical communication, a small-signal communication model is employed, as shown in Fig. 3.2 [84]. In this model, the diode present in the DC equivalent circuit is replaced by its small-signal representation, comprising a junction capacitance (C) in parallel with an equivalent resistance (r). Consequently, the dynamic response of the solar module can be characterized by a time constant given by

$$\tau = C \cdot r. \tag{3.3}$$

The junction capacitance plays a dominant role in limiting the temporal response of the solar module. A higher capacitance results in slower rise and fall times in response to variations in incident optical intensity, thereby limiting the effective switching speed of the solar module. As a result, conventional solar panels typically exhibit bandwidths limited to a few tens of kilohertz.

When intensity-modulated optical signals impinge on the solar module, both DC and AC components are generated across the load resistance. The DC component (V) corresponds to the average optical power and can be utilized for energy harvesting, whereas the AC component ($v(\omega)$) carries the modulated information signal. In receiver architectures, the selection of load resistance plays an important role. The overall output voltage of the solar module can be expressed as

$$V_{OUT} = V + v(\omega), \tag{3.4}$$

where the DC component is given by

$$V = \left[I_{PH} - I_d - \frac{V + IR_{sr}}{R_{sh}} \right] R_{load}, \tag{3.5}$$

and the small-signal AC voltage response is expressed as

$$v(\omega) = \frac{\frac{R_{load}}{R_{load}+R_{sr}}}{1/r + j\omega C + 1/R_{sh} + 1/(R_{sr} + R_{load})} i(\omega). \tag{3.6}$$

Here, ω denotes the angular frequency of the incident optical signal, and $i(\omega)$ represents the information-bearing component of the generated photocurrent.

3.3.2 Impact of Load Selection

The electrical current generated by the solar panel must flow through an external load to produce a measurable output voltage. As an initial and fundamental choice, a purely resistive load is considered. The value of this resistive load plays a crucial role in determining the voltage developed across the solar panel and, consequently, the overall receiver performance.

The selection of the load resistance is particularly critical, as it directly influences both the signal amplitude and the frequency response of the solar module. Specifically, the following trade-offs are observed:

- An increase in the load resistance results in a higher peak-to-peak output voltage, thereby improving the received signal strength.
- A higher load resistance leads to a reduction in the 3-dB bandwidth of the solar module due to the increased effective *RC* time constant.

- An increase in the load resistance also enhances the DC voltage component across the solar panel, which is beneficial for energy harvesting but may saturate subsequent signal conditioning stages.

These observations highlight the inherent trade-off between signal strength, bandwidth, and DC operating point, emphasizing the need for careful load selection or adaptive circuitry in solar panel-based optical receivers. To understand better, we have considered only the communication model of the solar panel as shown in Fig. 3.2. The overall impedance response of the solar panel is derived as:

$$\frac{v(\omega)}{i(\omega)} = \frac{\frac{R_{load}}{(R_{load}+R_{sr})}}{1/r + j\omega C + 1/R_{sh} + 1/(R_{sr} + R_{load})} \tag{3.7}$$

An increase in the switching frequency (ω) leads to a rise in the effective capacitive impedance of the solar panel, which in turn reduces the voltage response across the load. One straightforward approach to enhance the output voltage is to increase the load resistance. However, this approach is subject to inherent limitations.

First, increasing the resistive load raises the overall impedance gain of the system. Since gain and bandwidth are inversely related, an improvement in voltage gain results in a proportional reduction in the available bandwidth, and vice versa. Consequently, higher load resistance limits the high-frequency response of the solar panel.

Second, the DC voltage component across the load increases proportionally with the load resistance. While this may be advantageous for energy harvesting, it can drive the operating point toward saturation and degrade the dynamic range of the communication signal. These analytical observations are further corroborated through experimental validation, as illustrated in Fig. 3.3.

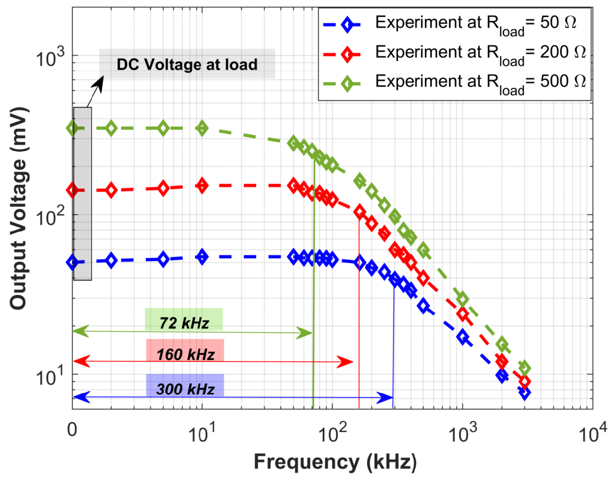

Figure 3.3: Raw solar module frequency response

3.4 Analog Receiver Design and Analytical Framework

To overcome the limitations associated with a purely resistive load, an analog front-end circuitry, referred to as the *Bandwidth Enhancement Circuit*, is designed. In this work, the focus is restricted to enhancing the communication capability of the solar panel, while the impact on energy harvesting is considered separately. Fig. 3.4 illustrates the modified solar receiver architecture incorporating the proposed BEC.

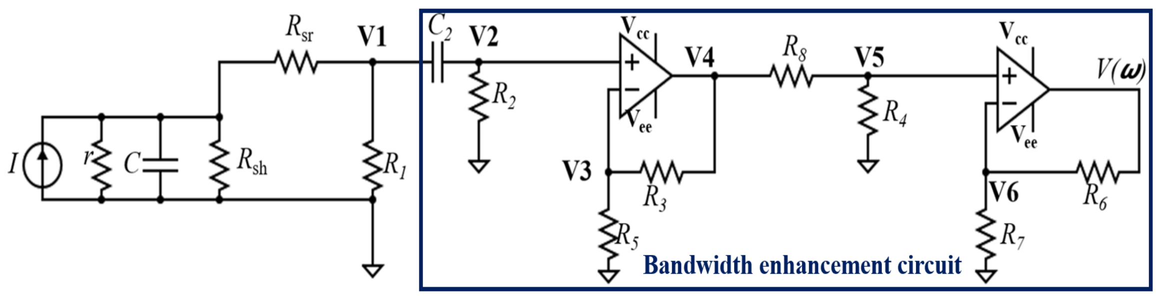

Figure 3.4: Solar panel with bandwidth enhancement circuit.

In an OOK modulation scheme, reliable detection at the receiver requires a clear distinction between the high- and low-power levels of the incident optical signal. However, when a solar panel is employed as the optical receiver, its inherently limited bandwidth imposes significant constraints on this detection process. Owing to the restricted 3-dB bandwidth, the peak-to-peak amplitude of the received electrical signal is severely attenuated. Furthermore, the dominant junction capacitance of the solar panel results in increased rise and fall times, thereby degrading the temporal response of the detected waveform.

As the switching frequency of the transmitted signal increases, these impairments become more pronounced, leading to substantial waveform distortion. In particular, duty-cycle distortion emerges as a critical issue, causing overlap between logic-high and logic-low levels. This degradation significantly reduces the reliability of threshold-based detection and poses a major challenge for achieving robust, high-speed communication using solar panel–based OOK receivers.

To mitigate these limitations, the incorporation of external signal-conditioning circuitry, an equalizer is essential. The primary role of the equalizer is to compensate for the bandwidth constraints imposed by the solar panel by extending the effective 3-dB bandwidth and improving the rise and fall times of the received signal. By reshaping the frequency response of the receiver, the equalizer enhances the separation between logic levels, thereby improving detection accuracy and overall communication reliability.

The complete receiver architecture consists of three main components: the solar panel, an equalizer, and a non-inverting amplifier. For the purpose of analysis and design simplicity, the equalizer and the non-inverting amplifier are collectively treated as a single functional block, termed the *Bandwidth Enhancement Circuit*. This abstraction facilitates a clearer evaluation of the performance improvements achieved through bandwidth extension and signal conditioning.

The BEC is specifically designed to process only the AC component of the photocurrent generated by the solar panel. At the input stage, the circuitry effectively suppresses the DC component, which primarily corresponds to harvested optical energy. Since the DC component is responsible for powering external loads or charging energy storage elements, isolating it ensures that the energy-harvesting capability of the solar panel remains unaffected. As a result, the proposed BEC enhances the communication performance of the receiver without compromising the inherent energy-harvesting functionality of the solar panel.

The mathematical analysis of the Fig. 3.4 is as follows:

$$\frac{V_1}{I} = \frac{\frac{R_1}{(R_1+R_{sr})}}{1/r + j\omega C + 1/R_{sh} + 1/(R_{sr}+R_1)} \tag{3.8}$$

$$\frac{V_2}{V_1} = \frac{R_2}{R_2 + (1/sC_2)} \tag{3.9}$$

As the circuit is having negative feedback, from virtual ground concept: $V_2 = V_3$

$$\frac{V_4}{V_3} = 1 + \frac{R_3}{R_5} \tag{3.10}$$

$$\frac{V_5}{V_4} = \frac{R_4}{R_4 + R_8} \tag{3.11}$$

$$\frac{V_{out}}{V_5} = 1 + \frac{R_6}{R_7} \tag{3.12}$$

Here, $V_{out} = v(\omega)$

from equation (3.11), equation (3.12) and from virtual ground concept $(V_5 = V_6)$

$$\frac{V_{out}}{V_4} = \left(\frac{R_4}{R_4 + R_8}\right) . \left(1 + \frac{R_6}{R_7}\right) \tag{3.13}$$

from equation (3.9), equation (3.10) and equation (3.13)

$$\frac{V_{out}}{V_1} = \left(\frac{R_4}{R_4 + R_8}\right) . \left(1 + \frac{R_3}{R_5}\right) . \left(1 + \frac{R_6}{R_7}\right) . \left(\frac{R_2}{R_2 + (1/sC_2)}\right) \tag{3.14}$$

from equation (3.8) and equation (3.13)

$$\frac{V_{out}}{I} = \left(\frac{\frac{R_1}{(R_1+R_{sr})}}{1/r + j\omega C + 1/R_{sh} + 1/(R_{sr}+R_1)}\right) . \left(\frac{R_4}{R_4 + R_8}\right) . \left(1 + \frac{R_3}{R_5}\right) . \left(1 + \frac{R_6}{R_7}\right) . \left(\frac{R_2}{R_2 + (1/sC_2)}\right) \tag{3.15}$$

The modified receiver transfer function is given in (3.15). The overall system response includes the solar panel response in cascade with the response of BEC. Parameters for the designed analog circuit are as follows: $R_1 = 200\ \Omega$, $R_2 = 100\ \Omega$, $C_2 = 10\ nF$ and op-amps are operating at five times gain. The frequency response and the time response of the designed receiver are described in the results section.

3.5 Experiment Setup

A 5 W polycrystalline solar panel is employed as the optical receiver for the experimental evaluation. The key electrical and physical parameters of the solar panel are summarized in Table 3.1. To assess the performance of the solar panel receiver both with and without the proposed BEC, experiments are conducted using the communication setup illustrated in Fig. 3.5.

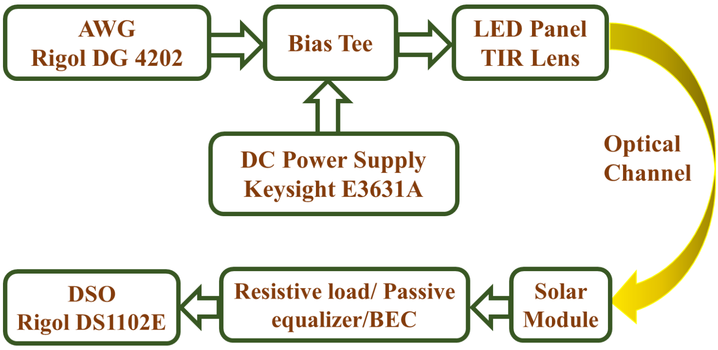

Figure 3.5: Block diagram of the communication setup.

Table 3.1: Solar panel parameters

Parameters	**Parameter values**
Number of cells	18 (9×2)
Open-circuit voltage (V_{oc})	11.24 V
Short-circuit current (I_{sc})	0.64 A
Rated voltage (V_{mp})	9.23 V
Rated current (I_{mp})	0.56 A
Module efficiency (η)	8.55%

Table 3.2: LED panel parameters

Parameters	**Parameter values**
Number of LEDs	24
Electrical power	14.4 W
Transmission distance	1 m
Average optical illuminance at solar panel	1800 lux
Ambient light at solar panel	130 lux

The experimental setup consists of an arbitrary waveform generator (AWG), an LED driver circuit, a panel comprising 24 LEDs, a 5 W solar panel, the proposed BEC, and an oscilloscope for signal observation and analysis. All experiments are carried out under ambient room lighting conditions with an illuminance level of approximately 130 lux. The employed solar panel comprises 18 cells arranged in a 9×2 configuration. The remaining experimental parameters related to the optical transmitter and illumination conditions are listed in Table 3.2.

The physical realization of the experimental testbed is shown in Fig. 3.6. The separation distance between the LED transmitter panel and the solar panel receiver is maintained at 1 m throughout the experiments. The receiver unit comprises the solar panel, the proposed BEC, DSP board for processing the received electrical signal, and a laptop for data acquisition and analysis.

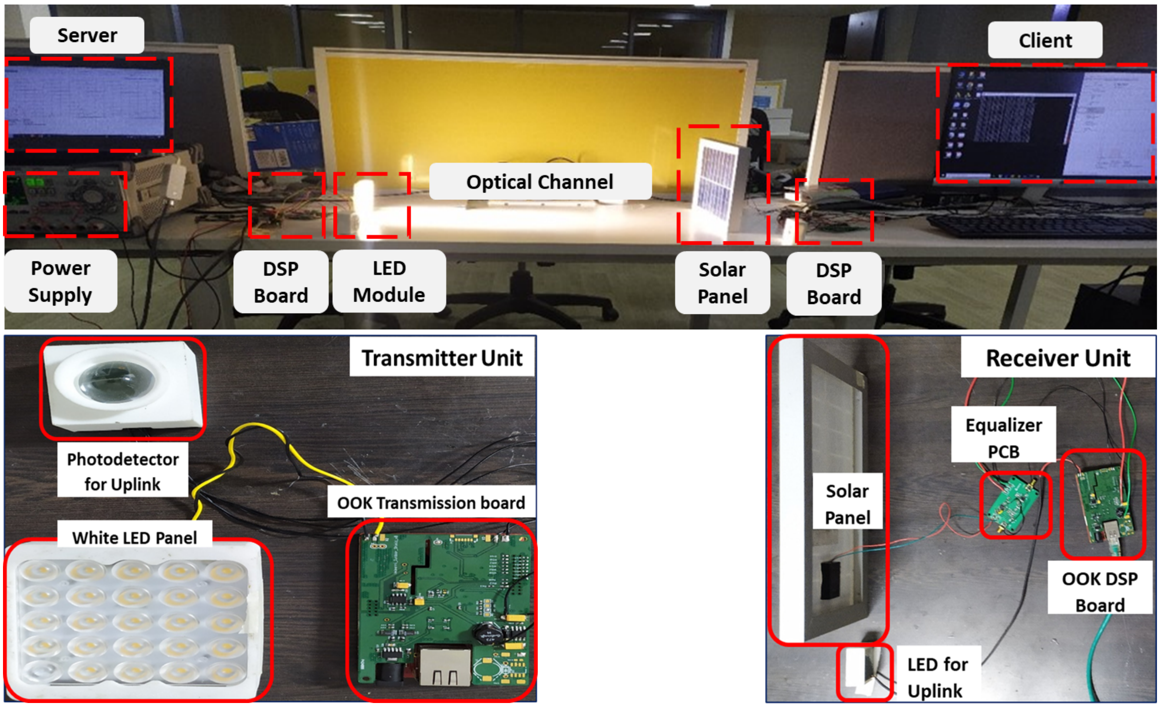

Figure 3.6: Experimental setup.

3.6 Performance Analysis

This section evaluates the performance of the proposed solar panel–based optical receiver with and without the BEC. The analysis focuses on the frequency-domain and time-domain characteristics, packet-level communication reliability, and the impact of transmitted optical power on system performance.

3.6.1 Frequency and Time Response

Solar panels are primarily designed to maximize energy-harvesting efficiency rather than high-speed signal detection [44, 85, 86]. Consequently, their electrical characteristics are optimized for low-frequency operation, and their effective bandwidth is typically limited to a few kilohertz. In this work, the measured 3-dB bandwidth of the employed solar panel is 163 kHz, as shown in Fig. 3.7. Experimental results further reveal that the solar panel can support communication signals up to approximately 400 kHz. Beyond this frequency, the peak-to-peak amplitude of the received signal is severely attenuated, and the temporal integrity of the waveform deteriorates due to pronounced distortion, as illustrated in Fig. 3.8.

Another inherent property of solar panels is their ability to pass both the DC and time-varying alternating current AC components of the incident optical signal. As a result, the electrical output of the solar panel comprises a strong DC offset superimposed on the modulated AC signal. This dominant DC component can drive subsequent signal-processing stages into saturation, thereby reducing the effective dynamic range available for communication signals. Such saturation significantly complicates the reliable discrimination between logic-low and logic-high levels, ultimately limiting the achievable data rate and degrading the overall performance of the optical communication link.

For reliable data recovery at the receiver, it is essential that the received signal exhibits a sufficiently large peak-to-peak voltage to enable accurate threshold-based detection. However, the presence of a dominant DC component in the solar panel output significantly reduces the available dynamic range for AC signal detection. Therefore, from a communication perspective, it becomes necessary to suppress the DC component and operate exclusively on the modulated AC portion of the photocurrent.

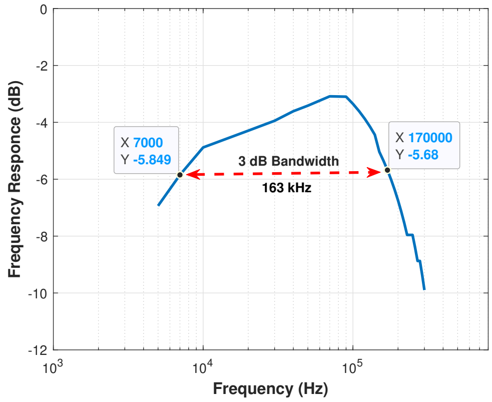

Figure 3.7: Frequency response of the solar panel.

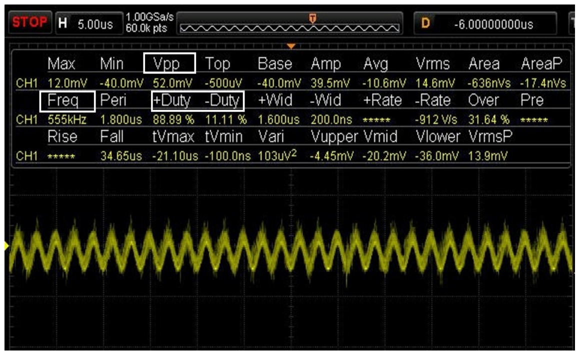

Figure 3.8: Time-domain response of the solar panel.

To address these limitations and to extend the effective bandwidth of the receiver, a BEC is introduced immediately after the solar panel. The incorporation of the BEC substantially improves the frequency response of the receiver, increasing the 3-dB bandwidth from 163 kHz to 1.62 MHz, as depicted in Fig. 3.9. This enhancement directly translates into an increased maximum switching frequency at which the transmitted data can be reliably recovered. With the proposed BEC, the received signal maintains a sufficiently high peak-to-peak amplitude even at modulation frequencies as high as 3 MHz, thereby enabling clear discrimination between logic-high and logic-low levels. Furthermore, the time-domain characteristics of the received waveform, particularly the duty-cycle fidelity, exhibit significant improvement, as shown in Fig. 3.10.

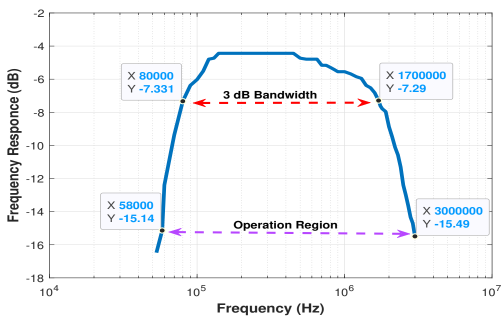

Figure 3.9: Frequency response of the modified receiver design.

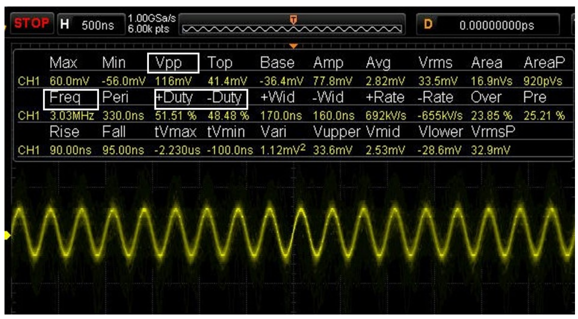

Figure 3.10: Time-domain response of the modified receiver.

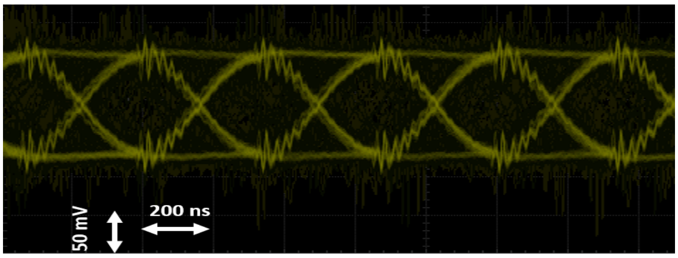

Figure 3.11: Eye diagram at a data rate of 1.5 Mbps.

A critical factor influencing the performance of the BEC is the value of the load resistor placed at the solar panel output. A low-valued load resistor reduces the effective RC time constant and thus increases the bandwidth; however, it simultaneously lowers the peak-to-peak voltage to a level that limits the effectiveness of the BEC. Conversely, an excessively high load resistance can push the receiver into saturation, resulting in clipping and nonlinear distortion of the received waveform. Therefore, an optimal trade-off must be achieved in selecting the load resistance in conjunction with the BEC design parameters, as both jointly determine the overall frequency response, linearity, and signal integrity of the receiver.

Following conditioning by the BEC, the signal is forwarded to an ADC for digital processing. To suppress high-frequency noise and prevent aliasing, a low-pass filter is employed at the ADC input stage. This filtering preserves the integrity of the communication signal and enhances the robustness of the detection process. The eye diagram corresponding to a data rate of 1.5 Mbps is presented in Fig. 3.11, demonstrating the improved signal quality and timing margin achieved with the proposed receiver design.

3.6.2 Packet Success Rate

The impact of the separation distance between the transmitter and the receiver on the packet success rate is illustrated in Fig. 3.12. To evaluate the reliability of the communication link, a total of 1000 packets, each with a payload size of 1518 bytes, were transmitted for every tested distance. The experimental results indicate that the packet loss begins to increase significantly when the separation distance exceeds approximately 100 cm.

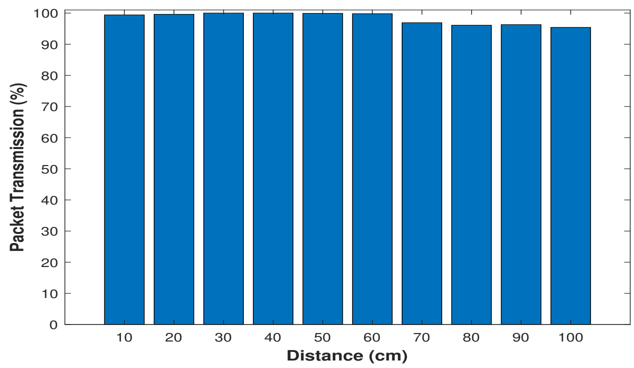

Figure 3.12: Packet success rate as a function of transmitter–receiver separation distance.

This performance degradation can be primarily attributed to two factors: optical beam divergence and the limited responsivity of individual solar cells. As the separation distance increases, the transmitted optical beam undergoes natural divergence, resulting in a reduced optical flux incident on the solar panel. Consequently, each solar cell collects a smaller fraction of the transmitted optical power. Under such reduced illumination conditions, the output of the receiver analog front-end fails to maintain the required peak-to-peak voltage necessary for reliable symbol detection. When the signal amplitude falls below the decision threshold, the ADC is unable to accurately distinguish between logic-high and logic-low levels, leading to an increased number of packet errors.

In addition, a slight degradation in performance is observed at very short separation distances, particularly below 30 cm. When the light source is placed extremely close to the solar panel, the optical beam becomes highly localized, resulting in non-uniform illumination across the panel surface. As a result, only a subset of the solar cells receives the majority of the incident optical power, while the remaining cells contribute minimally to the overall photocurrent. This uneven distribution reduces the effective utilization of the solar panel aperture, introduces minor signal distortions, and ultimately impacts the overall packet success rate.

3.6.3 Impact of Transmitted Power

The influence of transmission distance on the achievable data rate for different levels of transmitted optical power is illustrated in Fig. 3.13. A consistent trend is observed across all measured distances: as the transmitter moves closer to the solar panel, the optical power required to achieve the maximum data rate decreases. This behavior arises because, at shorter separation distances, the incident optical flux on the solar panel is sufficiently high to establish the required extinction ratio. Consequently, the receiver can reliably distinguish between logic-high and logic-low levels even at lower transmitted optical power levels.

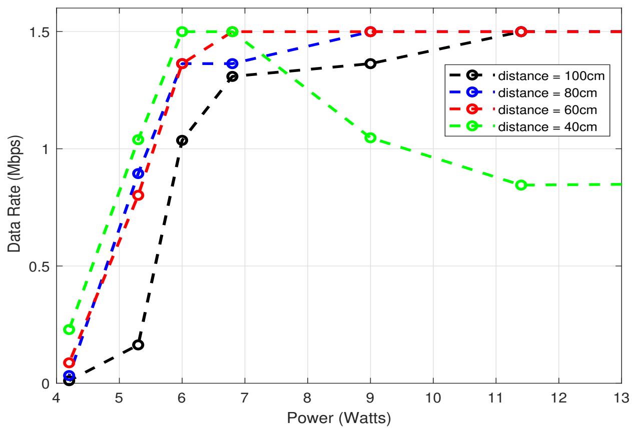

Figure 3.13: Achievable data rate as a function of transmitted optical power for different transmitter–receiver separation distances.

A notable observation is obtained at a separation distance of 40 cm. At this short distance, the solar panel is subjected to a relatively high optical intensity, resulting in enhanced photocurrent generation across the constituent cells. Under these conditions, the maximum data rate is achieved when the transmitted optical power is approximately 6 W. However, when the transmitted power exceeds 7 W, the peak-to-peak amplitude of the received electrical signal surpasses the linear operating range of the receiver amplification stage. This causes signal clipping in the analog front-end, leading to waveform distortion and a reduction in the effective extinction ratio. Such distortion increases symbol errors and, consequently, degrades the achievable data rate.

As the transmitted optical power is further increased, the severity of clipping intensifies, resulting in a continued decline in system performance. Eventually, the system enters a saturation regime in which additional increases in optical power no longer yield improvements in data rate. In this region, the data rate stabilizes at approximately 850 kbps for transmitted powers exceeding 11.5 W. This behavior indicates that the receiver front-end has reached its maximum tolerable illumination level and is no longer capable of processing the incoming signal without significant distortion.

3.7 Summary

This chapter presented the design and experimental validation of a solar-panel-based OWC receiver employing OOK modulation. By integrating a BEC with the solar panel, the receiver effectively operates as an optical communication detector. Experimental results demonstrate a significant improvement in the receiver's 3-dB bandwidth, enabling a 1-m VLC link with a data rate of 1.5 Mbps. The enhanced bandwidth further suggests the feasibility of higher-order modulation schemes, such as OFDM. Overall, the results confirm that, with suitable circuit-level enhancements, a solar panel can function as a communication receiver in sustainable optical wireless systems.

Chapter 4

Enhanced Solar Receiver Design and Extended Indoor Communication Range over Solar Panels

4.1 Motivation

The utilization of a solar panel as an optical receiver demonstrates a strong potential for enabling data communication, as previously established in Chapter 3. While the initial experiments successfully validated short-range communication capabilities, achieving reliable long-distance communication using a solar panel remains a significant challenge. This limitation primarily arises due to the inherent trade-off between communication distance and received signal strength. As the optical link distance increases, the incident optical power on the solar panel decreases substantially, leading to a lower photocurrent and reduced signal-to-noise ratio at the receiver.

Additionally, extracting the communication signal across a higher-value resistive load, commonly used to increase voltage sensitivity, introduces a severe loading effect that restricts the system's effective bandwidth. This bandwidth–resistance trade-off becomes a bottleneck when attempting to support higher data rates or longer communication distances.

These limitations collectively motivate the development of an improved analog front-end design that can boost the system bandwidth without compromising sensitivity. To further strengthen long-range communication performance, optical lenses are incorporated on the transmitter side to focus and collimate the emitted optical beam. This focused projection ensures that more optical power is delivered to the solar panel receiver over extended distances, thereby improving the overall link reliability and enabling longer communication ranges.

4.2 Chapter Contributions

The major contributions of this chapter are summarized as follows:

- Design of an analog front-end for a solar optical receiver aimed at mitigating the inherent bandwidth–resistance tradeoff, enabling improved signal integrity and higher data rates without sacrificing noise performance.

- Development of an optical front-end lens system focused on increasing optical coupling efficiency and beam directivity, thereby extending the achievable optical transmission distance and enhancing overall system performance.

4.3 Transmitter Optics

Optics plays a fundamental role in enabling long-distance communication, particularly when the goal is to deliver a highly concentrated optical beam onto the solar panel receiver. Among the various optical techniques available, TIR stands out as an exceptionally efficient mechanism for redirecting light. Unlike reflective surfaces that rely on metallic or dielectric coatings and inherently suffer from absorption losses, TIR provides an ideally lossless reflection when the incident ray exceeds a material-dependent critical angle. This makes TIR-based lenses highly attractive for applications requiring maximum optical power delivery.

In the proposed system, a custom TIR lens is positioned directly above the LED emitter. The lens geometry is designed such that photons emitted from the LED are efficiently captured and redirected toward the solar module, significantly improving power concentration at the receiver. During TIR, a light ray traveling inside a denser medium (e.g., PMMA or glass) strikes the interface with a less dense medium (air). When the incidence angle exceeds the critical angle, the ray undergoes complete reflection back into the denser medium. This phenomenon enables the lens to preserve most of the emitted power while steering the light in a desired propagation direction. The effective illumination area on the solar panel depends on both the

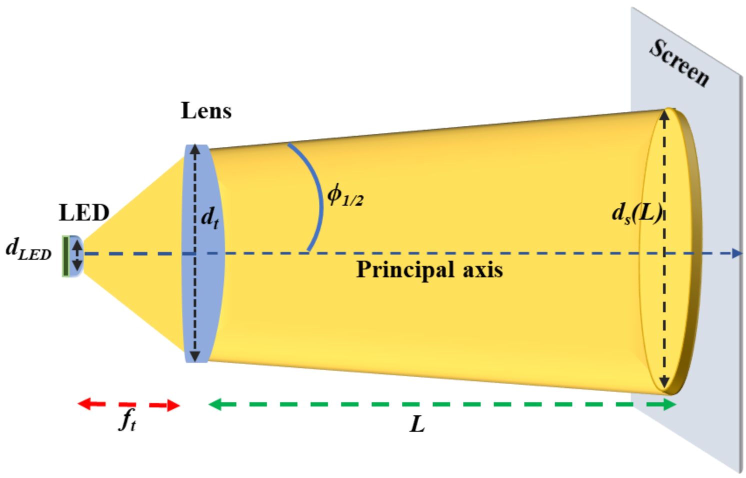

Figure 4.1: Illustration of the beam alignment of the LED after TIR lens optics.

LED size and the optical characteristics of the TIR lens. As illustrated in Fig. 4.1, the beam spot diameter at a transmission distance L can be expressed as [87]

$$d_s(L) = d_t + 2 \cdot L \cdot tan(\phi_{1/2}), \tag{4.1}$$

where d_t is the diameter of the transmitting aperture, and L is the transmission distance. With the application of a TIR lens, the overall beam angle of the light source reduces, resulting in a high amount of power that can be focused on the solar modules. The divergence half beam angle ($\phi_{1/2}$) is given by [87]:

$$\phi_{1/2} = arctan\left(0.5 \cdot \frac{d_{LED}}{f_t}\right), \tag{4.2}$$

where d_{LED} is the LED diameter, and f_t is the focal length of the transmitter lens. The focal length indicates how strongly the lens converges or diverges light, thereby governing the efficiency of beam focusing. In the designed TIR optics, the focal length f_t is 1 mm, and the transmitting aperture has a diameter of 37.8 mm. Using these values, the divergence angle $\phi_{1/2}$ can be calculated for subsequent link budget analysis. For VLC channels, the emitted light from an LED typically follows a Lambertian radiation pattern characterized by an order m. For the VLC system, the order of the Lambertian pattern *(m)* depends on the $\phi_{1/2}$ and is given by [88]:

$$m = \frac{-ln2}{ln(cos\phi_{1/2})}, \tag{4.3}$$

A decrease in $\phi_{1/2}$ by the application of the TIR lens results in an increase of m. This increased directivity improves the channel DC gain, which is essential for long-range communication. The channel gain for a Lambertian source is given by [89]:

$$G = \frac{(m+1)}{2\pi}\cos^m(\phi). \tag{4.4}$$

where ϕ is the transmission angle from the light source to the solar module. The geometric

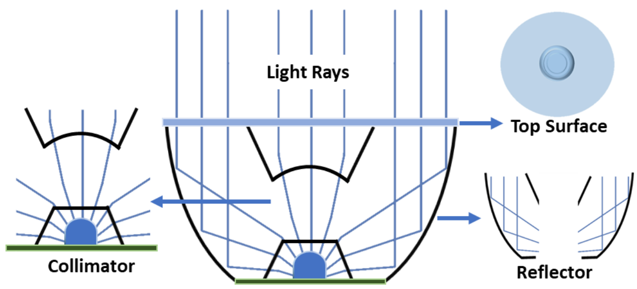

Figure 4.2: TIR lens optics.

structure of the designed TIR lens can be broadly segmented into three functional regions—the collimator, the reflector, and the top emitting surface, as illustrated in Fig. 4.2. Each region performs a distinct optical function that collectively contributes to efficient beam shaping and enhanced light concentration at the receiver.

The collimator section is responsible for straightening and aligning the light rays emerging from the LED chip. Light rays incident near the upper edge of this region are transformed into nearly parallel beams, thereby reducing the beam divergence at the source itself. Additionally, the side surfaces of the collimator guide and confine the emitted photons, directing a substantial portion of the light toward the reflector region with minimal spillover. Upon reaching the reflector section, light rays encounter surfaces specifically shaped to satisfy the conditions for total internal reflection. When these rays strike the reflector interface at angles greater than the critical angle, they are fully reflected back into the high-index medium of the lens, without any transmission loss. As a result, the reflector effectively channels and redirects the light toward the forward direction, ensuring that the optical power remains confined within the designed propagation path. The top surface of the TIR lens serves as the primary output interface. Its geometry is optimized to generate a concentrated optical intensity peak, which is crucial for delivering a high-power, focused beam to the solar module. This surface contributes to shaping the final beam profile, ensuring that the projected light exhibits minimal divergence and high spatial uniformity.

When these three elements—collimator, reflector, and top surface operate in unison, the overall TIR lens produces a sharply bounded light distribution characterized by a pronounced cut-off and a significantly enhanced intensity peak, as demonstrated in Fig. 4.3. This engineered optical behavior enables a more efficient coupling of optical power into the solar module, thereby improving the achievable communication distance and system performance in VLC applications. The advantage of incorporating a TIR lens into the optical transmitter design is illustrated in Fig. 4.4. At a transmission distance of 330 cm, an LED operating without a TIR lens generates a relatively weak and broadly distributed optical intensity, resulting in an almost uniform illumination pattern within a beam radius of approximately 10 cm. Such a

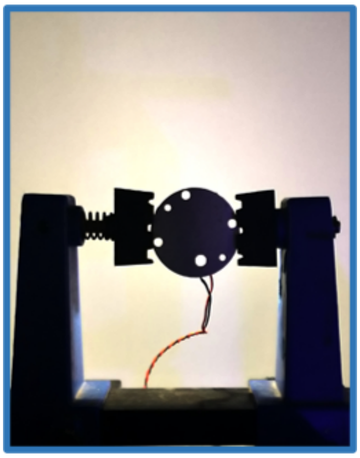

(a) Without TIR lens

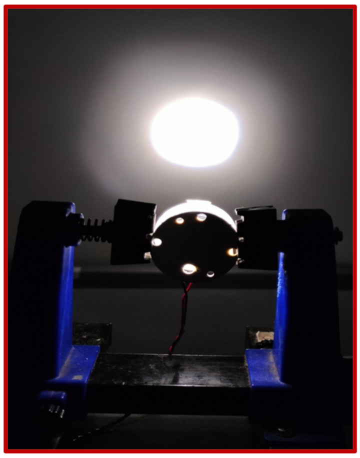

(b) With TIR lens

Figure 4.3: LED light intensity comparison with and without TIR lens.

diffuse distribution limits the amount of optical power that can be efficiently collected by the solar panel receiver, thereby constraining the achievable communication range. In contrast,

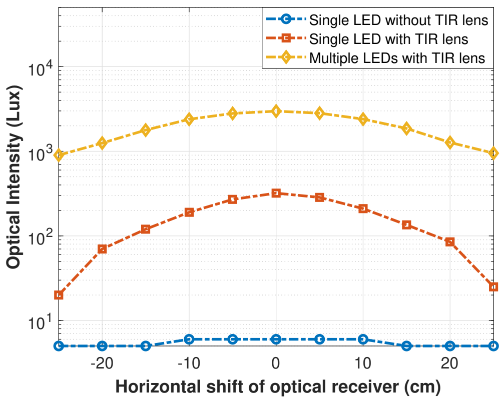

Figure 4.4: Optical intensity vs. horizontal shift of the irradiance receiver.

integrating a TIR lens with the LED significantly enhances the emitted optical intensity by narrowing and focusing the beam. The lens effectively redirects and concentrates the photons into a tighter spot, enabling more optical power to be delivered to the receiver over longer distances. Importantly, this improvement is achieved without increasing the LED's driving current, which means the communication link can be extended while maintaining the same electrical power budget. As a result, the use of TIR optics enables better management of the transmitter's overall power consumption while simultaneously improving the link margin.

To further increase the available optical power at the receiver, this work employs an LED panel consisting of 20 individual LEDs, each equipped with its own TIR lens. This array configuration not only enhances the total emitted optical flux but also ensures that the concentrated beams remain well-directed over the same 330 cm distance. The LED panel is driven at a current of 330 mA and modulated using an AC signal with a peak-to-peak voltage of 20 V, providing sufficient modulation depth for reliable data transmission. This combined optical and electrical configuration enables the establishment of a stronger and more focused illumination pattern, thereby improving the performance and reach of the solar-panel-based communication system.

4.4 Bandwidth Enhancement Circuit

Proper receiver design plays a pivotal role when employing solar modules as optical communication receivers. Although solar modules offer advantages such as large detection area and cost-effectiveness, they inherently suffer from low bandwidth, which directly constrains the achievable system throughput. Several approaches have been explored to overcome this bandwidth limitation, including resistive loading, passive equalization, and active equalization. Each technique, however, introduces its own set of challenges.

The simplest method uses a resistive load, which offers minimal circuit complexity. Despite this simplicity, a purely resistive load makes the receiver highly vulnerable to ambient light variations and introduces a substantial DC component at the solar module output. These DC levels shift the operating point of the signal and may cause decision threshold errors in subsequent stages such as comparators or analog-to-digital converters, thereby compromising link reliability.

To mitigate these issues, passive equalization techniques can be employed. Passive equalizers suppress the DC component and attenuate low-frequency ambient noise, improving the usability of the received signal. However, due to the inherently low-pass behavior of solar

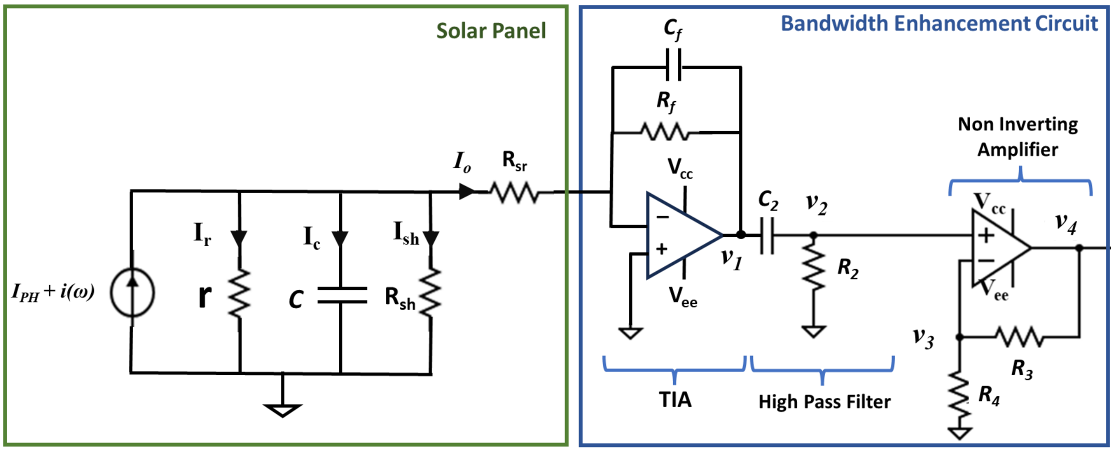

Figure 4.5: Modified solar module receiver.

modules, the signal amplitude decreases significantly at higher frequencies. Consequently, although passive equalization helps with noise reduction, the received voltage levels may still be insufficient to drive downstream digital circuitry, especially at higher data rates. To overcome these limitations, this work introduces a BEC, Design 2, specifically designed to augment the performance of solar modules in VLC applications, as illustrated in Fig. 4.5. The proposed receiver architecture comprises three key components: a solar module, a TIA stage, and an active equalizer. It is important to highlight the fundamental difference between photodiodes and solar panels in the context of optical detection. Photodiodes typically operate in photoconductive mode under reverse bias, which expands the depletion region, strengthens the internal electric field, and enhances the speed of carrier collection. This results in superior bandwidth and sensitivity. In contrast, solar panels operate in photovoltaic mode without external bias. While this mode is ideal for energy harvesting, it introduces high junction capacitance and limited electric field strength, resulting in slower response times and reduced bandwidth. Therefore, to interface a solar panel effectively with communication circuitry, a TIA becomes essential. The TIA serves two major roles:

- Providing a low-impedance load to counter the effects of the solar panel's high capacitance, thereby improving temporal response, and

- Converting the weak photocurrent generated by the solar panel into a voltage signal suitable for further processing.

The output of the TIA is then fed into the active equalizer, which consists of a high-pass filter followed by a non-inverting amplifier. This stage not only suppresses low-frequency and ambient-light-induced noise components but also amplifies the desired high-frequency communication signal. The combined effect of noise suppression and gain enhancement makes the active equalizer particularly beneficial for maintaining adequate signal strength at higher data rates. Fig. 4.5 can be analytically presented as:

$$I_o = I_{PH} + i(\omega) - (I_c + I_r + I_{sh}). \tag{4.5}$$

As optical intensity falls on the solar module, it converts it into an electrical equivalent output current (I_o) based on its responsivity. This output current consists of DC (I'_{PH}) and AC ($i'(\omega)$) electrical components, which reach the TIA stage after experiencing current leakage through the parasitic elements. The output voltage from TIA is given as:

$$v_1 = \frac{-Z_f(\omega)}{1 + R_{sr}(1/r + j\omega C + 1/R_{sh})}.(I'_{PH} + i'(\omega)), \tag{4.6}$$

where,

$$Z_f(\omega) = \frac{R_f(1/j\omega C_f)}{R_f + (1/j\omega C_f)}. \tag{4.7}$$

TIA circuit generates the voltage signal (v_1) based on the feedback branch impedance (Z_f). The Z_f is a parallel combination of feedback resistance (R_f) and feedback capacitance (C_f). The voltage, v_1, acts as an input to the high-pass filter stage, and the output of this stage is given by:

$$\frac{v_2}{v_1} = \frac{R_2}{R_2 + (1/j\omega C_2)}, \tag{4.8}$$

Proper selection of R_2 and C_2 allows only the required signal to pass, and the unwanted low-frequency signals get filtered out. This filtered output passes to the amplification stage.

Because the amplifier has negative feedback via the virtual-ground concept, v_2 equals v_3. The amplifier output voltage, v_4, is given as:

$$\frac{v_4}{v_3} = 1 + \frac{R_3}{R_4}, \tag{4.9}$$

from (4.6), (4.8), and (4.9) the output response obtained as:

$$v(\omega) = -\underbrace{\frac{Z_f}{1 + R_{sr}(1/r + j\omega C + 1/R_{sh})}}_{TIA\ output} \underbrace{\frac{R_2}{R_2 + (1/j\omega C_2)}\left(1 + \frac{R_3}{R_4}\right)}_{Active\ filtering} i'(\omega). \tag{4.10}$$

where, $v(\omega) = v_4$.

The amplified, filtered signal is obtained at the output terminal for further processing. The modified receiver output, expressed in (4.10), contains only the AC component of the incident optical signal, as all DC contributions are effectively removed by the filtering stage. Consequently, the overall system response is characterized by the cascaded behavior of the solar module followed by the BEC. Parameters for the designed analog circuit are as follows: $R_f = 100\ \Omega$, $R_2 = 100\ \Omega$, $C_2 = 10\ nF$ and op-amp is operating at five times gain. TIA at the solar panel output significantly improves the performance of the solar receiver with BEC design 2 compared to BEC design 1 discussed in the previous chapter.

As a result, the combined solar module–BEC architecture enhances signal integrity, improves high-frequency response, and enables significantly higher data rates compared to traditional resistive or passive equalization approaches. The measured frequency and time-domain performance of the proposed receiver configuration are presented and analyzed in the results section.

Table 4.1: Parameters for the conducted experiment.

Parameters	Parameter Values
Number of LEDs	20
Solar module open circuit voltage	5.88 V
Solar module short circuit current	60 mA
Ambient light at solar module	200 Lux
Distance	330 cm
BEC power consumption	120 mW
LED panel power consumption	9.6 W

4.5 Experiment Setup

Before performing the data transmission over a solar module, it is essential to determine the system's frequency and time response. Different load designs, such as resistive, passive equalizer, and BEC, are experimentally tested with the setup block diagram shown in Fig. 3.5. The setup consists of an AWG, Rigol DG 4202 with 200 MHz bandwidth, and a 500 MSa/s sampling rate, a bias tee, a 20 white light LEDs panel, a TIR lens on each LED, a solar module with different load designs, and a 100 MHz DSO with a 1 GSa/s maximum real-time sampling rate. Bias tee's one input comes from the AWG to send the sinusoidal waveform, and the other comes from the DC power supply, Keysight E3631A, to power up the LEDs. The LEDs are biased in the linear region to avoid signal clipping at the transmitter end. The experiment was conducted indoors, where ambient light sources provided 200 lux of illumination on the receiver in addition to the light received from the modulated LED panel. The other parameters are in Table 4.1.

Once the solar module frequency response is obtained, the communication capabilities are tested using data transmission. Light is modulated with a 16 QAM-OFDM modulation signal to transfer data. For further processing, a Li-Fi evaluation kit^{TM} from Velmenni is used [90]. The data transmission setup is shown in Fig. 4.6, where the transmission distance is 330 cm. The receiver unit comprises a solar module, BEC, and a digital signal processing board to process the incoming data.

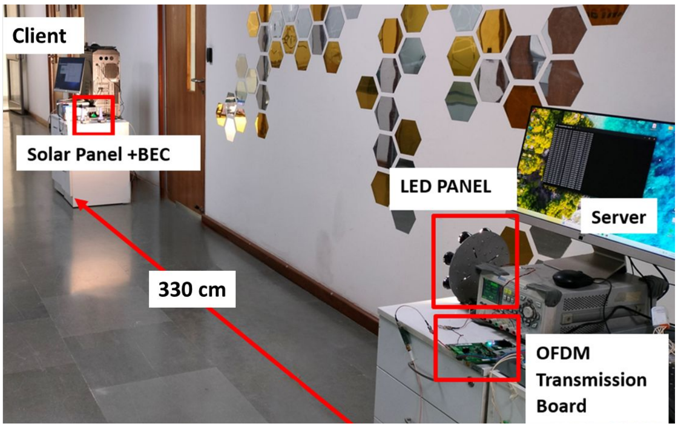

Figure 4.6: Solar module data transmission setup.

4.6 Performance Analysis

This section presents a comprehensive performance analysis of the proposed solar-panel-based optical wireless communication receiver. The evaluation focuses on both the temporal and spectral characteristics of the receiver, beginning with an examination of the time- and frequency-domain responses to quantify the effective bandwidth and signal fidelity. The impact of received optical power on key performance metrics, including data rate, signal distortion, and saturation behavior, is then analyzed to identify the operating limits of the receiver front-end.

Furthermore, the region of operation of the BEC is investigated to delineate its linear and saturation regimes and to assess its influence on overall system performance. Finally, the impact of receiver orientation on link reliability is examined to capture practical deployment considerations, particularly in dynamic scenarios where angular misalignment between the transmitter and the solar-panel receiver may occur. Together, these analyses provide a detailed understanding of the receiver's operational characteristics and practical performance constraints.

4.6.1 Time and Frequency Response

To enable the use of solar modules as practical optical receivers for communication, different load configurations were experimentally evaluated. In all experiments, a sinusoidal signal of

20 V peak-to-peak (V_{p-p}) was used to modulate a white LED source. Since the frequency response of the LED determines the strength of the transmitted optical signal, it directly influences the power received at the solar module. Therefore, before evaluating the receiver, the LED transmitter response was characterized using a standard PIN photodiode placed at the receiver. During transmission, a bias-tee was used to combine the AC modulation signal with a DC bias. The presence of the bias-tee introduces a reduced voltage swing at lower frequencies (approximately 5 kHz), resulting in reduced optical output. This phenomenon produces an upward slope in the measured frequency response between 1–10 kHz. However, at higher frequencies, the LED response stabilizes and remains nearly constant, ensuring that the transmitter does not impose additional bandwidth limitations on the designed receiver.

At the receiver end, the measured frequency response is shown in Fig. 4.7a. The 3-dB bandwidth (f_L, f_H) of the solar module was obtained by identifying the frequency range over which the response dropped by 3 dB from its maximum. As depicted in Fig. 4.7a, the solar module with a purely resistive load exhibits a 3-dB bandwidth of 206 kHz (spanning 4 kHz to 210 kHz). Although the resistive load offers a simple implementation, it also allows the passage of low-frequency and DC components of light. As a result, the received signal experiences a significant DC offset, making threshold-based decision circuitry, including ADCs, more prone to error within their operating range. To overcome this challenge, passive and active equalization techniques were evaluated. Passive equalization suppresses the DC and low-frequency components by employing a high-pass behavior, thereby increasing the usable bandwidth. However, this comes at the cost of reduced system gain. As shown in Fig. 4.7a, passive equalization increases the bandwidth to 289 kHz (between 21 kHz and 310 kHz) while effectively blocking low-frequency components, but the received signal amplitude decreases.

The impact of these approaches is shown in the time-domain responses in Fig. 4.7b. Fig. 4.7b(i) demonstrates the DC shift introduced by ambient and LED-originated DC light in the resistive load case. At higher switching frequencies (e.g., 800 kHz), the low-pass nature of the solar module further reduces the peak-to-peak voltage, as shown in Fig. 4.7b(ii). Passive

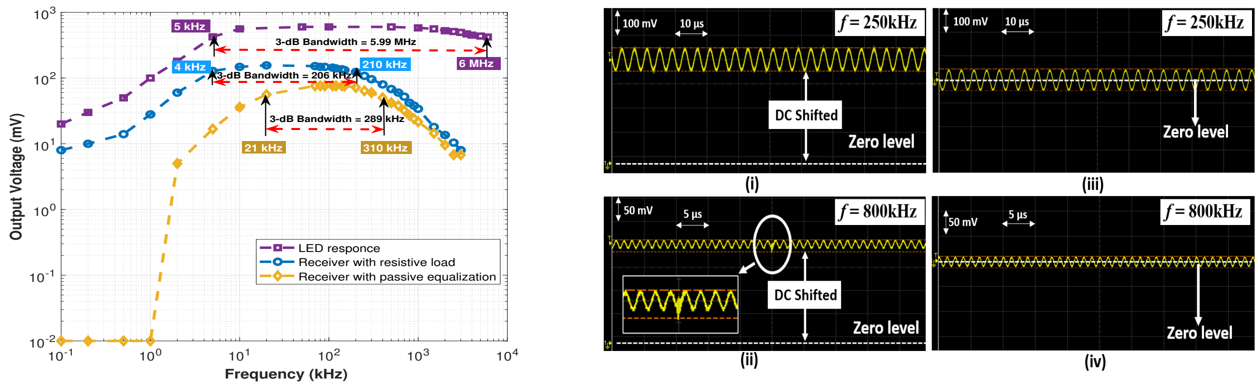

(a) (b)

Figure 4.7: (a) Frequency response depicting 3-dB bandwidth advantage of passive equalization over resistive load (b) Time response of solar module with i.) Resistive load at 250 kHz, ii.) Resistive load at 800 kHz, iii.) Passive equalization load at 250 kHz, iv.) Passive equalization load at 800 kHz.

equalization mitigates the DC shift by blocking low-frequency components, as illustrated in Fig. 4.7b(iii)–(iv), but it does not improve received signal strength. To address the limitations of both resistive and passive equalization loads, a bandwidth enhancement circuit (BEC) was designed and experimentally validated.

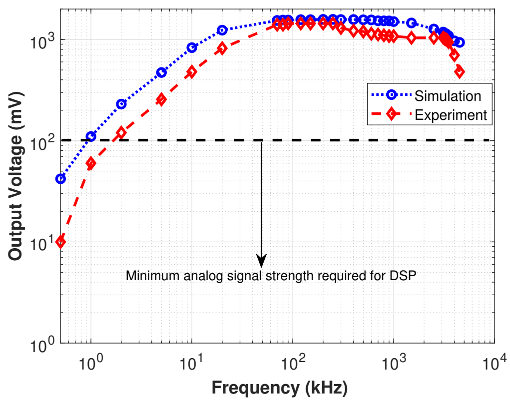

Figure 4.8: Simulation and experimental frequency response of the modified solar module receiver.

The LTspice simulated circuit and the frequency response of simulated and experimental observations of the raw solar receivers with resistive load are shown in Fig. 4.9 and Fig. 4.10, respectively. An additional circuit is designed ahead of the solar module's electrical equivalent circuit to capture the LED response in the LTspice simulation software. The LTspice simulated

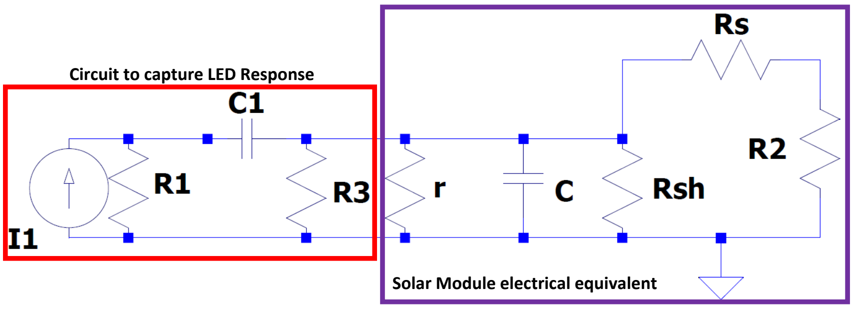

Figure 4.9: LTspice circuit simulation for raw solar module receiver

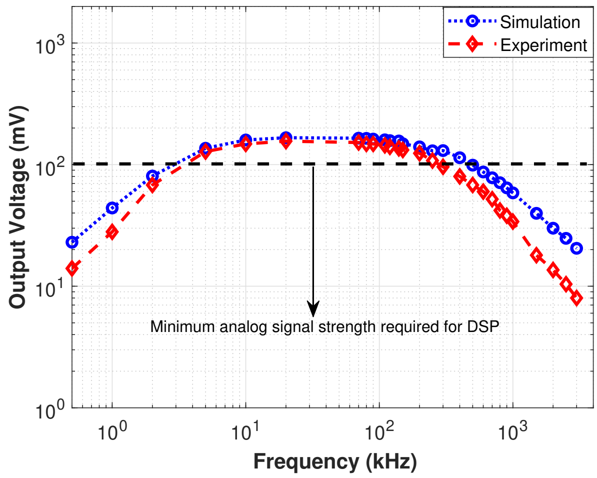

Figure 4.10: Frequency response of raw solar panel receiver

circuit and the frequency response of simulated and experimental observations of the modified solar receivers are shown in Fig. 4.11 and Fig 4.12, respectively. The results of circuit simulation and experimental results show a good match to confirm the bandwidth enhancement claim of solar module receivers using the designed analog circuitry.

Fig. 4.13(a) shows the frequency response of each stage. The TIA converts the photocurrent generated by the solar module into a voltage, achieving an upper cut-off frequency of approximately 38 MHz. The output then passes through the high-pass filter, which attenuates frequency components below 160 kHz and passes signals in the 160 kHz–38 MHz range. Thus, the combined response of the first two stages results in an effective passband of nearly

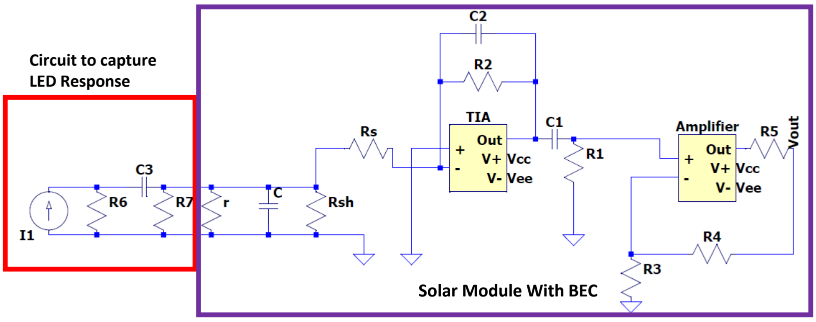

Figure 4.11: LTspice circuit simulation for modified solar module receiver

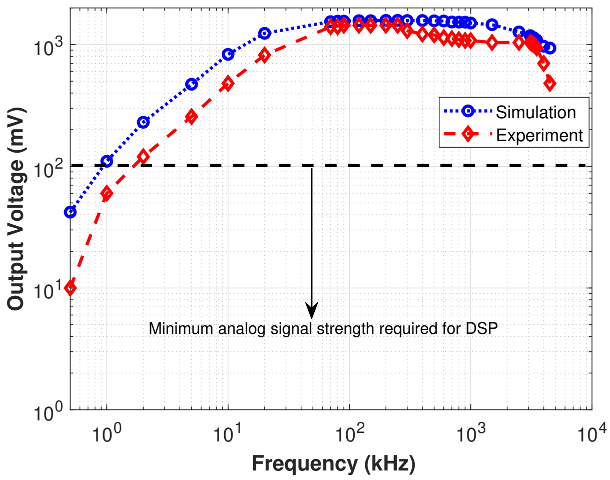

Figure 4.12: Frequency response of modified solar panel receiver

37.84 MHz, after which the gain decreases due to the TIA's high-frequency roll-off. The final stage consists of a non-inverting amplifier that ensures adequate signal amplitude for subsequent processing. With a bandwidth of approximately 33 MHz, this amplifier boosts all frequency components within range before its response begins to decline. Importantly, because the amplifier bandwidth is significantly greater than the intrinsic solar module bandwidth (33 MHz $\gg$ 3.5 MHz), it does not constrain the overall performance of the receiver. As a result of the BEC, the solar module achieves an enhanced 3-dB bandwidth of approximately 3.27 MHz (from 30 kHz to 3.3 MHz). The corresponding time-domain response, shown in Fig. 4.13b, indicates that unmodulated light components are effectively suppressed while providing a high peak-to-peak output signal. This confirms that the BEC design significantly improves the dynamic response of the solar module receiver.

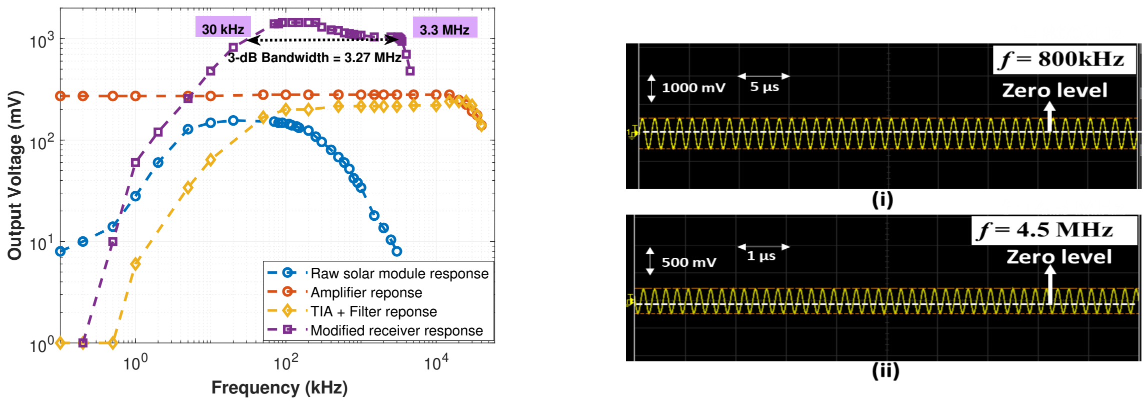

(a) (b)

Figure 4.13: (a) Frequency response of the modified solar module receiver (b) Time response of the solar module with (i) BEC load at 800 kHz, and (ii) BEC load at 4.5 MHz.

The results clearly demonstrate that the proposed BEC-based design substantially improves both the frequency and time-domain characteristics of the solar module receiver, enabling high-speed optical communication using low-cost, commercially available solar panels.

4.6.2 Receiver Region of Operation

The operational characteristics of the designed receiver are strongly influenced by the optical power incident on the solar module. Similar to conventional optical receivers, the modified solar receiver exhibits saturation behavior when subjected to excessively high optical intensity at a fixed link distance. To study this effect, the LED drive current was gradually increased, thereby increasing the emitted optical power, and the corresponding output of the BEC was recorded at a constant receiver position. As illustrated in Fig. 4.14, the output voltage of the designed receiver increases proportionally with the LED driving current up to a certain threshold. Beyond approximately 400 mA, the BEC output enters a saturation region where additional increases in optical power no longer translate into a proportional voltage increase. This saturation leads to clipping of the information-bearing signal, which can cause symbol distortion, amplitude compression, and degradation in bit-error performance. Such behavior is characteristic of photovoltaic-type receivers operating in conjunction with active amplification stages.

On the other end of the operating range, very low LED drive currents produce insufficient illuminance at the receiver. Due to the inherently low responsivity and high junction capacitance of the solar module, weak incident optical power results in small photocurrent generation, thereby producing a low-amplitude signal after the BEC. This weak signal may fall below the sensitivity threshold of the downstream comparator or demodulator, increasing the likelihood of detection errors. Experimental observations reveal that reliable operation is achieved only when the received optical intensity is maintained within an optimal illuminance window of approximately 180–3100 lux. Within this range, the BEC provides adequate gain without entering saturation, while also avoiding the low-signal regime where noise dominates.

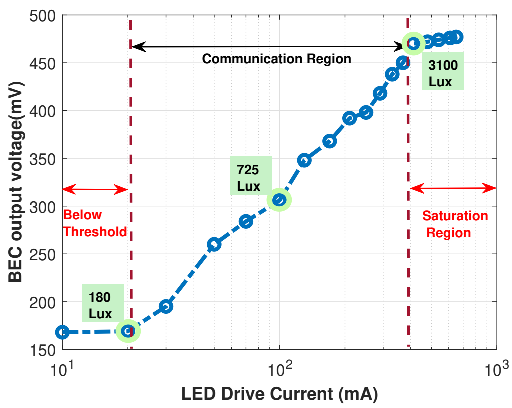

Figure 4.14: LED driving current versus BEC output voltage.

4.6.3 Impact of Distance on Data Rate

The performance of the designed solar-panel-based optical receiver in terms of achievable data rate as a function of transmission distance is illustrated in Fig. 4.15. The proposed receiver achieves a maximum data rate of 18.8 Mbps at a separation distance of 330 cm with zero packet loss, highlighting the optimal operating point of the system. Packet loss performance was evaluated using the *Iperf* network testing tool [91], where a total of 10^5 packets, each of size 1518 bytes, were transmitted for every tested distance. At separation distances below

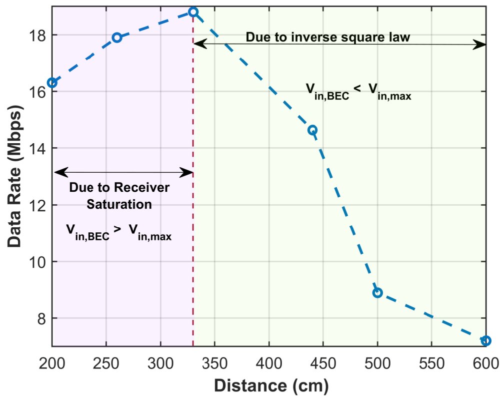

Figure 4.15: Distance vs Data rate.

330 cm, the receiver operates in a saturation regime due to excessive received optical power. In this region, the input voltage to the BEC exceeds its maximum linear operating limit ($V_{in,\text{BEC}} > V_{in,\text{max}}$), resulting in signal clipping at the output of the analog front-end. This nonlinear distortion degrades the effective extinction ratio and introduces symbol errors, which manifest as packet losses. For instance, at a distance of 200 cm, a data rate of 16.9 Mbps was achieved; however, a loss of 51 packets was observed due to pronounced clipping effects.

As the transmission distance increases beyond 330 cm, the received optical power decreases in accordance with the inverse square law, leading to a gradual reduction in the achievable data rate. Despite this reduction, reliable communication is maintained without any packet loss up to a distance of 600 cm. This behavior indicates that, although the signal amplitude decreases with distance, it remains within the linear operating region of the receiver front-end and above the minimum sensitivity threshold required for error-free packet detection.

Overall, these results demonstrate that the proposed receiver exhibits a well-defined operational region, with saturation-induced performance degradation at short distances and power-limited data rate reduction at longer distances. The absence of packet loss over a wide range of distances underscores the robustness of the receiver design and its suitability for practical optical wireless communication links.

4.6.4 Impact of Receiver Orientation

Device orientation plays a critical role in determining the performance and reliability of optical wireless communication links. Conventional VLC receivers, such as photodiodes, are highly susceptible to misalignment due to their small active area and narrow field of view. Under ideal conditions, the optical receiver should be oriented perpendicular to the incident light beam to ensure maximum signal reception. Any deviation by an angle θ° from this optimal alignment results in reduced received optical power and, consequently, degraded communication performance.

In contrast, solar modules offer a significantly larger active area,[1] which helps mitigate misalignment issues. This inherent advantage makes solar modules more robust for practical VLC deployments where the receiver may not always be ideally aligned.

Figure 4.16 illustrates the experimental setup used to study the effect of receiver orientation, where the solar module is rotated along the XY plane by an angle θ°. The corresponding impact on achievable data rate is presented in Fig. 4.17.

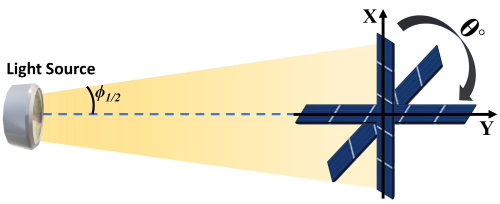

Figure 4.16: Solar module orientation setup.

As shown in Fig. 4.17, at an orientation of 0°, the solar module directly faces the LED source, enabling maximum optical power capture and achieving the peak data rate of 18.8 Mbps. As the orientation angle increases, the effective incident optical power reduces due to geometric misalignment, resulting in a gradual degradation in received signal strength and data rate.

Nevertheless, despite a significant 40° rotation, the solar module still maintains a data rate of 7.6 Mbps. This demonstrates the robustness of solar receivers against angular misalignment.

[1] Although a larger solar panel area can improve the SNR due to increased optical collection, the associated parasitic capacitances may cause nonlinear distortions and limit the achievable system bandwidth.

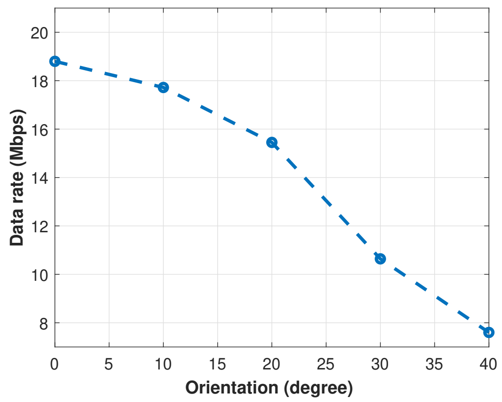

Figure 4.17: Data rate performance for varying receiver orientation.

For comparison, a conventional photodiode under the same rotational conditions experiences a complete outage, highlighting the superior tolerance of solar modules in practical VLC scenarios.

4.7 Summary

This chapter presented the design, implementation, and experimental validation of a solar-panel-based OWC receiver for high-speed VLC. To address the inherent limitations of solar modules, namely low bandwidth and strong sensitivity to DC ambient light, a BEC comprising a TIA, a high-pass filter, and a non-inverting amplifier was developed. The proposed circuitry effectively suppresses DC components, mitigates ambient light noise, and provides an optimal electrical load to the solar panel, resulting in a 3-dB bandwidth enhancement to 3.27 MHz.

On the transmitter side, TIR lenses were employed with white LEDs to reduce beam divergence, increase the Lambertian order, and enhance the channel gain without increasing the LED drive current. An LED panel consisting of 20 TIR-assisted LEDs enabled improved optical intensity and extended communication range. Experimental results using 16-QAM OFDM demonstrated a peak data rate of 18.8 Mbps over a 330 cm link and a maximum distance–data-rate combination of 600 cm at 7.8 Mbps. The system also exhibited strong robustness to receiver misalignment, achieving 7.6 Mbps at a 40° rotation in the XY plane.

The results confirm that the large active area of solar panels significantly alleviates alignment and orientation constraints compared to conventional photodiode receivers, thereby reducing system complexity while enhancing practical deployability.

Chapter 5

Simultaneous Light Information and Power Transfer using Solar Panels in Indoor Environment

5.1 Motivation

Earlier, the communication capabilities of solar panels were discussed, and it was demonstrated that the inherent 3-dB bandwidth limitation can be significantly improved through appropriate analog circuit design. While these enhancements enable reliable data reception, solar panels inherently offer dual functionality by supporting both optical communication and energy harvesting. Therefore, the analog front-end was further modified and experimentally evaluated to enable simultaneous optical communication and energy harvesting, thereby extending the utility of the solar panel beyond standalone receiver operation.

5.2 Chapter Contributions

The major contributions of this chapter are summarized as follows:

- The analog front-end was further enhanced and experimentally validated to support simultaneous optical wireless communication and energy harvesting, demonstrating its dual-function capability without compromising system performance.
- The influence of solar panel size on both communication quality and energy harvesting efficiency was also investigated through experimental evaluation, providing insights into the tradeoffs and design considerations for integrated systems.

5.3 Frequency-Selective Receiver Design for Simultaneous Communication and Energy Harvesting

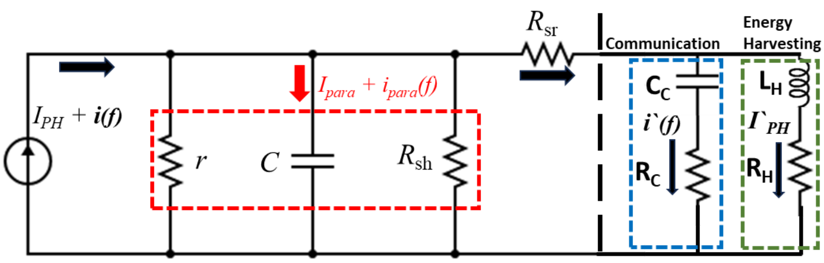

Figure 5.1: Simultaneously power harvesting and communication circuit

Fig. 5.1 illustrates the proposed frequency-selective receiver architecture for simultaneous power harvesting and optical communication using a photovoltaic (PV) cell. The received optical signal consists of a DC component generated by continuous illumination and a high-frequency AC component corresponding to the intensity-modulated communication signal. Accordingly, the photovoltaic cell is represented by an equivalent circuit comprising the photocurrent source, dynamic resistance r, junction capacitance C, shunt resistance R_{sh}, and series resistance R_{sr}. The generated photocurrent is divided into an internal parasitic current associated with the intrinsic PV characteristics and an external current delivered to the receiver circuit. To enable simultaneous communication and power harvesting, the external circuit is divided into two frequency-selective branches. The communication branch employs a series RC high-pass filter formed by the coupling capacitor C_C and load resistance R_C, allowing only the high-frequency modulation components to reach the communication receiver while blocking the DC photocurrent. Conversely, the energy harvesting branch consists of an RL low-pass filter formed by the harvesting inductor L_H and load resistance R_H. The inductor provides a low-impedance path for the DC photocurrent while presenting a high impedance to the communication signal, thereby preventing the AC modulation from being dissipated in the harvesting circuit. Consequently, the proposed architecture performs frequency-domain separation of the harvested power and communication signal without requiring active switching or signal processing.

The effectiveness of the filtering approach is evaluated by varying the communication load resistance, R_C, while maintaining the remaining circuit parameters unchanged. The corresponding communication and energy harvesting characteristics are summarized in Table 5.1. As expected from the first-order high-pass filter, the communication cutoff frequency decreases according to

$$f_c = \frac{1}{2\pi R_C C_C},$$

decreasing from 159.15 kHz to 1.59 kHz as R_C increases from 100 Ω to 10 kΩ. The reduction in cutoff frequency directly influences the communication response, where the upper cutoff frequency decreases from 445.31 kHz to 48.21 kHz, resulting in a reduction of the available 3-dB communication bandwidth from 432.31 kHz to 45.94 kHz. These results indicate that increasing the communication load resistance progressively limits the high-frequency response of the communication branch.

A notable observation from Table 5.1 is that the communication branch has a negligible impact on the energy harvesting performance. Throughout the investigated range of R_C, the peak harvested power remains nearly constant at approximately 14.81 mW, while the harvested

Table 5.1: Effect of Communication Load Resistance on Communication and Energy Harvesting Performance

R_C (Ω)	f_c (kHz)	$f_{\max}$ (kHz)	$f_{\min}$ (kHz)	BW (kHz)	P_{peak} (mW)	BW_H (kHz)
100	159.15	445.31	13.00	432.31	14.81	2.75
1200	13.26	83.08	6.69	76.39	14.81	2.67
2300	6.92	64.28	4.86	59.42	14.81	2.59
3400	4.68	58.10	3.91	54.19	14.81	2.55
4500	3.54	54.60	3.40	51.20	14.81	2.53
5600	2.84	52.51	3.00	49.51	14.81	2.51
6700	2.38	51.30	2.75	48.55	14.81	2.51
7800	2.04	49.73	2.55	47.18	14.81	2.51
8900	1.79	49.35	2.39	46.96	14.81	2.51
10000	1.59	48.21	2.27	45.94	14.81	2.51

bandwidth changes only slightly from 2.75 kHz to 2.51 kHz. This demonstrates that the communication filter introduces minimal electrical loading on the harvesting branch. Unlike conventional receiver architectures, where communication and harvesting circuits compete for the received signal energy, the proposed frequency-selective design effectively decouples the two functionalities by exploiting their distinct frequency characteristics.

These results highlight that the selection of the communication and harvesting filter components is critical for achieving effective branch isolation. Appropriate design of the RC high-pass communication filter and RL low-pass harvesting filter enables independent optimization of the communication bandwidth while preserving the harvested power.

5.4 Modified Optical Receiver Design

In the previous chapter, the feasibility of using a solar panel as an optical communication receiver was established by systematically addressing several inherent limitations. In particular, the following challenges associated with solar-panel-based receivers were identified and mitigated through appropriate analog front-end design:

- ***Impact of unmodulated light components***, which introduce strong DC offsets and degrade the detection of weak modulated signals.
- ***High capacitive effect of the solar panel***, arising from its large junction area, which limits the receiver's high-frequency response.
- ***Limited 3-dB bandwidth***, which constrains the achievable data rate in optical wireless communication systems.

While these challenges were effectively addressed to enhance the communication performance, an important aspect remains to be explored: the ability of a solar panel to support *simultaneous optical communication and energy harvesting*. Exploiting this dual functionality is crucial for realizing sustainable and energy-efficient optical wireless systems, particularly in applications such as intelligent transportation systems and outdoor deployments.

To this end, a modified analog optical receiver architecture is proposed in this chapter. The new design enables concurrent extraction of the AC communication signal and the DC power component from the received optical signal, allowing the solar panel to function as both an information receiver and an energy harvester. Furthermore, the impact of solar panel size on communication performance and harvested energy is investigated, providing insights into the trade-offs between bandwidth, received signal strength, and energy harvesting efficiency. This analysis lays the foundation for a unified framework supporting SLIPT using solar-panel-based optical receivers. The designed analog circuitry, along with the solar panel, is shown in Fig. 5.2. When the light-carrying information falls over a solar panel, it generates a DC component (I_{PH}) and an information-carrying component (i_{ω}). These generated current components will reach the load after loss due to parasitic impedance (r, C, R_{sh}, R_{sr}). The designed analog circuitry receives the DC component (I'_{PH}) and information carrying component (i'_{ω}). At node v_{DC}, these components will be divided into an energy harvesting branch consisting of a series combination of inductance (L_{DC}) and resistance (R_{DC}), and a communication branch.

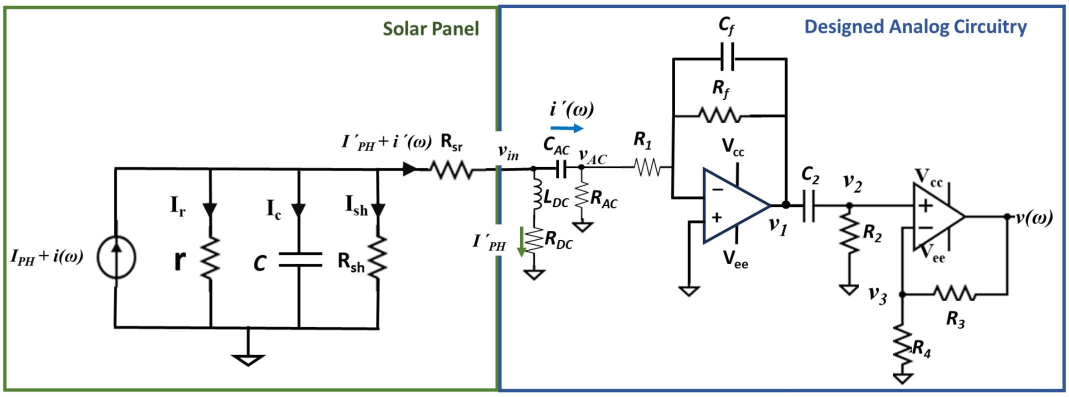

Figure 5.2: Modified solar receiver design

The voltage received at node, v_{AC}, is given as follows:

$$v_{AC} = v_{in} \cdot \left(1 + \frac{X_{AC}}{Z + R_{sr}} + \frac{X_{AC}}{Z_L}\right) - i'(\omega)\left(\frac{X_{AC}}{1 + \frac{R_{sr}}{Z}}\right) \tag{5.1}$$

where the parasitic branch impedance is, $Z = 1/r + j\omega C + 1/R_{sh}$, the energy harvesting branch impedance is, $Z_L = j\omega L_{DC} + R_{DC}$, the capacitive impedance is $X_{AC} = 1/j\omega C_{AC}$, and, the switching frequency (f), $\omega = 2\pi f$. Proper selection of R_{AC} and C_{AC} will decide the high-pass filter cut-off, allowing only the required signal to pass, and the unwanted low-frequency signals get filtered out. This filtered output passes to the amplification stage. The amplifier output voltage, v_1, is given as:

$$v_1 = \left(1 + \frac{R_f}{R_1}\right) v_{AC}. \tag{5.2}$$

This generated signal is again passed to the high-pass filter to suppress the lower frequency component, which is amplified due to the amplifier stage, and provides the voltage gain to the required band of frequency. The output response obtained is:

$$v(\omega) = \underbrace{v_{in} \cdot \left(1 + \frac{X_{AC}}{Z + R_{sr}} + \frac{X_{AC}}{Z_L}\right) - i'(\omega)\left(\frac{X_{AC}}{1 + \frac{R_{sr}}{Z}}\right)}_{Solar\ panel\ output} \underbrace{\left(1 + \frac{R_f}{R_1}\right)}_{First\ stage\ amplifier} \underbrace{\left(\frac{R_2}{R\ 2} + (1/j\omega C_2)\right)\left(1 + \frac{R_3}{R_4}.\right)}_{Active\ filtering} \tag{5.3}$$

The amplified, filtered signal is obtained at the output terminal for further processing.

After filtering the received optical signal at node v_{in}, the modulated information-bearing AC component is routed towards the communication branch, while the remaining photocurrent component, denoted as I'_{PH}, is directed to the energy harvesting branch. This current represents the effective DC photocurrent generated due to the incident optical power after the removal of high-frequency signal components.

The harvested electrical power is determined by the magnitude of the extracted photocurrent I'_{PH} and the voltage developed across the DC load resistance R_{DC}. Assuming steady-state operation, the harvested power can be expressed as

$$P_{\text{harvested}} = I'_{PH} V_{DC}. \tag{5.4}$$

where V_{DC} is the voltage across R_{DC} and is directly influenced by the incident optical intensity, the electrical characteristics of the solar panel, and the chosen load resistance. This relationship highlights the inherent trade-off between energy harvesting and communication performance, as circuit parameters optimized for maximizing I'_{PH} and V_{DC} may impact the bandwidth and signal quality of the communication branch.

5.5 Experiment Setup

To determine the system's frequency and time response solar panels are experimentally tested with the setup block diagram illustrated in Fig. 3.5. The setup consists of an AWG, Rigol DG 4202, a bias tee, a 20-white-light-LED panel, a TIR lens on each LED, a solar module with different load designs, and a DSO, DS 1102E. Bias tee's one input comes from the AWG to send the sinusoidal waveform, and the other comes from the DC power supply, Keysight E3631A, to power up the LEDs. The LEDs are biased in the linear region to avoid signal clipping at the transmitter end. The experiments are conducted in a room with ambient lighting of 200 lux and the other parameters listed in Table 5.2. After determining the frequency response of the solar module, data transmission tests are carried out to evaluate communication capabilities. The light is modulated using a 16 QAM-OFDM signal for data transfer using Velmenni Li-Fi Evaluation Kit^{TM} [90]. The data transmission setup, shown in Fig. 5.3, has a transmission distance of 2 meters.

Table 5.2: Testing parameters.

Parameters	Parameter Values
Number of LEDs with TIR lens	20
Solar Panel 1 open circuit voltage	11.24 V
Solar Panel 1 short circuit current	0.64 A
Solar Panel 2 open circuit voltage	5.88 V
Solar Panel 2 short circuit current	60 mA
Ambient light at solar module	200 Lux
Distance between transmitter and receiver	2 m
Analog circuit power consumption	100 mW
LED panel power consumption	8 W

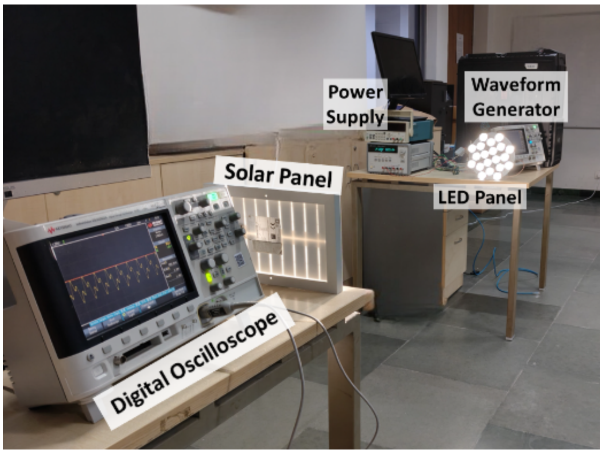

Figure 5.3: Solar module data transmission setup.

5.6 Results and Discussion

This section presents a comparative analysis of the impact of solar panel cell size on both optical communication performance and energy harvesting capability. Two solar panel configurations are considered. Solar Panel 1 consists of cells with dimensions of 2.5 cm $\times$ 8 cm, with all cells connected in series, whereas Solar Panel 2 comprises smaller cells of size 0.7 cm $\times$ 3 cm, also connected in series. These two configurations enable an investigation into the role of active area and junction capacitance on system performance.

The analysis includes frequency-domain measurements to quantify the effect of the proposed analog circuitry on the achievable 3-dB bandwidth, as well as time-domain evaluations to illustrate signal conditioning before and after the designed circuitry for both solar panels. In addition, the harvested electrical power is measured and correlated with the achieved data rates, thereby highlighting the trade-offs between communication performance and energy harvesting. Together, these results provide comprehensive insights into the influence of solar panel size on simultaneous optical communication and energy harvesting.

5.6.1 Experimental Outcomes of Frequency Response Analysis

Solar panels are conventionally designed for energy harvesting applications, which restricts their effective operation to low-frequency regimes. As a consequence, when directly used as optical receivers, solar panels typically exhibit a limited 3-dB bandwidth on the order of a few tens of kilohertz. This inherent limitation primarily arises from the large junction capacitance associated with the extensive active area of solar cells.

The experimental observations corroborate this behavior. Solar Panel 1, characterized by a larger cell area, exhibits a 3-dB bandwidth of approximately 40 kHz, as shown in Fig. 5.4. In contrast, Solar Panel 2, which has a smaller cell area, demonstrates an improved 3-dB bandwidth of about 80 kHz, as illustrated in Fig. 5.5. These results highlight the inverse relationship between solar cell area and achievable bandwidth.

While such bandwidths are insufficient to support high data rate communication, the proposed analog front-end significantly enhances the receiver frequency response. Specifically, the designed active high-pass filter suppresses low-frequency components and selectively amplifies higher-frequency signal content. As a result, the effective 3-dB bandwidth is extended to 2.47 MHz and 2.77 MHz for Solar Panel 1 and Solar Panel 2, respectively, while maintaining

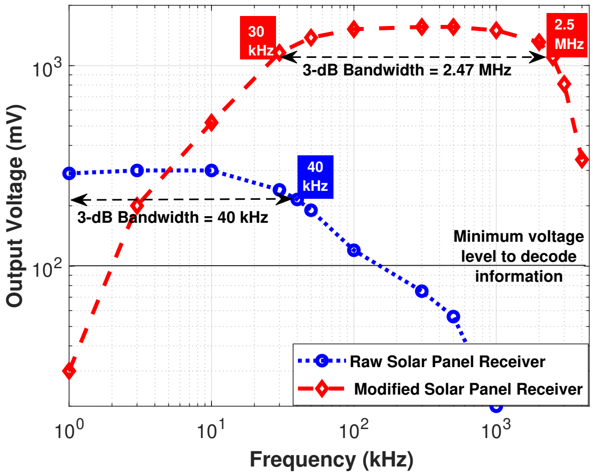

Figure 5.4: Frequency response of modified receiver with solar panel 1 (11.24 V, 0.64 A).

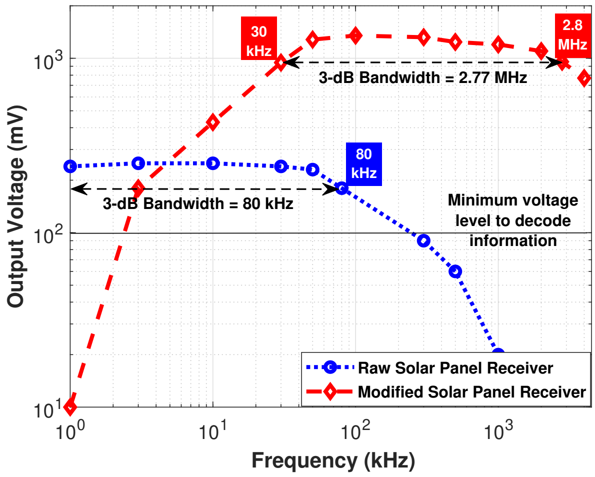

Figure 5.5: Frequency response of modified receiver with solar panel 2 (5.88V, 60 mA).

a minimum output voltage level of 100 mV. This improvement enables reliable high-speed optical communication without compromising the energy harvesting functionality of the solar panels.

5.6.2 Experimental Outcomes of Time-Domain Response Analysis

For successful data transmission, proper signal conditioning at the receiver is a critical performance metric. Although the frequency-domain analysis demonstrated a significant enhancement in the receiver bandwidth after employing the modified analog circuitry, the time-domain behavior of the received signal is also strongly influenced by the inherent capacitive characteristics of the solar panel. In particular, the higher junction capacitance associated with larger-area solar panels can lead to waveform distortion, even when sufficient bandwidth is available.

To investigate this effect, a square waveform was generated using AWG and transmitted over the optical link. At the receiver, the time-domain response of the solar panels was analyzed both without and with the proposed analog circuitry. The received waveforms without analog

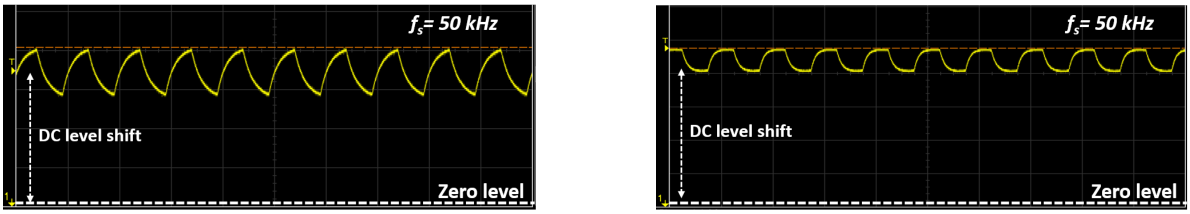

(a) Solar panel 1 (11.24 V, 0.64 A) (b) Solar panel 2 (5.88V, 60 mA)

Figure 5.6: Time-domain response without analog circuitry: (a) Solar Panel 1, (b) Solar Panel 2.

circuitry are shown in Fig. 5.6. A 30 kHz square waveform was transmitted, which lies well within the intrinsic 3-dB bandwidth of both solar panels. Owing to its larger cell area and consequently higher capacitance, Solar Panel 1 exhibits slow charging and discharging behavior, resulting in an exponential rise and decay rather than a sharp square waveform. In contrast, Solar Panel 2, with a smaller effective capacitance, is able to regenerate the square waveform with significantly reduced distortion. Additionally, both solar panels generate a DC photocurrent due to ambient illumination, leading to a noticeable DC level shift in the received signal. If left unfiltered, this DC offset can drive the amplifier beyond its linear operating region, causing signal clipping and distortion.

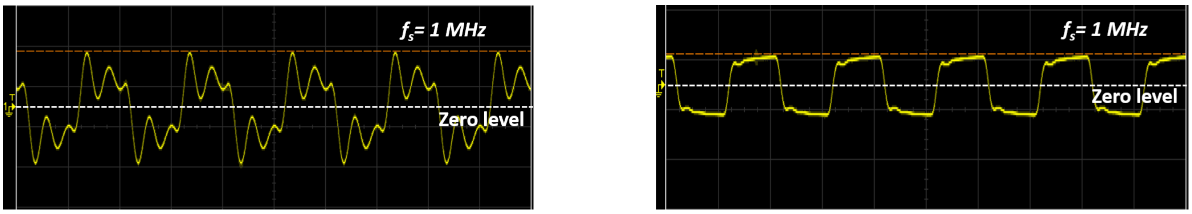

(a) Solar panel 1 (11.24 V, 0.64 A) (b) Solar panel 2 (5.88V, 60 mA)

Figure 5.7: Time-domain response with analog circuitry: (a) Solar Panel 1, (b) Solar Panel 2.

With the inclusion of the designed analog circuitry, the effective 3-dB bandwidth of both solar panels is significantly enhanced. To evaluate the corresponding signal conditioning performance, a 1 MHz square waveform was transmitted, and the received responses are shown in Fig. 5.7. The results clearly indicate that bandwidth enhancement alone does not guarantee improved time-domain signal fidelity. Due to the inherently high capacitive nature of large-area solar cells, nonlinear distortion remains prominent in Solar Panel 1, as observed in Fig. 5.7a. In comparison, Solar Panel 2 exhibits a substantially cleaner waveform, as shown in Fig. 5.7b. Importantly, the designed analog circuitry effectively suppresses the DC level shift in both cases, ensuring that the received signal remains within the linear operating range of the amplification stages.

5.6.3 Data Rate and Energy Harvested

Solar panels functioning as simultaneous information and power receivers are a key enabler for future energy-efficient communication networks. However, the performance of such systems is strongly influenced by intrinsic solar panel characteristics, including active area, number of cells, and panel material, which jointly determine both the communication quality and the energy harvesting capability. As shown in Fig. 5.8, Solar Panel 1, with a larger cell area, collects a higher amount of incident optical power and consequently harvests 38.4 mW of electrical power. Nevertheless, the high capacitive effect associated with the larger area leads to poor signal conditioning, resulting in information loss and limiting the achievable data rate to 1.84 Mbps. In contrast, Solar Panel 2 exhibits superior signal conditioning due to its smaller cell area, enabling a significantly higher data rate of 12.4 Mbps. However, the reduced active area limits the collected optical energy, yielding a harvested power of only 4.5 mW. These results clearly illustrate the fundamental trade-off between communication performance and energy harvesting in solar-panel-based simultaneous light information and power transfer systems.

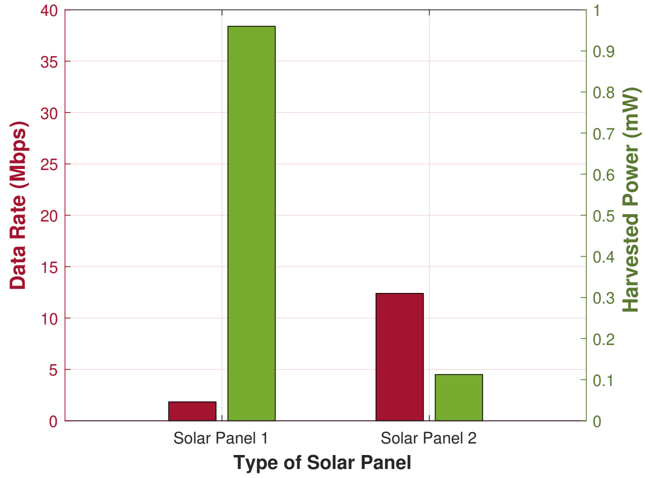

Figure 5.8: Data rate and harvested energy for solar panel 1 (11.24 V, 0.64 A) and solar panel 2 (5.88V, 60 mA).

5.7 Summary

This chapter investigated the feasibility of using solar panels as simultaneous information and power receivers for optical wireless communication systems. A modified analog front-end was developed to enable concurrent extraction of communication signals and harvested energy, while mitigating the effects of ambient light and limited intrinsic bandwidth. Through frequency- and time-domain analyses, the impact of solar panel cell size on bandwidth, signal conditioning, and nonlinear distortion was systematically evaluated.

Experimental results demonstrated that larger-area solar panels harvest higher electrical power but suffer from increased capacitive effects that degrade signal quality and limit achievable data rates. In contrast, smaller-area solar panels provide improved signal conditioning and support significantly higher data rates at the cost of reduced harvested power. These findings highlight the fundamental trade-off between communication performance and energy harvesting capability, and establish design guidelines for selecting solar panel characteristics in sustainable SLIPT systems.

Chapter 6

Comparative Evaluation of Solar Panel Configurations and Their Impact on Communication Performance

6.1 Motivation

Despite growing interest in solar panels as optical wireless communication receivers, existing studies have largely focused on validating feasibility rather than examining how different electrical configurations influence receiver performance. In particular, the impact of solar module interconnection configuration schemes on key communication metrics remains unexplored. The effects of configurations on bandwidth, achievable data rate, communication range, and simultaneous energy harvesting have not been systematically investigated. This lack of comparative analysis limits the ability to optimize solar panel–based receivers for practical communication systems. Motivated by this gap, this chapter presents an experimental evaluation of different solar panel configurations, providing quantitative insights into their influence on communication performance and energy harvesting efficiency.

6.2 Chapter Contribution

The major contribution of this chapter is summarized as follows:

- Different solar panel configurations are used in the real world based on the applications. To examine the impact of the same on the communication performance, this chapter experimentally compares the communication performance of a single solar panel and a parallel-connected solar panel.

6.3 Impact of Configuration

At the receiver side, off-the-shelf solar panels provide a low-cost and environmentally sustainable alternative to conventional photodiodes for optical wireless communication. However, due to their inherently low responsivity and large junction capacitance, the generated photocurrent under LED illumination is weak, which fundamentally limits the achievable communication range and data rate. Consequently, the electrical interconnection configuration of multiple solar modules plays a critical role in determining the overall receiver performance.

Among the possible interconnection schemes, the parallel configuration is of particular interest from a communication perspective, as it directly enhances the detected photocurrent without increasing the operating voltage. By summing the individual photocurrent of multiple modules, a higher received signal amplitude can be achieved, leading to improved signal strength and extended communication distance.

6.4 Solar Panel as Communication Receiver

This section examines the effects of parallel configurations, parameter extraction, and the impact of the proposed analog circuitry through analytical modeling.

6.4.1 Extension of AC Small-Signal Model for Parallel Solar Panel Configurations

To enhance the output photocurrent, multiple solar modules can be connected in a parallel configuration as shown in Fig. 6.1. Total output current across the resistive load is given by:

$$I_{Parallel} = I_{Parallel_1} + I_{Parallel_1} + \ldots + I_{Parallel_N}. \tag{6.1}$$

Effective output current increases, although this will impact the communication bandwidth.

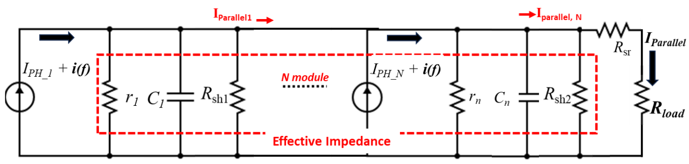

Figure 6.1: Parallel configuration of solar modules.

Starting from the AC small-signal model of a solar panel given in (**??**), the voltage-to-current transfer function can be expressed as

$$H(f) = \frac{v(f)}{i(f)} = \frac{\frac{R_{load}}{(R_{load}+R_{sr})}}{G + j2\pi f C}, \tag{6.2}$$

The conductance term G in (6.2) is defined as:

$$G = \frac{1}{r} + \frac{1}{R_{sh}} + \frac{1}{(R_{sr} + R_{load})}, \tag{6.3}$$

which accounts for the combined contribution of the diode dynamic resistance, shunt leakage path, and the load-dependent branch. From (6.2), the -3 dB cutoff frequency of the system is obtained as:

$$f_c = \frac{G}{2\pi C}, \tag{6.4}$$

indicating that the receiver bandwidth is fundamentally governed by the ratio between the effective conductance and the junction capacitance.

6.4.1.1 Parallel Solar Panel Configuration

For N identical solar panels connected in parallel, the effective junction capacitance increases linearly with N, while the resistive parameters scale inversely with N, yielding

$$\begin{aligned} C_{\text{parallel}} &= NC, \qquad r_{\text{parallel}} = \frac{r}{N}, \\ R_{sr,\text{parallel}} &= \frac{R_{sr}}{N}, \quad R_{sh,\text{parallel}} = \frac{R_{sh}}{N}. \end{aligned} \tag{6.5}$$

Substituting these equivalent parameters into the conductance expression leads to the parallel configuration conductance

$$G_{\text{parallel}} = \frac{N}{r} + \frac{N}{R_{sh}} + \frac{1}{(R_{sr}/N + R_{load})}. \tag{6.6}$$

Accordingly, the cutoff frequency for the parallel-connected solar panels is given by

$$f_{c,\text{parallel}} = \frac{G_{\text{parallel}}}{2\pi C_{\text{parallel}}} = \frac{G_{\text{parallel}}}{2\pi (NC)}. \tag{6.7}$$

For the practical case where the load resistance is much larger than the scaled series resistance ($R_{load} \gg \frac{R_{sr}}{N}$) the (6.7) simplifies to:

$$f_{c,\text{parallel}} \approx \frac{1}{N} f_c, \tag{6.8}$$

which highlights that increasing the number of parallel-connected panels reduces the bandwidth due to the linear growth of junction capacitance.

6.4.1.2 Asymptotic Saturation Behavior

Substituting (6.6) into (6.7), the cutoff frequency can be expressed explicitly as

$$f_{c,\text{parallel}} = \frac{1}{2\pi C} \left[\frac{1}{r} + \frac{1}{R_{sh}} + \frac{1}{N(R_{sr}/N + R_{load})} \right]. \tag{6.9}$$

As the number of parallel-connected panels increases, the term $(R_{sr}/N + R_{load})$ becomes increasingly dominated by R_{load}. Consequently,

$$\lim_{N\to\infty} \frac{1}{N(R_{sr}/N + R_{load})} \approx \frac{1}{NR_{load}} \to 0. \tag{6.10}$$

Therefore, the cutoff frequency approaches a finite upper bound given by

$$f_{c,\text{parallel}}^{\text{sat}} = \frac{1}{2\pi C}\left(\frac{1}{r} + \frac{1}{R_{sh}}\right). \tag{6.11}$$

This result demonstrates that beyond a certain number of parallel-connected solar panels, further increase in N does not yield a proportional bandwidth improvement. Instead, the system bandwidth becomes limited by the intrinsic diode resistance and shunt leakage paths of the solar panel, leading to the experimentally observed saturation behavior. This result indicates that increasing the number of parallel solar panels beyond a threshold does not further improve the bandwidth, since the dominant limitation arises from the intrinsic diode resistance and shunt leakage paths rather than the load resistance. Similarly, the output voltage in the parallel configuration is given by:

$$v_{out}(f) = \frac{R_{load}}{(R_{load} + R_{sr,parallel})} \cdot \frac{i(f)}{G_{parallel} + j2\pi f C_{parallel}}. \tag{6.12}$$

As N increases, $R_{sr,parallel} = R_{sr}/N \to 0$, and hence

$$\frac{R_{load}}{(R_{load} + R_{sr,parallel})} \to 1. \tag{6.13}$$

Moreover, since $G_{parallel}$ grows linearly with N while $C_{parallel}$ also grows linearly with N, their ratio approaches a constant value. Consequently, the output voltage magnitude converges to

$$\lim_{N\to\infty} |v_{out}(f)| = \text{constant}. \tag{6.14}$$

Therefore, both the cutoff frequency and output voltage exhibit saturation behavior beyond a critical number of parallel-connected solar panels. This effect is experimentally illustrated in Fig. 6.2, where the response of the receiver is shown for different numbers of parallel-connected modules.

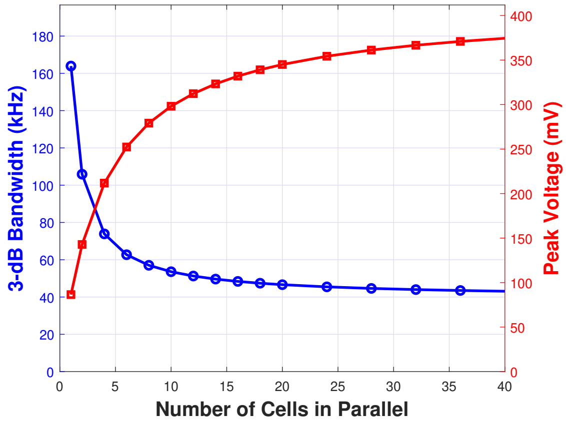

Figure 6.2: Response of parallel solar modules.

The results indicate that increasing the number of parallel-connected modules leads to a higher peak output voltage due to the increased photocurrent. However, this improvement is accompanied by a reduction in the 3-dB bandwidth of the receiver. A pronounced bandwidth degradation is observed up to eight parallel modules, beyond which the rate of deterioration becomes more gradual. This behavior reveals a fundamental trade-off between signal amplitude and bandwidth when scaling the receiver using parallel-connected solar modules.

Based on these observations, this study focuses on a comparative analysis between a single-module receiver and an eight-module parallel configuration, which represents a practical operating point that balances signal enhancement and bandwidth reduction. The experimentally measured frequency responses of the single-module and parallel configurations are presented in Fig. 6.3.

The results demonstrate that the single solar module achieves a 3-dB bandwidth approximately three times higher than that of the parallel configuration. In contrast, the parallel configuration provides a voltage gain exceeding five times that of the single-module receiver within its 3-dB bandwidth region. These findings clearly highlight the configuration-dependent

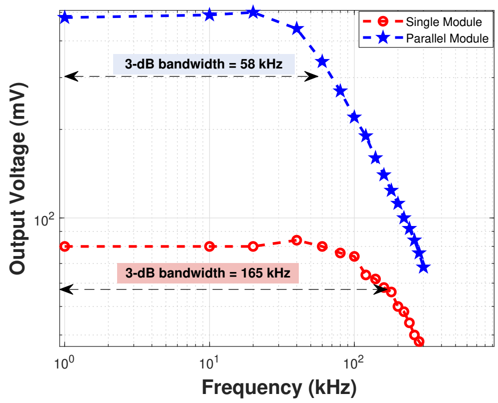

Figure 6.3: Frequency response of single solar module and parallel configuration.

trade-off between bandwidth and received signal strength, which is a key design consideration for solar panel–based optical communication receivers. The experimental setup used to evaluate the impact of receiver configuration is shown in Fig. 6.4.

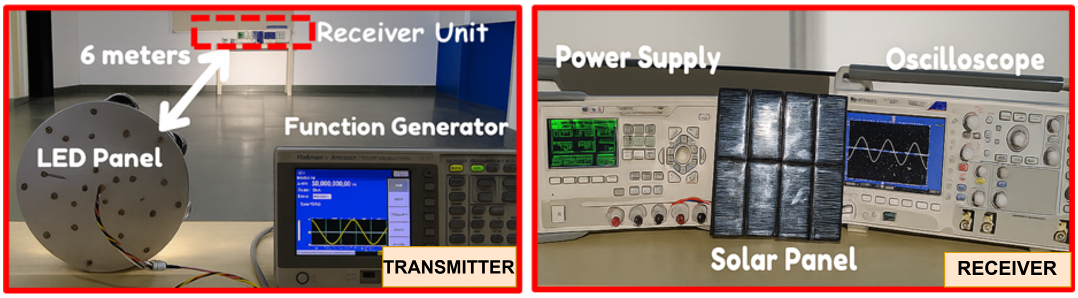

Figure 6.4: Experimental setup.

6.5 Performance Analysis

This section presents an experimental comparison between a single standalone solar module and a multi-module parallel configuration from both communication and energy harvesting perspectives. Although the parallel configuration increases the harvested electrical power by summing the photocurrent contributions of multiple modules, it also introduces a reduction in the effective communication bandwidth due to the increased junction capacitance. To mitigate this limitation, a dedicated analog front-end circuit was designed and integrated at the receiver to enhance the 3-dB bandwidth and support higher data rates over extended transmission distances. A comprehensive performance evaluation is carried out by jointly analyzing the frequency response, achievable data rate, and harvested energy for both configurations.

6.5.1 Experimental Outcomes of Frequency Response Analysis

Conventional solar panels inherently exhibit limited frequency response, typically restricted to the order of tens of kilohertz due to their large junction capacitance, as observed in Fig. 6.3. This characteristic severely constrains their direct applicability as high-speed optical communication receivers. To overcome this limitation, an analog front-end circuit was developed

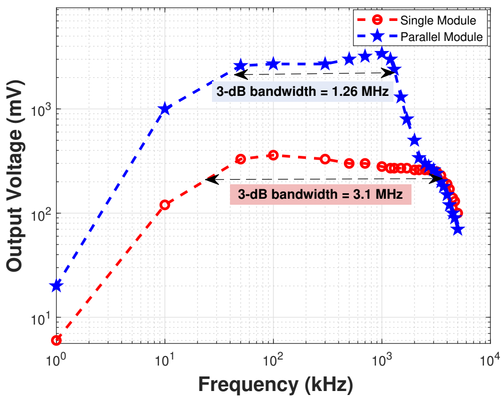

Figure 6.5: Modified receiver's frequency response.

to simultaneously suppress near-DC components and enhance the effective 3-dB bandwidth of the received signal. As illustrated in Fig. 6.5, the proposed circuit significantly attenuates low-frequency components while extending the usable bandwidth for both the single-module and parallel configurations.

The single-module configuration achieves a higher bandwidth compared to the parallel configuration, primarily due to its lower equivalent junction capacitance. In contrast, the parallel interconnection of multiple solar modules increases the total capacitance seen at the receiver input, which results in a more pronounced roll-off in the high-frequency response. To ensure a fair and consistent comparison, all circuit parameters, including load resistance and amplifier settings, were maintained identically for both configurations.

6.5.2 Data Rate and Energy Harvested

The combined performance in terms of achievable data rate and harvested electrical energy as a function of transmission distance is presented in Fig. 6.6. At a transmission distance of 1 m,

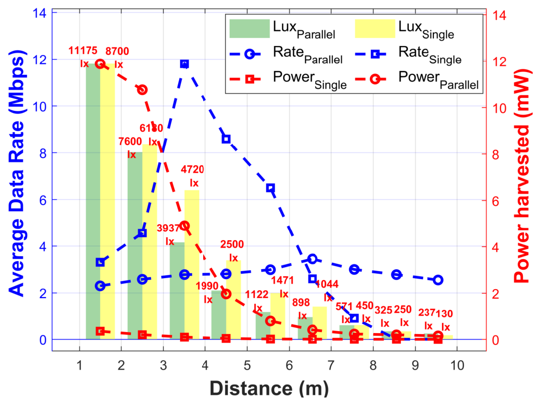

Figure 6.6: Data rate and harvested energy with distance.

the received optical intensity is sufficiently high to enable substantial energy harvesting in both configurations. Owing to the cumulative photocurrent contribution from multiple modules, the parallel configuration consistently achieves higher harvested energy than the single-module receiver. However, despite its superior energy harvesting capability, the parallel configuration yields lower achievable data rates when compared to the single-module case. This behavior is attributed to its reduced communication bandwidth, which limits the maximum symbol rate that can be reliably supported. The single-module receiver, benefiting from a wider bandwidth, is therefore able to sustain higher data rates across most transmission distances.

The variation of data rate with distance exhibits a non-monotonic trend for both configurations. For the single-module receiver, saturation occurs at short distances due to excessive photocurrent, which results in signal clipping and constrains the achievable throughput. As the distance increases and the received optical power decreases, the system transitions out of the saturation region, reaching a peak data rate of approximately 11.8 Mbps at around 3.5 m. Beyond this point, the data rate gradually declines as optical path loss dominates.

A similar trend is observed for the parallel configuration; however, the peak data rate occurs at a larger distance of approximately 6.5 m. This shift is a consequence of the higher photocurrent generated by the parallel modules, which extends the saturation region over a longer distance range. Consequently, while the parallel configuration supports improved energy harvesting and longer operational range, it experiences a trade-off in terms of reduced bandwidth and lower peak data rate compared to the single-module configuration.

6.6 Summary

This study experimentally investigates two receiver configurations: a single standalone solar module and an array of eight solar modules connected in parallel. To overcome the intrinsic bandwidth limitations of solar panels, a dedicated analog front-end circuit is employed in both configurations to enhance the effective 3-dB bandwidth. The single-module receiver achieves a bandwidth of 3.1 MHz and supports a maximum data rate of 11.8 Mbps, making it well suited for short-range, high-speed VLC applications. In contrast, the parallel configuration significantly increases the generated photocurrent, thereby extending the achievable communication distance to 9.5 m. This characteristic makes the parallel receiver particularly attractive for long-range and energy-constrained communication scenarios, such as intelligent transportation systems and rural connectivity networks. The investigations presented in Chapters 3–6 were intentionally conducted under controlled indoor laboratory conditions to systematically characterize the communication performance of commercial solar panels and to develop the underlying receiver architecture, bandwidth enhancement techniques, SLIPT framework, and comparative performance analysis. These controlled experiments enabled the isolation of key system parameters and provided a rigorous understanding of the factors influencing optical wireless communication performance. Building upon these validated findings, the subsequent chapter extends the proposed communication system to real-world outdoor environments, where practical challenges such as ambient sunlight, environmental noise, and long-distance transmission are addressed through infrared-based communication and ambient-light suppression techniques. This progression from controlled laboratory validation to outdoor field deployment demonstrates the practical applicability and scalability of the proposed solar panel-based optical wireless communication system.

Chapter 7

Outdoor Optical Communication Using Solar Panels with Ambient Light Suppression

7.1 Motivation

Solar panels employed as optical receivers represent a promising paradigm for OWC, enabling simultaneous high-speed data transmission and self-sustainable operation through energy harvesting. This work primarily investigates the communication capabilities of solar panels to address critical limitations of conventional photodiode-based receivers, including signal misalignment, dead zones, and performance degradation due to partial shading caused by lateral vehicular motion during sharp turns.

Experimental evaluations are conducted over a communication distance of 2 m, corresponding to typical short inter-vehicular spacing in platooning scenarios. Maintaining reliable communication at such distances is essential for improving road throughput and reducing traffic congestion [92]. However, the inherently low bandwidth of solar panels, mainly due to their large junction capacitance, restricts their direct use in high-speed communication systems.

To address this limitation, the analog front-end circuit is specifically optimized for outdoor operation and infrared LED transmitters, which simultaneously enhance the receiver bandwidth and suppress strong ambient light interference, thereby enabling reliable data transmission in the Mbps regime.

Previous studies on LC have predominantly employed white LEDs as optical transmitters. In contrast, the IR spectrum remains largely unexplored for solar-based communication systems. IR LEDs offer important advantages for vehicular environments, as they are invisible to the human eye and therefore do not introduce glare for vehicles in the same or adjacent lanes. This work proposes the integration of a compact IR LED transmitter panel that maintains uniform brightness, ensuring stable inter-vehicular communication links. Furthermore, the proposed approach mitigates the adverse effects of automatic headlamp brightness control, which can otherwise introduce asymmetric beam patterns and degrade communication performance.

PV modules exhibit a broad spectral responsivity range, typically spanning from the visible to the near-infrared region (approximately 300–1100 nm), depending on the semiconductor material [93]. The IR spectrum aligns well with the high-responsivity region of silicon-based PV cells, thereby enhancing detection efficiency while reducing interference from ambient visible light. In addition, compared to shorter visible wavelengths, IR wavelengths around 850 nm exhibit improved propagation characteristics under scattering conditions such as fog, dust, and smoke [94, 95].

Motivated by these advantages and the growing demands of ITS, this work presents an IR LED–based optical communication link utilizing solar panels as optical receivers. Furthermore, the large active area of solar panels effectively mitigates the dead-zone problem associated with conventional small-area photodiodes, as validated through experimental results.

7.2 Chapter Contributions

The major contributions of this work are summarized as follows:

1. First Demonstration of Infrared Solar-Based Receiver with Bandwidth Enhancement: Unlike prior work using white LEDs with solar panels, this study demonstrates IR LEDs for vehicular optical communication due to their invisibility and reduced glare. The narrow bandwidth of solar panels is overcome using a custom bandwidth enhancement circuit, extending the receiver bandwidth from 160 kHz to 4.18 MHz and enabling OFDM transmission.

2. Quantitative Dead-Zone and Mobility-Constrained Performance Analysis:
A comprehensive evaluation of link performance under realistic vehicular dynamics is carried out, including:

- *Receiver misalignment:* Reliable communication is maintained for lateral displacements up to $\pm$40 cm, achieving data rates up to 17.9 Mbps and not falling below 2.4 Mbps.
- *Partial blockage:* The solar panel receiver sustains a communication link even under 90% shading, whereas a silicon photodiode fails beyond 60–70% blockage.
- *Receiver tilt:* Operation is supported up to $\pm 50^\circ$ tilt with a throughput of 4.01 Mbps, significantly exceeding the $\pm 10^\circ$ tolerance of conventional photodiodes. These results are consistent with reported vehicular roll and yaw dynamics.

3. Integrated Prototype under Realistic Outdoor Conditions:
The proposed system is validated using an integrated prototype operating under bright outdoor illumination over a 2 m vehicular link. The experimental setup emulates real-world vehicular challenges, including misalignment, motion, and partial shading. The system achieves key link-layer performance metrics, including latency below 20 ms, link reliability of 99.99%, and negligible packet loss for packet sizes up to 1518 bytes. These results satisfy real-time vehicular communication requirements outlined in [96] and [97].

7.3 Experimental Setup

The frequency response and communication performance of the proposed system are evaluated using the setup shown in Fig. 7.1. The transmitter consists of an AWG, RIGOL DG4202, a bias tee, and four 850 nm IR LEDs. The bias tee combines the modulating signal with a DC bias to ensure linear LED operation. A TIR lens is used to narrow the LED beam for long-distance transmission. At the receiver, a solar module integrated with a BEC captures the optical signal, and the output is observed using a DSO, DS1102E. The receiver also interfaces with a digital signal processing board for data recovery. After characterizing the frequency response of the solar module, real-time communication experiments are conducted in an outdoor vehicular scenario, as shown in Fig. 7.2. Data transmission is performed using 16-QAM OFDM over an optical wireless link of up to 3.5 m under ambient illumination of approximately 94,800 lux. The system employs four IR LEDs at the transmitter and a solar module rated at 5.88 V and 60 mA at the receiver.

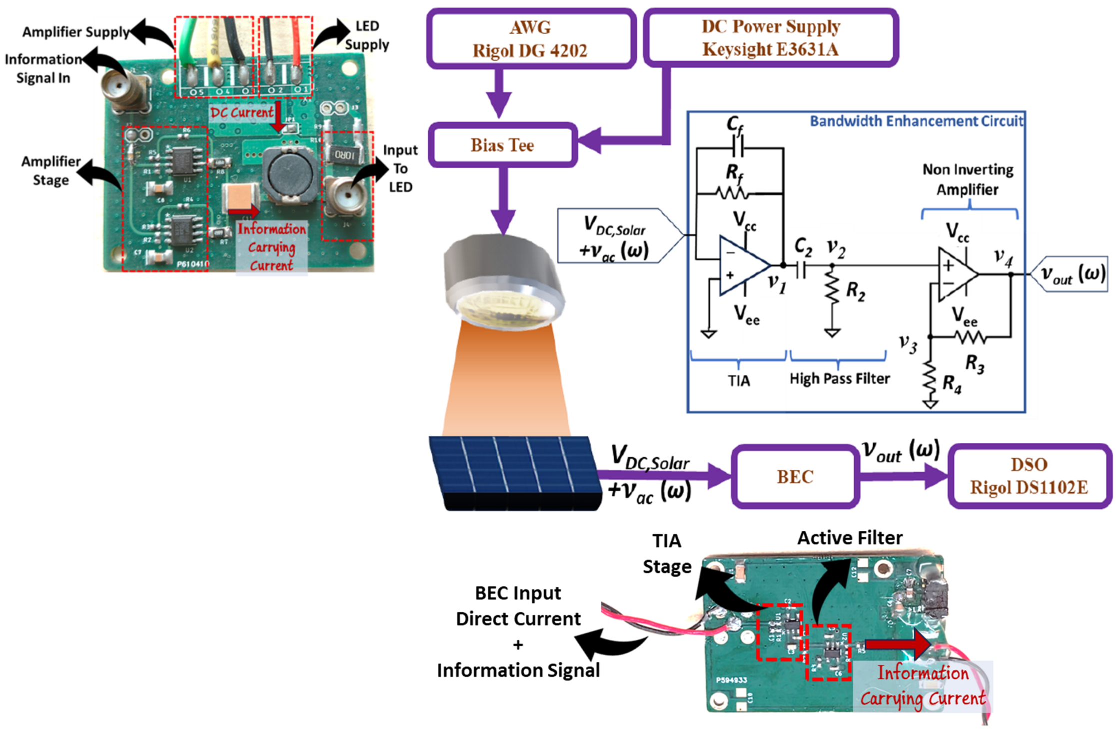

Figure 7.1: Block diagram of communication setup.

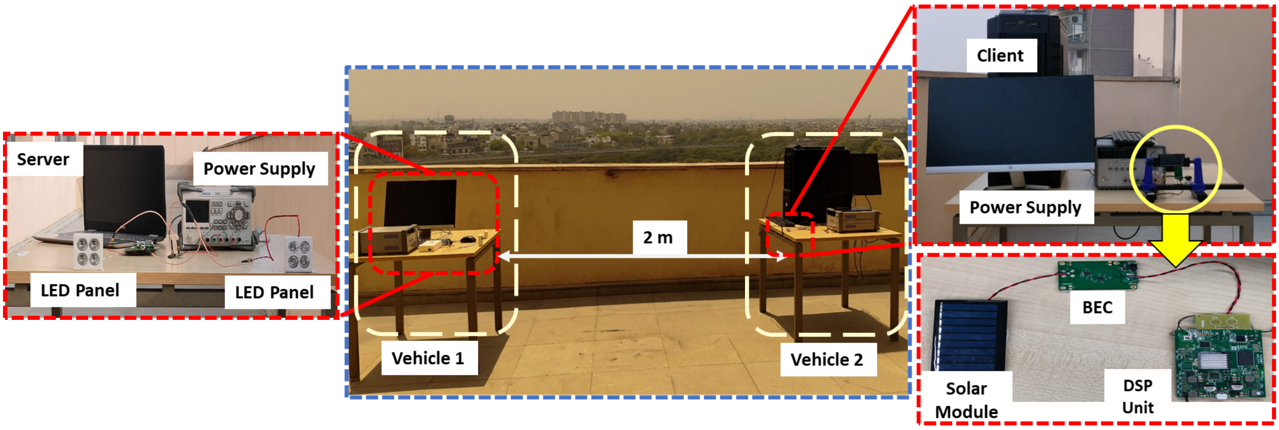

Figure 7.2: Outdoor testing setup considering vehicle 1 as the leading vehicle transmitting information and vehicle 2 as the following vehicle receiving information over a solar panel.

7.3.1 Frequency Response of Raw Solar Module

To characterize the frequency response of the solar module without the BEC, both simulation and experimental measurements are performed using the LTspice circuit simulator and the experimental setup described earlier. The results in Fig. 7.3 confirm that a raw solar panel exhibits inherently low bandwidth when used as an optical communication receiver. A minimum output

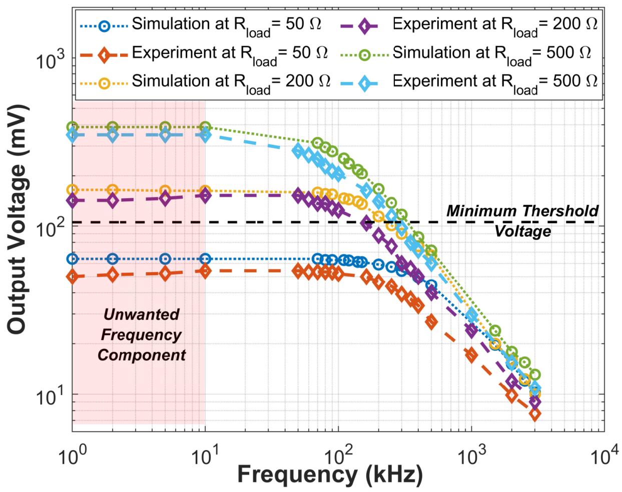

Figure 7.3: Frequency response of raw solar receiver.

voltage of approximately 100 mV is required for reliable signal recovery. Although selecting a low load resistance ($R_{load} = 50\ \Omega$) increases the bandwidth, the received signal amplitude becomes insufficient for data detection. This limitation can be partially addressed by increasing the transmitted optical power; however, this approach leads to higher power consumption and increased noise due to additional amplification stages. Alternatively, increasing R_{load} improves the output voltage at low frequencies and enhances energy harvesting capability, but significantly reduces the 3-dB bandwidth. This inverse relationship highlights the fundamental trade-off between harvested energy and communication bandwidth. Consequently, high-speed data transmission using a raw solar panel is not feasible. To mitigate this bandwidth constraint and suppress low-frequency components, BEC is designed and experimentally evaluated in an outdoor environment.

7.3.2 Frequency Response of Modified Solar Receiver

The frequency response of the solar receiver integrated with the BEC is shown in Fig. 7.4. The corresponding lower (f_L) and upper (f_H) 3-dB cutoff frequencies are indicated. For comparison, the experimentally measured 3-dB bandwidth of the raw solar receiver is 160 kHz, spanning from 1 kHz to 161 kHz. The BEC consists of a TIA stage, followed by a high-pass

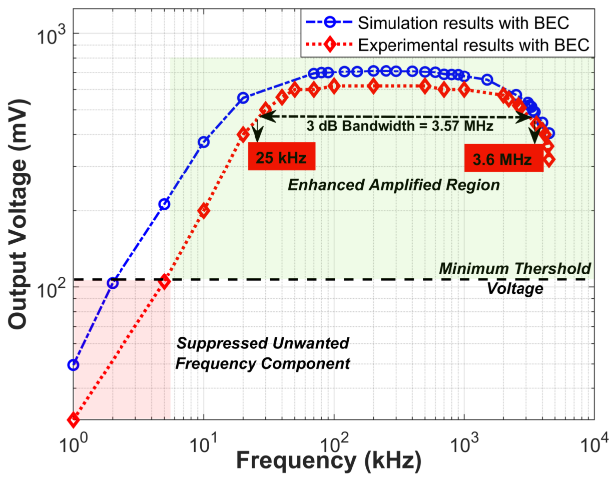

Figure 7.4: Frequency response of modified solar receiver.

filter with a cutoff frequency of 60 kHz to suppress low-frequency and DC components, and a non-inverting amplifier to provide sufficient gain for high-frequency signals. With the proposed

BEC, the receiver achieves an enhanced 3-dB bandwidth of 3.57 MHz, extending from 25 kHz to 3.6 MHz, with an output amplitude of approximately 460 mV at the 3-dB frequency points. These results demonstrate that the designed BEC significantly improves the bandwidth of the solar receiver while effectively mitigating the DC offset caused by ambient illumination.

7.4 Effect of Ambient Illumination on Solar Panel Optical Receiver

The influence of diurnal solar illumination on the performance of the proposed solar panel optical receiver is experimentally investigated in an uncontrolled outdoor environment. Ambient light introduces strong low-frequency and DC components that can distort the received signal and degrade demodulation accuracy. Hence, robust receiver design and appropriate parameter selection are essential for reliable outdoor optical communication. To address this challenge, the proposed receiver with optimized BEC parameters is evaluated under varying illumination conditions throughout the day.

The solar module orientation and corresponding sun profile are illustrated in Fig. 7.5a. Experiments are conducted at different times of the day under varying atmospheric temperatures and solar illuminance levels. Solar illuminance is measured using an HTC LX-101A digital lux

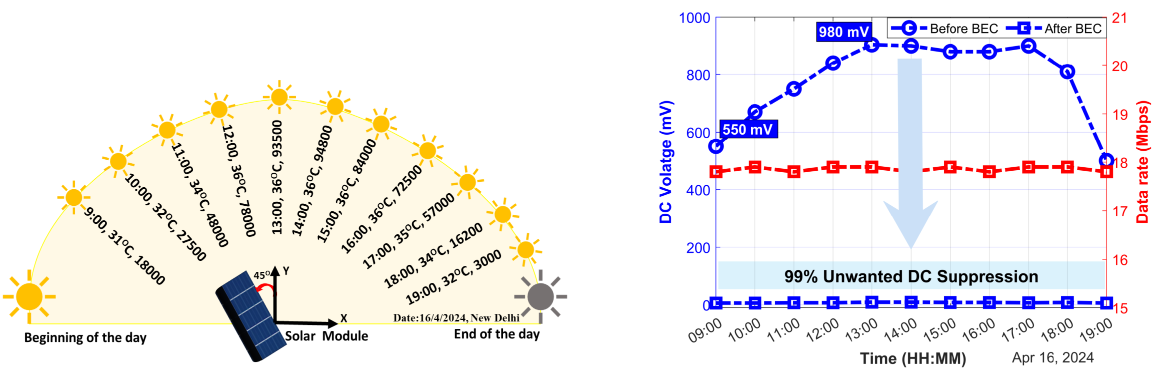

(a) Sun profile throughout a day (Time, Temperature, Lux)

(b) Uniform data rate with 99% suppressed ambient light

Figure 7.5: Impact of ambient illumination on BEC performance.

meter. During the early morning hours, the ambient lux level is relatively low and gradually increases with solar elevation. The corresponding DC voltage generated by the solar module follows this trend, as shown in Fig. 7.5b. At 09:00 hours, the measured DC voltage is approximately 550 mV and increases until midday.

The power output of the solar panel depends strongly on its orientation with respect to the sun, with maximum efficiency achieved under near-normal incidence. Although peak illuminance occurs around 13:00 hours, the non-perpendicular angle of incidence limits the generated voltage. As the sun moves toward the horizon, the incidence angle becomes more favorable, resulting in nearly constant DC voltage between 13:00 and 17:00 hours despite a gradual reduction in flux intensity. Environmental factors such as cloud cover, wind, and temperature variations further contribute to fluctuations in the measured output voltage. Beyond 17:00 hours, the decrease in daylight intensity leads to a corresponding reduction in DC voltage. These time-varying DC levels introduce baseline shifts in the received signal and may cause clipping in the amplifier stages. The designed BEC effectively suppresses the DC and low-frequency components, achieving approximately 99% ambient light rejection with only minor residual fluctuations of 5–9 mV.

Fig. 7.6 presents the data rate (left Y-axis) and received optical power (right Y-axis) measured as functions of transmission distance using *iperf-2.0.14a*. The non-monotonic data rate behavior observed in Fig. 7.6 results from receiver saturation at short distances (< 2 m) and signal attenuation at longer distances. At close proximity, the received optical power exceeds the maximum allowable limit ($P_{RX,max} = 6.1$ mW), causing amplifier saturation and signal clipping, which reduces the achievable data rate. At an optimal distance of approximately 2 m, the system achieves a peak data rate of 17.9 Mbps.

Beyond this point, the received optical power decreases due to beam divergence and atmospheric propagation losses, leading to a gradual reduction in data rate. When the received signal falls below the required peak-to-peak threshold beyond 3.2 m, reliable demodulation becomes challenging. The communication range can be further extended by employing optical

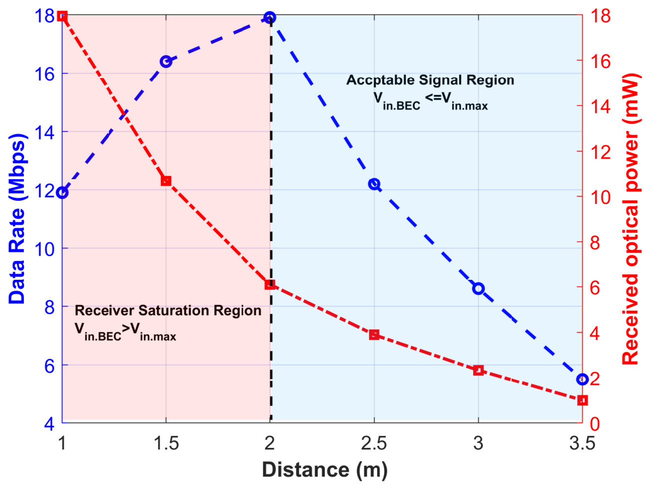

Figure 7.6: Impact of distance on data rate and received optical power

lenses for beam collimation, increasing the number of transmitting LEDs, or using solar panels with higher responsivity.

7.5 Dead Zone

The previous sections demonstrated the outdoor performance of the proposed solar receiver and the effectiveness of the designed circuitry in suppressing ambient light interference. This section highlights the advantage of such a communication link in vehicular applications, particularly for short-range scenarios such as vehicular platooning. Prior studies have shown that automated vehicles operating with inter-vehicle distances of approximately 2 m can significantly improve road throughput and reduce traffic congestion [92]. Platooning, therefore, represents a key application requiring reliable short-range vehicle-to-vehicle communication.

In vehicular environments, conventional photodiode-based receivers suffer from the dead-zone problem due to their limited active area. Dead zones arise when the receiver becomes misaligned or when its orientation exceeds the acceptable field-of-view during steering maneuvers, lane changes, road slopes, or curved paths, as illustrated in Fig. 7.7. These orientation variations lead to intermittent signal loss and reduced link reliability.

In contrast, solar panels provide a substantially larger optical collection area, making them more tolerant to angular misalignment and orientation changes. This characteristic significantly mitigates the dead-zone effect and enables more robust communication under realistic driving conditions. Consequently, solar panel–based optical receivers offer a promising solution for maintaining reliable links in short-range vehicular platooning scenarios.

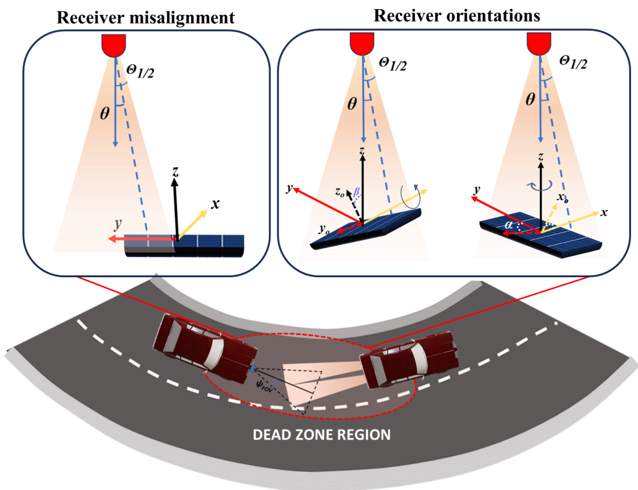

Figure 7.7: Dead-zone caused due to receiver misalignment and receiver orientation.

7.5.1 Receiver Misalignment

Receiver misalignment in LC systems commonly arises due to road banking and curved trajectories, which disrupt the line-of-sight alignment between the transmitter and receiver and create dead-zone regions. In vehicular platooning scenarios, such link interruptions during sharp turns may lead to unsafe operating conditions. The use of a solar panel receiver with a substantially larger effective collection area mitigates this limitation by increasing tolerance to lateral displacement.

Fig. 7.8 illustrates the dead-zone condition caused by lateral misalignment. The LED transmitter is assumed to be mounted near the tail lamp of the leading vehicle (LV), while the solar panel receiver is positioned at the center of the bumper of the following vehicle (FV). The

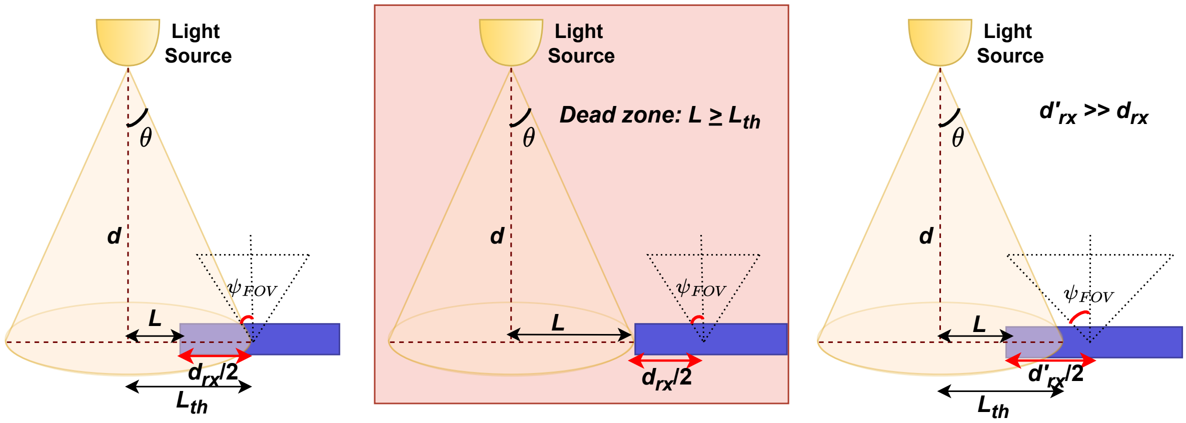

Figure 7.8: Impact of the horizontal shift of solar module.

communication link is governed by the LED semi-half angle, the receiver field-of-view (FOV), and the relative lateral displacement between the LV and FV.

When the lateral displacement exceeds a threshold value L_{th}, the receiver moves outside the illuminated footprint, and a dead zone occurs due to insufficient optical power. The geometric relationship defining this threshold is expressed as

$$\tan\big(\min(\theta_{1/2}, \psi_{FOV})\big) = \frac{L_{th} - (d_{rx}/2)}{d}, \tag{7.1}$$

$$L_{th} = d \tan\big(\min(\theta_{1/2}, \psi_{FOV})\big) + \frac{d_{rx}}{2}. \tag{7.2}$$

Here, L_{th} denotes the maximum allowable lateral displacement, d_{rx} is the lateral width of the receiver, d represents the distance between the transmitter and the center of the illuminated footprint, $\theta_{1/2}$ is the LED semi-angle, and ψ_{FOV} is the receiver field-of-view.

The outdoor LC channel is further affected by atmospheric absorption and scattering, which can be modeled using the Beer-Lambert law. The differential received power over an elemental area dA, assuming Lambertian radiation, is given by [98]

$$dP = \frac{(m+1)}{2\pi D_d^2} \cos^m(\theta) \cos(\psi) \tau(D_d) P_{emit}\, dA, \tag{7.3}$$

where $\tau(D_d)$ denotes the atmospheric transmittance at distance D_d, m is the Lambertian order of the LED, P_{emit} is the emitted optical power, θ is the radiation angle, and ψ is the incidence angle at the receiver.

For fixed P_{emit}, θ, and ψ, the total received power is obtained as

$$P = \frac{(m+1)}{2\pi D_d^2} \cos^m(\theta)\cos(\psi)\tau(D_d)P_{emit}\int dA, \tag{7.4}$$

$$P = \frac{(m+1)}{2\pi D_d^2} \cos^m(\theta)\cos(\psi)\tau(D_d)P_{emit}\int_{L_{th}-\kappa d'_{rx}}^{L_{th}}\int_{0}^{a} dx\,dy, \tag{7.5}$$

where κ denotes the fractional overlap between the receiver area and the illuminated footprint, ranging from zero (no overlap) to unity (full overlap). The parameter d'_{rx} represents the lateral width of the solar panel, and a denotes the horizontal extent of the illuminated region. Accordingly, the received optical power becomes

$$P = \frac{(m+1)}{2\pi D_d^2} \cos^m(\theta)\cos(\psi)\tau(D_d)P_{emit}\kappa a d'_{rx}. \tag{7.6}$$

Since the effective collection area of a solar panel is significantly larger than that of a conventional photodiode ($d'_{rx} \gg d_{rx_{PD}}$), the solar receiver captures higher optical power, particularly near the boundary of the illuminated footprint. This property provides increased tolerance to lateral displacement and enhances link robustness compared with photodiode-based receivers.

7.5.2 Orientation Impact

Receiver orientation represents a critical limitation in photodiode-based LC systems due to their narrow aperture. Even small angular deviations may result in link outage. In contrast, the large collection area of solar panels enables sustained communication under substantial orientation variations.

According to Euler's rotation theorem, the three-dimensional orientation of a rigid body can be described by yaw (α), pitch (γ), and roll (β) angles [99, 100], as illustrated in Fig. 7.9. Yaw corresponds to rotation about the vertical axis during turning or lane changes, pitch describes rotation about the lateral axis during acceleration and braking, and roll denotes rotation about the longitudinal axis due to road inclination and vehicle dynamics. In this study, the combined

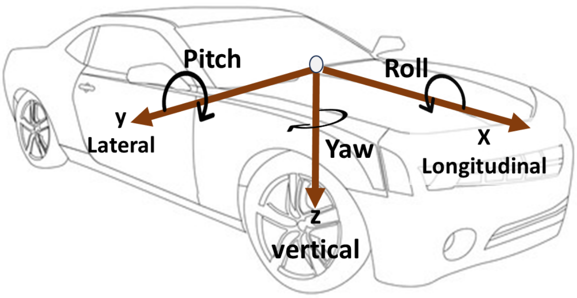

Figure 7.9: Vehicular orientation system

effects of yaw and roll are considered, as these dominate orientation variations during normal vehicle operation. Reported vehicular dynamics indicate that yaw and roll angles may vary up to $\pm 50^\circ$ and $\pm 17^\circ$, respectively [101, 102]. The corresponding rotation matrices are defined as [99]

$$\mathbf{R}(\alpha) = \begin{bmatrix} \cos\alpha & \sin\alpha & 0 \\ -\sin\alpha & \cos\alpha & 0 \\ 0 & 0 & 1 \end{bmatrix}, \tag{7.7}$$

$$\mathbf{R}(\beta) = \begin{bmatrix} 1 & 0 & 0 \\ 0 & \cos\beta & \sin\beta \\ 0 & -\sin\beta & \cos\beta \end{bmatrix}, \tag{7.8}$$

$$\mathbf{R}(\gamma) = \begin{bmatrix} \cos\gamma & 0 & -\sin\gamma \\ 0 & 1 & 0 \\ \sin\gamma & 0 & \cos\gamma \end{bmatrix}. \tag{7.9}$$

The overall rotation matrix is expressed as $\mathbf{R}(\alpha,\beta,\gamma) = \mathbf{R}(\alpha)\mathbf{R}(\beta)\mathbf{R}(\gamma)$. If $\mathbf{n}_z$ denotes the initial unit normal vector of the receiver, the rotated normal vector $\mathbf{n}_r$ is given by

$$\mathbf{n}_r = \mathbf{R}(\alpha,\beta,\gamma)\mathbf{n}_z. \tag{7.10}$$

Accordingly, the incidence angle ψ is obtained as

$$\cos(\psi) = \frac{\mathbf{n}_r \cdot \mathbf{D}_d}{||\mathbf{D}_d||}, \tag{7.11}$$

where $\mathbf{D}_d$ and $||\mathbf{D}_d||$ denote the distance vector and Euclidean distance between the transmitter and receiver, respectively.

7.6 Experimental Observations and Insights

This work investigates the communication capability of solar panels when employed as optical receivers. A series of experiments is conducted to demonstrate that solar panel–based receivers effectively address key challenges encountered in vehicular LC systems. An IR LED operating at a wavelength of 850 nm is used as the optical transmitter.

7.6.1 Optical Link Reliability

The reliability of the proposed solar panel–based optical link is experimentally evaluated using the outdoor testbed shown in Fig. 7.2. Key performance metrics, including packet loss, average round-trip time (RTT), lateral misalignment tolerance, and receiver orientation sensitivity, are investigated. Two IR LED panels are positioned 40 cm apart to emulate the spatial separation of vehicular tail lamps.

Link reliability is first assessed by analyzing the effect of packet size on packet loss and average RTT, as shown in Fig. 7.10. The *iperf* network tool is employed to transmit 10^5 packets for each packet size configuration. The minimum average RTT of 16 ms is observed

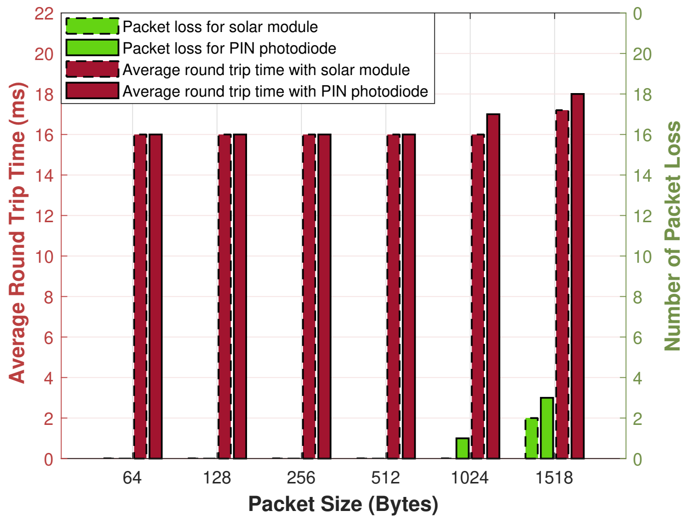

Figure 7.10: Packet loss and average round-trip time versus packet size.

for 64-byte packets, while the maximum RTT of 18 ms occurs for 1518-byte packets. Packet loss remains negligible for packet sizes up to 512 bytes. For 1518-byte packets, a maximum loss of only three packets is recorded, demonstrating stable link performance.

To further evaluate reliability over different inter-vehicular distances, packet error measurements are conducted using 10^5 packets of 1518 bytes at each distance. At a separation of 1 m, a maximum of seven packet losses is observed. Between 2 m and 4 m, packet loss remains extremely low, with only three lost packets, corresponding to a link reliability exceeding 99.99%. Beyond 4 m, the received optical power drops below 0.01 mW, resulting in a rapid increase in packet loss. These results confirm robust communication up to 4 m and indicate that the operating range can be extended through higher optical transmit power or solar panels with improved responsivity.

The impact of lateral displacement of the solar receiver is examined in the experiment shown in Fig. 7.11. The LED transmitters are placed symmetrically at ±20 cm from the centerline. At these positions, the maximum data rate of 17.9 Mbps is achieved with a received optical intensity of 0.86 mW. As the receiver moves toward the center position, the received intensity decreases, resulting in a reduced data rate of 10.8 Mbps.

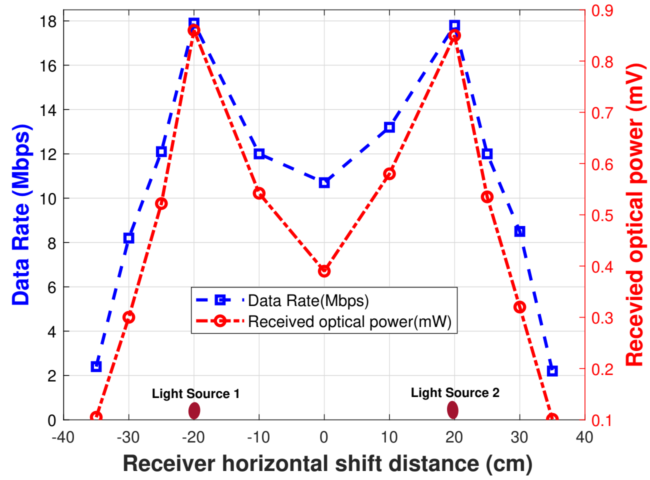

Figure 7.11: Impact of the horizontal shift of the solar module.

At the extreme lateral edges, the received optical intensity drops to approximately 0.1 mW, yielding a data rate of 2.4 Mbps. These observations demonstrate that the solar receiver maintains functional communication over a wide lateral displacement range, highlighting its suitability for vehicular platooning scenarios where relative alignment continuously varies.

7.6.2 Dead Zone Impact

The impact of the dead zone on communication performance is presented in this section.

7.6.2.1 Receiver Misalignment

The effect of receiver misalignment and partial optical blockage on data rate performance is experimentally investigated and illustrated in Fig. 7.12. The shaded region represents the portion of the receiver area that does not receive incident optical power. Performance is compared between a conventional silicon photodiode and the proposed solar panel receiver.

When the receivers are positioned at the center of the illumination cone, both devices experience maximum received optical intensity. Under zero shading, the solar panel achieves a data rate of 17.9 Mbps, while the silicon photodiode attains 23.2 Mbps. As the shaded area increases, the data rate decreases for both receivers. However, the photodiode exhibits a sharp

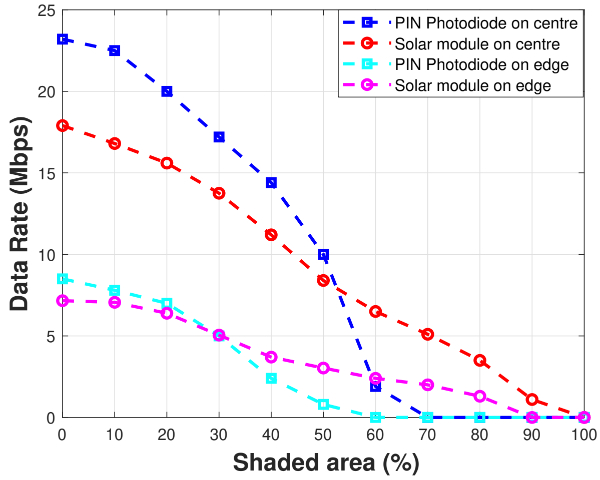

Figure 7.12: Data rate versus shaded area of the optical receiver.

degradation beyond 50% shading and experiences complete outage at approximately 70% shading. In contrast, the solar panel maintains an active link up to nearly 90% shaded area due to its substantially larger collection surface.

A second experiment places the receivers at the edge of the illumination cone, where the initial received optical power is inherently lower. In this configuration, both receivers exhibit reduced peak data rates even under zero shading. The silicon photodiode undergoes rapid performance degradation beyond 30% shading and reaches complete outage at 60% shading. Conversely, the solar panel shows gradual performance degradation and continues to outperform the photodiode beyond 30% shaded area, sustaining communication up to 90% shading.

This performance difference is primarily attributed to the inherent limitations of photodiodes, namely their small active area and narrow FOV. With an active area of approximately 100 mm^2, photodiodes collect significantly less optical power and are highly sensitive to misalignment and partial blockage. Additionally, their restricted angular acceptance limits off-axis reception. Solar panels, with their substantially larger surface area, effectively operate as wide-FOV receivers, providing improved tolerance to angular deviations and partial shading. This property makes them well-suited for dynamic vehicular environments where relative orientation continuously changes. The achieved data rates are sufficient to support video transmission at 1280×720 resolution along with safety messages and vehicle trajectory information [97, 103].

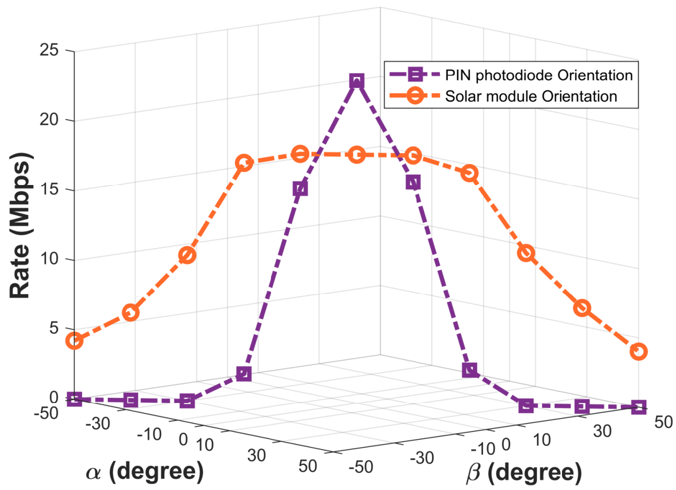

Figure 7.13: Receiver orientation versus data rate.

7.6.2.2 Orientation Impact

Receiver orientation varies significantly during vehicle maneuvers such as sharp turns, lane changes, and road banking, potentially causing dead-zone conditions. Experimental validation is therefore performed to quantify the angular tolerance of the proposed solar receiver and compare it with a silicon photodiode, as shown in Fig. 7.13.

To emulate vehicular roll and yaw motions, a custom-designed mechanical pan–tilt servo gimbal is employed. The fixture enables yaw rotation from -60° to $+60^\circ$ and roll (vertical tilt) from -60° to $+60^\circ$ in steps of 5°.

Under perfect alignment, the silicon photodiode achieves a higher peak data rate than the solar receiver. However, even small angular deviations result in a rapid performance decline for the photodiode, leading to link outage beyond 10° of misorientation. In contrast, the solar receiver exhibits stable performance up to 10° of rotation and maintains an active communication link even at extreme angular deviations of $\pm 50^\circ$, achieving a data rate of 4.01 Mbps. These results confirm the superior robustness of solar panel receivers against orientation-induced dead zones, making them highly suitable for vehicular platooning and short-range vehicle-to-vehicle optical communication.

7.7 Summary

This chapter experimentally demonstrates high-speed optical communication using a solar panel as a vehicular receiver, addressing the dead-zone problem associated with conventional photodiode-based systems. Owing to its large collection area, the solar receiver maintains link connectivity under severe misalignment, partial shading (up to 90%), and extreme orientation variations (up to $\pm 50^\circ$). To overcome the intrinsic bandwidth limitation of solar panels (160 kHz), an analog circuit is designed, extending the receiver bandwidth to 3.57 MHz and enabling data rates up to 17.9 Mbps. These results confirm the suitability of solar panel-based receivers for robust short-range vehicular communication and highlight their potential for future intelligent transportation systems.

Chapter 8

Conclusion and Future Work

This dissertation presented a comprehensive investigation into the design, modeling, and experimental validation of **solar panel–based optical wireless communication receiver**. Motivated by the limitations of conventional photodiode-based receivers, particularly their susceptibility to dead zones caused by misalignment, orientation variations, and partial blockage, this research aimed to develop a robust and practical optical receiver architecture suitable for dynamic environments. Through analytical modeling, circuit-level design, and extensive outdoor experimentation, this thesis establishes solar panels as viable and reliable optical receivers for simultaneous communication and energy harvesting.

8.1 Summary of Contributions

The main contributions of this dissertation are summarized as follows:

- This research demonstrated through systematic experimentation that commercial solar panels can be effectively utilized as optical communication receivers. Unlike conventional photodiodes with limited active area, solar panels provide a significantly larger optical collection surface, enabling improved tolerance to receiver misalignment, orientation changes, and partial shading. This directly addresses the dead-zone problem commonly observed in VLC systems.

- A key technical challenge associated with solar panels is their inherently low electrical bandwidth (approximately 160 kHz), which restricts achievable data rates. To overcome this limitation, custom analog circuits were designed and implemented. The proposed BEC extends the effective receiver bandwidth to 3.57 MHz while suppressing low-frequency and DC components induced by ambient light. This enabled reliable high-speed data transmission with data rates up to 17.9 Mbps using an IR LED in an outdoor environment and 18.8 Mbps using indoor white LED with 16-QAM OFDM modulation.

- The outdoor performance of the proposed solar receiver was extensively evaluated under varying ambient illumination conditions throughout the day. Experimental results demonstrated that the designed BEC suppresses more than 99% of the ambient light–induced DC component, ensuring stable communication even under high solar lux levels. These findings confirm the robustness of the receiver architecture in uncontrolled outdoor environments.

- The impact of lateral displacement and partial blockage on link reliability was experimentally investigated to quantify the dead-zone mitigation capability of solar receivers. Results showed that the communication link remains operational even when up to 90% of the receiver area is shaded. Compared with silicon photodiodes, solar panels exhibited significantly higher resilience to misalignment and maintained connectivity at the edges of the illumination footprint.

- Receiver orientation effects were studied using controlled roll and yaw rotations to emulate real vehicular motion. While conventional photodiodes experienced link outage beyond small angular deviations (approximately 10°), the solar receiver maintained active communication even at extreme orientations of up to ±50°, achieving data rates of 4.01 Mbps. This highlights the suitability of solar panel receivers for vehicular platooning and short-range vehicle-to-vehicle optical links.

- Overall, the experimental and analytical results demonstrate that solar panel–based optical receivers provide a low-cost, lens-free, and bias-free alternative to conventional photodiode receivers. By simultaneously offering large-area optical collection and communication capability, the proposed approach simplifies receiver design and improves robustness in dynamic vehicular scenarios.

8.2 Future Research Directions

Building upon the foundations established in this dissertation, several promising research directions can be pursued:

8.2.1 Advanced Modulation and Receiver Architectures

Although the experimental validation presented in this thesis employs OOK due to the inherent bandwidth limitations and non-ideal characteristics of commercial photovoltaic receivers, the proposed bandwidth enhancement techniques significantly improve the communication capability of solar-panel-based optical receivers. These advancements establish a practical pathway toward supporting higher-order modulation schemes, which demand greater bandwidth and signal quality. The scalability of the proposed receiver architecture has been validated in our subsequent studies, where OFDM with 16-QAM was successfully demonstrated using the bandwidth-enhanced solar-panel receiver. These results confirm that the proposed analog front-end design is not restricted to low-order modulation but provides a foundation for implementing spectrally efficient modulation schemes, thereby enabling higher data rates and facilitating the evolution of solar-panel-based optical wireless communication systems toward future high-capacity LiFi and intelligent transportation applications. The current system can be extended to support higher-order modulation schemes and wider bandwidths through improved analog front-end design and adaptive filtering. Future research may explore adaptive gain control, digital equalization, and multi-band reception techniques to further increase achievable data rates and link reliability.

8.2.2 Environmental Robustness and Weather-Aware Communication

Extensive field trials under diverse weather conditions, such as rain, fog, dust, and fluctuating sunlight intensity, will be conducted to evaluate long-term reliability. Incorporating atmospheric attenuation and scattering models into system design will enable weather-aware adaptive communication strategies for vehicular optical links.

8.2.3 Angle-Diversity and Multi-Panel Reception

The spatial and angular response characteristics of solar panels offer the potential for angle-diversity reception. Future work will investigate multi-panel receiver configurations to exploit spatial diversity and further mitigate dead zones caused by extreme misalignment and shadowing in dynamic vehicular environments.

8.2.4 Dynamic Vehicular Experiments and Channel Modeling

The proposed solar-panel-based optical receiver architecture provides a strong foundation for next-generation Intelligent Transportation Systems (ITS). Future research will focus on extending the communication range using higher-power optical transmitters, optimized optics, adaptive beam steering, receiver diversity, and MIMO-based optical communication techniques. Large-scale dynamic vehicle-to-vehicle (V2V) experiments will be conducted to characterize path loss, mobility-induced fading, and vehicular light distributions, enabling the development of realistic channel models for platooning and cooperative driving applications. Furthermore, the proposed receiver can be extended beyond vehicle platooning to support broader ITS applications, including V2I communication, intelligent traffic intersections, and smart transportation infrastructure. Additional validation under diverse outdoor conditions will further enhance the robustness and scalability of the proposed system for practical vehicular optical wireless communication.

8.3 Concluding Remarks

In conclusion, this dissertation demonstrates that solar panel–based optical receivers constitute a promising alternative to conventional photodiode-based LC systems. By overcoming dead-zone limitations through large-area reception and bandwidth enhancement, the proposed architecture enables robust, high-speed, and alignment-tolerant optical links suitable for intelligent transportation systems. The analytical insights, circuit designs, and experimental validations presented in this work provide a strong foundation for future research on sustainable, affordable, resilient, and high-performance optical wireless communication networks.

Appendix A

Author’s Publications

Journals (Published)

1. **Rahul**, V. A. Bohara, A. Srivastava, D. Solanki and A. Mitra, "Dead Zone Mitigation in Vehicular Platoon via Solar Panel as a Communication Receiver," in IEEE Transactions on Intelligent Transportation Systems, doi: 10.1109/TITS. 2025. 3627293.

2. **Rahul**, A. Srivastava, V. A. Bohara, D. Solanki and A. Mitra, "Demonstration of Broadband Data Link over off-the-shelf Solar Module with White LED," in IEEE/OSA Journal of Lightwave Technology, 2025, doi: 10.1109/JLT. 2025. 3541831.

3. **Rahul**, A. Mitra, A. Srivastava, V. A. Bohara and D. Solanki, "Solar Module as a High-Speed Data Receiver with Ambient Light Suppression in an Outdoor Scenario" OPTICA Optics Letters (2025), https://doi.org/10.1364/OL.545006.

4. **Rahul**, S. Chaturvedi, A. Srivastava, V. A. Bohara and A. Mitra, “Energy Management Strategy for Drone-Based Optical Wireless Communication Network," in *Physical Communication*, vol. 76, p. 103075, 2026, doi: 10.1016/j.phycom.2026.103075.

Journals (Under Review)

1. **Rahul**, A. K. Pal, P. Aggarwal, V. A. Bohara, and A. Mitra, “Modeling and Measurement of Communication Characteristics in Parallel-Configured Solar Panel Optical Receivers,” *IEEE Transactions on Green Communications and Networking*, 2026.

2. D. Solanki, **Rahul**, A. Mitra, A. Srivastava and V. A. Bohara, “ Long Range High Speed Optical Wireless Communication Link", submitted to *Optics Letters*, 2026.

Conferences(Published)

1. **Rahul**, A. Mitra, A. Srivastava, V. A. Bohara, and D. Solanki, “Experimental Validation of Optical Wireless Receiver using Solar Panel with Bandwidth Enhancement Circuit,” *2022 IEEE 95th Vehicular Technology Conference (VTC2022-Spring)*, Helsinki, Finland, 2022, pp. 1–6, doi:10.1109/VTC2022Spring54318. 2022. 9860765.

2. **Rahul**, V. A. Bohara, A. Mitra, D. Solanki and A. Srivastava, "Experimental Validation of Simultaneous Power and Data Transfer over Solar Panels for 5G and Future Network," 2024 IEEE Future Networks World Forum (FNWF), Dubai, United Arab Emirates, 2024, pp. 867-872, doi: 10.1109/FNWF63303. 2024. 11028868.

3. **Rahul**, K. Joshi, V. A. Bohara, A. Mitra, D. Solanki and A. Srivastava, "Experimental Validation of Solar Panel Communication with Various Phase Shift Keying Modulation Schemes for Light Communication," 2024 IEEE International Conference on Advanced Networks and Telecommunications Systems (ANTS), Guwahati, India, 2024, pp. 1-6, doi: 10.1109/ANTS63515.2024.10898847.

4. **Rahul**, V. A. Bohara, A. Mitra, D. Solanki, and A. Srivastava, “Sunlight to Signals: Solar Panel as Active Data Receiver,” *17th International Conference on COMmunication Systems and NETworks (COMSNETS)*, Bengaluru, India, 2025, pp. 1359–1361, doi:10.1109/COMSNETS63942.2025.10885740.

5. **Rahul**, A. Mitra, V. A. Bohara, A. Srivastava and D. Solanki, "POSTER: Leveraging Solar Panels for Light Communication: Analyzing the Role of Configuration in Signal Reception," 2025 IEEE 26th International Conference on High Performance Switching and Routing (HPSR), Suita, Osaka, Japan, 2025, pp. 1-3, doi: 10.1109/HPSR64165. 2025. 11038895.

6. A. K. Pal, **Rahul**, V. A. Bohara, and A. Mitra, "Toward Low-Power Free-Space Optical Communication over Solar Panel," *Proc. of 19th IEEE ANTS*, Delhi, India, 2025.

7. A. K. Pal, **Rahul**, A. Mitra, and V. A. Bohara, "Mirror-Assisted Non-Line-of-Sight Voice Communication Over Solar Panels as Receivers for Long-Range Low-Power Links," *18th International Conference on COMmunication Systems and NETworks (COMSNETS)*, Bengaluru, India, 2026.

8. Naman Singhal, A. K. Pal, **Rahul**, V. A. Bohara, and A. Mitra, "A Graphical User Interface Driven Method for Static and Dynamic Parameter Extraction of Solar Panels for Optical Communication," *18th International Conference on COMmunication Systems and NETworks (COMSNETS)*, Bengaluru, India, 2026.

Patent

1. "A system to amplify bandwidth capacity in a Li-Fi network system", Inventors: **Rahul**, A. Mitra, D. Solanki, A. Srivastava, V.A. Bohara, Indian Patent, 557160, Grant Date: Dec. 31, 2024

Standardization

1. TSDSI Standardization Activity on Solar Panel Based Optical Wireless Communication leading to the approved study item "Solar Panel Based Optical Wireless Communication

(TR 6050 V1.0.0)"; Contributors: **Rahul**, A. Mitra A. Srivastava, V.A. Bohara, Technical Report Accepted and Published, Nov. 2025.

Awards and Achievements

1. Secured **first place** at the **18th International Conference on Communication Systems and Networks (COMSNETS 2025)** for the live demonstration titled *"Mirror-Assisted Non-Line-of-Sight Communication over Solar Panels as Receivers for Long-Range Low-Power Links."*

2. Selected among the **top 20 participants worldwide** in the **IEEE ComSoc 4-Minute Thesis (4MT) Competition** and presented the research at **IEEE GLOBECOM 2025**, Taiwan.

3. Awarded **second place** at the **17th International Conference on Communication Systems and Networks (COMSNETS 2025)** for the demonstration *"Sunlight to Signals: Solar Panels as Active Data Receivers."*

4. Received **first prize** at the **IEEE Communications Society (ComSoc) Student Technical Leadership Conference 2024**, Dubai, UAE, for the work *"Solar-Panel-Based LC Receivers for Sustainable Intelligent Transportation Systems"*

5. Earned an **Honorable Mention** for the paper *"Experimental Validation of Solar Panel Communication with Various Phase-Shift Keying Modulation Schemes for Light Communication"* at the **IEEE International Conference on Advanced Networks and Telecommunications Systems (ANTS 2024)**, Guwahati, India.

6. Received the **Dean's Excellence in Research Award**, **IIIT Delhi**, 2023.

7. Won **first prize** at the **Research Innovation and Incubation Showcase (RIISE)**, **IIIT Delhi**, for hardware demonstration of solar panel based communication 2023.

References

[1] H. Burchardt, N. Serafimovski, D. Tsonev, S. Videv, and H. Haas, “Vlc: Beyond point-to-point communication,” *IEEE Communications Magazine*, vol. 52, no. 7, pp. 98–105, 2014.

[2] V. A. Bohara and R. Swaminathan, *Optical and Wireless Access Networks*. Springer, 2025.

[3] I. Stefan, H. Burchardt, and H. Haas, “Area spectral efficiency performance comparison between vlc and rf femtocell networks,” in *2013 IEEE international conference on communications (ICC)*. IEEE, 2013, pp. 3825–3829.

[4] H. Abuella, M. Elamassie, M. Uysal, Z. Xu, E. Serpedin, K. A. Qaraqe, and S. Ekin, “Hybrid rf/vlc systems: A comprehensive survey on network topologies, performance analyses, applications, and future directions,” *IEEE Access*, vol. 9, pp. 160 402–160 436, 2021.

[5] “Ieee standard for local and metropolitan area networks–part 15.7: Short-range optical wireless communications,” *IEEE Std 802.15.7-2018 (Revision of IEEE Std 802.15.7-2011)*, pp. 1–407, 2019.

[6] “Ieee standard for information technology–telecommunications and information exchange between systems local and metropolitan area networks–specific requirements part 11: Wireless lan medium access control (mac) and physical layer (phy) specifications amendment 6: Light communications,” *IEEE Std 802.11bb-2023 (Amendment to IEEE Std 802.11-2020 as amended by IEEE Std 802.11ax-2021, IEEE Std 802.11ay-2021, IEEE Std 802.11ba-2021, IEEE Std 802.11az-2022, IEEE Std 802.11-2020/Cor 1-2022, and IEEE Std 802.11bd-2023)*, pp. 1–37, 2023.

[7] X. Huang, S. Chen, Z. Wang, J. Shi, Y. Wang, J. Xiao, and N. Chi, “2.0-Gb/s visible light link based on adaptive bit allocation OFDM of a single phosphorescent white LED,” *IEEE Photonics Journal*, vol. 7, no. 5, pp. 1–8, 2015.

[8] W.-C. Wang, C.-H. Cheng, H.-Y. Wang, and G.-R. Lin, “White-light color conversion with red/green/violet laser diodes and yellow light-emitting diode mixing for 34.8 gbit/s visible lighting communication,” *Photonics Research*, vol. 8, no. 8, pp. 1398–1408, 2020.

[9] R. Bian, I. Tavakkolnia, and H. Haas, “15.73 gb/s visible light communication with off-the-shelf leds,” *Journal of Lightwave Technology*, vol. 37, no. 10, pp. 2418–2424, 2019.

[10] D. Milovančev, N. Vokić, H. Hübel, and B. Schrenk, “Gb/s visible light communication with low-cost receiver based on single-color led,” *Journal of Lightwave Technology*, vol. 38, no. 12, pp. 3305–3314, 2020.

[11] A. Khalid, G. Cossu, R. Corsini, P. Choudhury, and E. Ciaramella, “1-Gb/s transmission over a phosphorescent white LED by using rate-adaptive discrete multitone modulation,” *IEEE photonics journal*, vol. 4, no. 5, pp. 1465–1473, 2012.

[12] J. Gancarz, H. Elgala, and T. D. Little, “Impact of lighting requirements on vlc systems,” *IEEE Communications Magazine*, vol. 51, no. 12, pp. 34–41, 2013.

[13] G. Cossu, A. Khalid, P. Choudhury, R. Corsini, and E. Ciaramella, “3.4 gbit/s visible optical wireless transmission based on RGB LED,” *Optics express*, vol. 20, no. 26, pp. B501–B506, 2012.

[14] E. Xie, C. Chen, C. Ouyang, J. Hill, J. J. D. McKendry, Y. Zhang, E. Gu, J. Herrnsdorf, H. Haas, and M. D. Dawson, “Gan-based series hybrid led array: A dual-function light source with illumination and high-speed visible light communication capabilities,” *Journal of Lightwave Technology*, vol. 42, no. 1, pp. 243–250, 2024.

[15] C. He and C. Chen, “A review of advanced transceiver technologies in visible light communications,” in *Photonics*, vol. 10, no. 6. MDPI, 2023, p. 648.

[16] S. Ramachandrapura, F. Ahmad, A. Prosad, and V. Raghunathan, “Dual-carrier multiplexed laser-based hybrid transmitter for high data-rate indoor optical wireless communication,” *Optik*, vol. 274, p. 170522, 2023.

[17] T. Lu, X. Lin, W. Guo, C.-C. Tu, S. Liu, C.-J. Lin, Z. Chen, H.-C. Kuo, and T. Wu, “High-speed visible light communication based on micro-led: A technology with wide applications in next generation communication,” *Opto-Electronic Science*, vol. 1, no. 12, pp. 220 020–1, 2022.

[18] P. Nabavi, S. Saghaye-Polkoo, M. Yuksel, and C. K. Renshaw, “A multi-led dome bulb prototype for dense visible light communication networks,” *Journal of Lightwave Technology*, vol. 40, no. 14, pp. 4621–4634, 2022.

[19] A. Beling and J. C. Campbell, “Advances in photodetectors and optical receivers,” *Optical Fiber Telecommunications VIA: Components and Subsystems*, pp. 99–154, 2013.

[20] V. Brückner, “Optical receivers,” in *Elements of Optical Networking: Basics and Practice of Glass Fiber Optical Data Communication*. Springer, 2024, pp. 125–138.

[21] P.-S. Lin, K. Circir, C.-C. Kuo, K.-P. Wang, C.-C. Yu, S. Yang, H.-S. Chen, J. J.-S. Huang, Y.-C. Chang, J. C. Campbell, and J.-W. Shi, “Optimization of the launched optical beam profile for high-speed avalanche photodiodes to enhance the wide dynamic range performance,” *Journal of Lightwave Technology*, vol. 43, no. 21, pp. 9834–9841, 2025.

[22] S. M. Laube, C. Gasser, K. Schneider-Hornstein, and H. Zimmermann, “Highly-sensitive integrating optical receiver with large pin photodiode,” *IEEE Photonics Journal*, 2024.

[23] Y. Shi, M. Zou, Z. Li, Y. Yu, and X. Zhang, “Ultrafast avalanche photodiode exceeding 100 ghz bandwidth,” *Nature Communications*, vol. 16, no. 1, p. 11058, 2025.

[24] A. Celik, I. Romdhane, G. Kaddoum, and A. M. Eltawil, “A top-down survey on optical wireless communications for the internet of things,” *IEEE Communications Surveys & Tutorials*, vol. 25, no. 1, pp. 1–45, 2022.

[25] A. G. Bell, “Upon the production and reproduction of sound by light,” *Journal of the Society of Telegraph Engineers*, vol. 9, no. 34, pp. 404–426, 1880.

[26] M. A. Khalighi and M. Uysal, “Survey on free space optical communication: A communication theory perspective,” *IEEE Communications Surveys Tutorials*, vol. 16, no. 4, pp. 2231–2258, 2014.

[27] H. Kaushal and G. Kaddoum, “Optical communication in space: Challenges and mitigation techniques,” *IEEE Communications Surveys Tutorials*, vol. 19, no. 1, pp. 57–96, 2017.

[28] Z. Zeng, S. Fu, H. Zhang, Y. Dong, and J. Cheng, “A survey of underwater optical wireless communications,” *IEEE Communications Surveys Tutorials*, vol. 19, no. 1, pp. 204–238, 2017.

[29] A. S. Hamza, J. S. Deogun, and D. R. Alexander, “Classification framework for free space optical communication links and systems,” *IEEE Communications Surveys Tutorials*, vol. 21, no. 2, pp. 1346–1382, 2019.

[30] S. Karmous, N. Adem, M. Atiquzzaman, and S. Samarakoon, “How can optical communications shape the future of deep space communications? a survey,” *IEEE Communications Surveys Tutorials*, vol. 27, no. 1, pp. 725–747, 2025.

[31] V. W. S. Chan, “Free space optical communication and network architecture - fundamentals, history and looking forward,” *IEEE Journal of Selected Topics in Quantum Electronics*, vol. 32, no. 1: Advances in Free Space Laser Communications, pp. 1–20, 2026.

[32] P. H. Pathak, X. Feng, P. Hu, and P. Mohapatra, “Visible light communication, networking, and sensing: A survey, potential and challenges,” *IEEE Communications Surveys & Tutorials*, vol. 17, no. 4, pp. 2047–2077, 2015.

[33] T. Komine and M. Nakagawa, “Fundamental analysis for visible-light communication system using led lights,” *IEEE Transactions on Consumer Electronics*, vol. 50, no. 1, pp. 100–107, 2004.

[34] H. Haas, L. Yin, Y. Wang, and C. Chen, “What is lifi?” *Journal of Lightwave Technology*, vol. 34, no. 6, pp. 1533–1544, 2016.

[35] D. Karunatilaka, F. Zafar, V. Kalavally, and R. Parthiban, “Led based indoor visible light communications: State of the art,” *IEEE Communications Surveys Tutorials*, vol. 17, no. 3, pp. 1649–1678, 2015.

[36] S. Rajagopal, R. D. Roberts, and S.-K. Lim, “Ieee 802.15.7 visible light communication: modulation schemes and dimming support,” *IEEE Communications Magazine*, vol. 50, no. 3, pp. 72–82, 2012.

[37] J. Armstrong, “Ofdm for optical communications,” *Journal of Lightwave Technology*, vol. 27, no. 3, pp. 189–204, 2009.

[38] C. Li and H. Haas, Eds., *Visible Light Communication: Theory and Applications*. CRC Press, 2015.

[39] R. W. Zaki, H. A. Fayed, A. Abd El Aziz, and M. H. Aly, “Outdoor visible light communication in intelligent transportation systems: Impact of snow and rain,” *Applied Sciences*, vol. 9, no. 24, p. 5453, 2019.

[40] O. Kharraz and D. Forsyth, “Performance comparisons between PIN and APD photodetectors for use in optical communication systems,” *Optik*, vol. 124, no. 13, pp. 1493–1498, 2013.

[41] G. P. Agrawal, *Fiber-Optic Communication Systems*, 4th ed. Hoboken, NJ, USA: Wiley, 2010.

[42] J. C. Campbell, “Recent advances in telecommunications avalanche photodiodes,” *Journal of Lightwave Technology*, vol. 25, no. 1, pp. 109–121, 2007.

[43] J. M. Kahn and J. R. Barry, “Wireless infrared communications,” *Proceedings of the IEEE*, vol. 85, no. 2, pp. 265–298, 1997.

[44] M. Kong, C. H. Kang, O. Alkhazragi, X. Sun, Y. Guo, M. Sait, J. A. Holguin-Lerma, T. K. Ng, and B. S. Ooi, “Survey of energy-autonomous solar cell receivers for satellite–air–ground–ocean optical wireless communication,” *Progress in Quantum Electronics*, vol. 74, p. 100300, 2020.

[45] S.-M. Kim and J.-S. Won, “Simultaneous reception of solar power and visible light communication using a solar cell,” *Optical Engineering*, vol. 53, no. 4, p. 046103, 2014.

[46] J. Fakidis, S. Videv, H. Helmers, and H. Haas, “0.5-Gb/s OFDM-based laser data and power transfer using a GaAs photovoltaic cell,” *IEEE Photonics Technology Letters*, vol. 30, no. 9, pp. 841–844, 2018.

[47] Z. Wang, D. Tsonev, S. Videv, and H. Haas, “On the Design of a Solar-Panel Receiver for Optical Wireless Communications With Simultaneous Energy Harvesting,” *IEEE Journal on Selected Areas in Communications*, vol. 33, no. 8, pp. 1612–1623, Aug. 2015.

[48] W.-H. Shin, S.-H. Yang, D.-H. Kwon, and S.-K. Han, “Self-reverse-biased solar panel optical receiver for simultaneous visible light communication and energy harvesting,” *Optics Express*, vol. 24, no. 22, p. A1300, Oct. 2016.

[49] M. Kong, B. Sun, R. Sarwar, J. Shen, Y. Chen, F. Qu, J. Han, J. Chen, H. Qin, and J. Xu, “Underwater wireless optical communication using a lens-free solar panel receiver,” *Optics Communications*, vol. 426, pp. 94–98, 2018.

[50] Z. Wang, D. Tsonev, S. Videv, and H. Haas, “Towards self-powered solar panel receiver for optical wireless communication,” in *2014 IEEE International Conference on Communications (ICC)*. Sydney, NSW: IEEE, Jun. 2014, pp. 3348–3353.

[51] S.-M. Kim and J.-S. Won, “Simultaneous reception of visible light communication and optical energy using a solar cell receiver,” in *2013 International Conference on ICT Convergence (ICTC)*. IEEE, 2013, pp. 896–897.

[52] W. Zhao, M. Kamezaki, K. Yamaguchi, M. Konno, A. Onuki, and S. Sugano, “An experimental analysis of pipe inspection using solar panel receiver for visible light communication and energy harvesting,” in *2020 IEEE/ASME International Conference on Advanced Intelligent Mechatronics (AIM)*, 2020, pp. 1848–1853.

[53] C.-W. Hsu, J.-T. Wu, H.-Y. Wang, C.-W. Chow, C.-H. Lee, M.-T. Chu, and C.-H. Yeh, “Visible light positioning and lighting based on identity positioning and rf carrier allocation technique using a solar cell receiver,” *IEEE Photonics Journal*, vol. 8, no. 4, pp. 1–7, 2016.

[54] K. Sindhubala and B. Vijayalakshmi, “Receiver Intend to Reduce Ambient Light Noise in Visible - Light Communication using Solar Panels,” *Journal of Engineering Science and Technology Review*, vol. 10, no. 1, pp. 84–90, Feb. 2017.

[55] H.-Y. Wang, J.-T. Wu, C.-W. Chow, Y. Liu, C.-H. Yeh, X.-L. Liao, K.-H. Lin, W.-L. Wu, and Y.-Y. Chen, “Using pre-distorted PAM-4 signal and parallel resistance circuit to enhance the passive solar cell based visible light communication,” *Optics Communications*, vol. 407, pp. 245–249, Jan. 2018.

[56] N. Lorrière, N. Bétrancourt, M. Pasquinelli, G. Chabriel, J. Barrère, L. Escoubas, J.-L. Wu, V. Bermudez, C. M. Ruiz, and J.-J. Simon, “Photovoltaic solar cells for outdoor Li-Fi communications,” *Journal of Lightwave Technology*, vol. 38, no. 15, pp. 3822–3831, 2020.

[57] A. Zaiton, H. Muhammad, and F. Jasman, “Solar panel receiver characterisation for indoor visible light communication system,” in *Journal of Physics: Conference Series*, vol. 1502, no. 1. IOP Publishing, 2020, p. 012016.

[58] S. Das, E. Poves, J. Fakidis, A. Sparks, S. Videv, and H. Haas, “Towards energy neutral wireless communications: Photovoltaic cells to connect remote areas,” *Energies*, vol. 12, no. 19, p. 3772, 2019.

[59] S. Das, A. Sparks, E. Poves, S. Videv, J. Fakidis, and H. Haas, “Effect of sunlight on photovoltaics as optical wireless communication receivers,” *Journal of Lightwave Technology*, vol. 39, no. 19, pp. 6182–6190, 2021.

[60] D. Ma, G. Lan, M. Hassan, W. Hu, and S. K. Das, “Sensing, computing, and communications for energy harvesting iots: A survey,” *IEEE Communications Surveys & Tutorials*, vol. 22, no. 2, pp. 1222–1250, 2019.

[61] M. T. Neukom, “Charge carrier dynamics of methylammonium lead-iodide perovskite solar cells,” *arXiv preprint arXiv:1611.06425*, 2016.

[62] Wijewardane, Samantha, "Flexible and lightweight thin-film solar PV based on CIGS, CdTe, and a-Si:H," in *Inventions, Innovations, and New Technologies*. Elsevier ScienceDirect, 2023, presented in part at the 50th IEEE Photovoltaic Specialists Conference (PVSC), San Juan, Puerto Rico, June 2023.

[63] "Perovskite solar cells: An in-depth guide and comparison with other technologies," Solar Magazine, 2022. [Online]. Available: https://solarmagazine.com/solar-panels/perovskite-solar-cells/

[64] C. Carrascal, I. Demirkol, and J. Paradells, "On-demand sensor node wake-up using solar panels and visible light communication," *Sensors*, vol. 16, no. 3, p. 418, 2016.

[65] J. Fakidis, S. Videv, H. Helmers, and H. Haas, "Simultaneous wireless data and power transfer for a 1-Gb/s GaAs VCSEL and photovoltaic link," *IEEE Photonics Technology Letters*, vol. 32, pp. 1277–1280, 2020.

[66] ——, "0.5-Gb/s OFDM-based laser data and power transfer using a GaAs photovoltaic cell," in *2018 IEEE Photonics Conference (IPC)*. IEEE, 2018, pp. 1–4.

[67] "Comparison of renewables: Perovskite vs. silicon vs. thin-film solar," Sustainable Atlas, 2026, citing NREL Best Research-Cell Efficiency Chart (2026) and Oxford PV commercial tandem module data (2025). [Online]. Available: https://sustainableatlas.org/post/comparison-renewables-innovation-perovskite-vs-silicon-vs-thin-film-solar-1793

[68] N. A. Mica *et al.*, "Triple-cation perovskite solar cells for visible light communications," *Photonics Research*, vol. 8, pp. A16–A24, 2020.

[69] N. A. Mica, R. Bian, P. Manousiadis, L. K. Jagadamma, I. Tavakkolnia, H. Haas, G. A. Turnbull, and I. D. Samuel, "Triple-cation perovskite solar cells for visible light communications," *Photonics research*, vol. 8, no. 8, pp. A16–A24, 2020.

[70] E. Tavakkolnia *et al.*, "Organic photovoltaics for simultaneous energy harvesting and high-speed MIMO optical wireless communications," *Light: Science & Applications*, vol. 10, no. 41, 2021.

[71] S. Zhang, D. Tsonev, S. Videv, S. Ghosh, G. A. Turnbull, I. D. Samuel, and H. Haas, "Organic solar cells as high-speed data detectors for visible light communication," *Optica*, vol. 2, no. 7, pp. 607–610, 2015.

[72] N. Lorrière, G. Chabriel, J. Barrère, M. Pasquinelli, G. Pic, N. Vannieuwenhuyse, L. Escoubas, and J.-J. Simon, "Lifi reception from organic photovoltaic modules subject to additional dc illuminations and shading effects," in *2019 Global LIFI Congress (GLC)*. IEEE, 2019, pp. 1–5.

[73] D. Tettey, K. A. Mahmoodi, R. Bonakdar, and M. Uysal, "Vehicular visible light communications with a solar panel receiver," in *Proceedings of the 29th Annual International Conference on Mobile Computing and Networking*, 2023, pp. 1–3.

[74] N. Lorrière *et al.*, "Photovoltaic solar cells for outdoor LiFi communications," *Journal of Lightwave Technology*, vol. 38, no. 15, pp. 3822–3831, 2020.

[75] P. D. Diamantoulakis and G. K. Karagiannidis, "Simultaneous lightwave information and power transfer (slipt) for indoor iot applications," in *GLOBECOM 2017-2017 IEEE Global Communications Conference*. IEEE, 2017, pp. 1–6.

[76] M. Liu, M. Xiong, Q. Liu, S. Zhou, and H. Deng, "Mobility-enhanced simultaneous lightwave information and power transfer," *IEEE Transactions on Wireless Communications*, vol. 20, no. 10, pp. 6927–6939, 2021.

[77] M. Xiong, Q. Liu, H. Deng, G. Wang, G. Li, and B. He, "Duplex self-aligning resonant beam communications and power transfer with coupled spatially distributed laser resonator," *arXiv preprint arXiv:2505.05107*, 2025.

[78] S. Han, W. Fang, M. Liu, M. Xu, S. Xia, and Q. Liu, "Field of view expansion for resonant beam information and power transfer," *arXiv preprint arXiv:2408.04274*, 2024.

[79] M. Uysal, S. Ghasvarianjahromi, M. Karbalayghareh, P. D. Diamantoulakis, G. K. Karagiannidis, and S. M. Sait, "Slipt for underwater visible light communications: Performance analysis and optimization," *IEEE Transactions on Wireless Communications*, vol. 20, no. 10, pp. 6715–6728, 2021.

[80] J. I. De Oliveira Filho, A. Trichili, O. Alkhazragi, M.-S. Alouini, B. S. Ooi, and K. N. Salama, "Reconfigurable mimo-based self-powered battery-less light communication system," *Light: Science & Applications*, vol. 13, no. 1, p. 218, 2024.

[81] S. Bader, X. Ma, and B. Oelmann, "One-diode photovoltaic model parameters at indoor illumination levels – A comparison," *Solar Energy*, vol. 180, pp. 707–716, Mar. 2019.

[82] D. Sera, R. Teodorescu, and P. Rodriguez, "PV panel model based on datasheet values," in *2007 IEEE International Symposium on Industrial Electronics*. Vigo, Spain: IEEE, Jun. 2007, pp. 2392–2396.

[83] J. Cubas, S. Pindado, and M. Victoria, "On the analytical approach for modeling photovoltaic systems behavior," *Journal of power sources*, vol. 247, pp. 467–474, 2014.

[84] Rahul, A. Mitra, A. Srivastava, V. A. Bohara, and D. Solanki, "Experimental validation of optical wireless receiver using solar panel with bandwidth enhancement circuit," in *2022 IEEE 95th Vehicular Technology Conference: (VTC2022-Spring)*, 2022, pp. 1–6.

[85] R. King, D. Bhusari, D. Larrabee, X.-Q. Liu, E. Rehder, K. Edmondson, H. Cotal, R. Jones, J. Ermer, C. Fetzer *et al.*, "Solar cell generations over 40% efficiency," *Progress in Photovoltaics: Research and Applications*, vol. 20, no. 6, pp. 801–815, 2012.

[86] M. A. Green, K. Emery, Y. Hishikawa, W. Warta, and E. D. Dunlop, "Solar cell efficiency tables (version 39)," *Progress in photovoltaics: research and applications*, vol. 20, no. 1, pp. 12–20, 2012.

[87] D. Schulz, J. Hohmann, P. Hellwig, J. Hilt, C. Schmidt, R. Freund, and V. Jungnickel, "Outdoor measurements using an optical wireless link for fixed-access applications," *Journal of Lightwave Technology*, vol. 37, no. 2, pp. 634–642, 2019.

[88] S. Naser, P. C. Sofotasios, L. Bariah, W. Jaafar, S. Muhaidat, M. Al-Qutayri, and O. A. Dobre, "Rate-splitting multiple access: Unifying noma and sdma in miso vlc channels," *IEEE Open Journal of Vehicular Technology*, vol. 1, pp. 393–413, 2020.

[89] I. Abdalla, M. Rahaim, and T. Little, “Impact of receiver fov and orientation on dense optical networks,” in *2018 IEEE Global Communications Conference (GLOBECOM)*. IEEE, 2018, pp. 1–6.

[90] Velmenni. "Li-Fi evaluation kit", 2022. [Online]. Available: https://www.velmenni.com/lifi-dongle-access-points

[91] iPerf Development Team, “iPerf - The ultimate speed test tool for TCP, UDP, and SCTP,” 2025, accessed: 2025-02-02. [Online]. Available: https://iperf.fr/iperf-doc.php#tuningtcp

[92] M. Y. Abualhoul, M. Marouf, O. Shagdar, and F. Nashashibi, “Platooning control using visible light communications: A feasibility study,” in *16th International IEEE Conference on Intelligent Transportation Systems (ITSC 2013)*. IEEE, 2013, pp. 1535–1540.

[93] L. Dingpu, X. Limin, M. Haifeng, H. Yingwei, and Z. Jieyu, “Research on outdoor testing of solar modules,” in *Proc. of SPIE Vol*, vol. 8419, 2012, pp. 84 193E–1.

[94] A. K. Majumdar, *Free-Space Laser Communications: Principles and Advances*. New York: Springer, 2008.

[95] T. Komine and M. Nakagawa, “Performance evaluation of visible-light wireless communication system using white led lightings,” in *Proceedings. ISCC 2004. Ninth International Symposium on Computers And Communications (IEEE Cat. No. 04TH8769)*, vol. 1. IEEE, 2004, pp. 258–263.

[96] WHO. "road traffic injuries", 2023. [Online]. Available: https://www.who.int/news-room/fact-sheets/detail/road-traffic-injuries

[97] 5GCAR project. [Online]. Available: https://5gcar.eu/wp-content/uploads/2017/05/5GCAR_D2.1_v1.0.pdf

[98] Q. Chen, W. Zheng, T. Zhang, W. Cui, and Z. Cui, “A power analysis model for outdoor long-distance visible light communication,” in *2017 Ninth International Conference on Ubiquitous and Future Networks (ICUFN)*. IEEE, 2017, pp. 131–136.

[99] J. Ryu and J. C. Gerdes, “Estimation of vehicle roll and road bank angle,” in *Proceedings of the 2004 American control conference*, vol. 3. IEEE, 2004, pp. 2110–2115.

[100] E. Vinande, P. Axelrad, and D. Akos, “Mounting-angle estimation for personal navigation devices,” *IEEE Transactions on Vehicular Technology*, vol. 59, no. 3, pp. 1129–1138, 2009.

[101] F. Xiao, J. Hu, P. Zhu, and C. Deng, “A method of three-dimensional stability region and ideal roll angle to improve vehicle stability,” *Nonlinear Dynamics*, vol. 111, no. 3, pp. 2353–2377, 2023.

[102] R. Tchamna and I. Youn, “Yaw rate and side-slip control considering vehicle longitudinal dynamics,” *International Journal of Automotive Technology*, vol. 14, pp. 53–60, 2013.

[103] K. Antonakoglou, N. Brahmi, T. Abbas, A. E. Fernandez Barciela, M. Boban, K. Cordes, M. Fallgren, L. Gallo, A. Kousaridas, Z. Li *et al.*, “On the needs and requirements arising from connected and automated driving,” *Journal of Sensor and Actuator Networks*, vol. 9, no. 2, p. 24, 2020.